AN ABSTRACT OF THE THESIS OF

Jong-Bum Kim for the degree of Doctor of Philosophy in Mechanical Engineering presented on March 5, 1992.

Title: Dynamic Finite Element Analysis of Micropolar Elastic Materials

Abstract approved: Signature redacted for privacy.
Timothy C. Kennedy

In granular or fibrous materials, in which the dimensions of the internal structure can be of the same order of magnitude as major flaws or holes, classical elasticity theory does not consistently provide accurate models of the large stress gradients that may develop. With the incorporation of additional rotational degrees of freedom, the development of micropolar elasticity theory offers promise for the modeling of these phenomena.

The principal objective of this investigation was to develop a plane-strain, dynamic, finite element method for the dynamic response of micropolar elastic media. For purposes of analysis, an eight-node isoparametric, quadrilateral element was used, and the dynamic finite element model was verified by comparing its output, including both displacement and microrotational solutions, with analytic solutions for micropolar plate material subject to shear loads. In addition, plates with circular holes under dynamic loads were analyzed. The results obtained for a special case of a classically elastic material were in good agreement with previously obtained analytical solutions. Materials with significant micropolar behavior were found to cause significant reductions in the dynamic stress concentrations caused by the diffraction of plane dilatational waves adjacent to circular holes. Similar trends were observed from the analysis of plates with elliptical holes subject to suddenly applied loads.

Finally, two cases were considered: 1) A stationary crack subject to dynamic loads, and 2) a crack propagating at a constant velocity while under constant load. The method for the calculation of dynamic energy release rates, and node releasing techniques for the simulation of crack propagation, were developed for micropolar elastic materials. In both cases, materials with strong micropolar properties were found to have significantly lower dynamic energy release rates than classically elastic material counterparts.

Dynamic Finite Element Analysis of Micropolar Elastic Materials

by

Jong-Bum Kim

A THESIS

submitted to

Oregon State University

in partial fulfillment of
the requirements for the
degree of

Doctor of Philosophy

Completed March 5, 1992

Commencement June 1992

APPROVED:

Signature redacted for privacy.

Associate Professor of Mechanical Engineering in charge of major

Signature redacted for privacy.

Head of Department of Mechanical Engineering

Signature redacted for privacy.

Dean of Graduate School

Date thesis is presented March 5, 1992

Typed by B. McMechan for Jong-Bum Kim

ACKNOWLEDGEMENTS

I would like to express my heartfelt gratitude to my major advisor, Dr. Timothy C. Kennedy, for his guidance and consistent support throughout the period of this study. Without his interest and assistance, this work could not have been completed. I would also like to thank Drs. Charles E. Smith, Clarence A. Calder, Andrzej Olas, and Larry Boersma for serving as members of my graduate commitee as well as for their kind advice and encouragement.

I would like to thank Duhwoe Jung for special help with the computer requirements for this thesis and for his warm friendship. In addition, my thanks to all of the Korean students in the Mechanical and Civil Engineering departments, whom it has been my pleasure to know during my period of study at Oregon State University. I would also like to extend my appreciation to the Department of Mechanical Engineering for financial support during my graduate education.

Most important, I would like to express my deep gratitude to my parents for their endless love and continuing encouragement. Special thanks are due to my wife, Hyunsook, my son, Hanjoon, and my lovely daughter, Sohyun, for their patience and love. Finally, I would like to extend my appreciation to Bill McMechan for his help with the thesis format.

TABLE OF CONTENTS

TABLE OF CONTENTS (continued)

LIST OF FIGURES

LIST OF FIGURES (continued)

Page

LIST OF FIGURES (continued)

Page

LIST OF TABLES

LIST OF APPENDIX FIGURES

Dynamic Finite Element Analysis of Micropolar Elastic Materials

1. INTRODUCTION

The classical theory of elasticity is based on the ideal assumptions that all balance laws are valid for every part of a body, however small that body may be, and that all material bodies possess continuous mass densities. It follows that load transfers through a surface element situated within the interior of a body occur only by means of the force stress vector. Based upon these assumptions, body strain can be described in terms of symmetric stress and strain tensors. Below the elasticity limit of the material, the behavior of numerous structural materials can be explained from these factors. However, essential differences have been observed between theory and experimentation in a number of cases. This is primarily true of states of stress in which large stress gradients occur. Stress concentrations around holes or in the proximity of cracks in granular or fibrous materials are typical examples of this state. Therefore, the classical theory of elasticity provides only an inadequate representation of the behavior of such materials as granular bodies with large molecules (polymers), composite fibrous materials, or liquid crystals, and the theory of oriented media must be incorporated to analyze these types of materials. Thus, micropolar theory has been one of the alternatives used to describe the behavior of these types of material.

1.1 Review of Micropolar Elasticity Theory and the Dynamic Finite Element Method

Micropolar elasticity theory, as introduced and developed by Eringen and Suhubi [1,2], incorporates the properties of the microstructure of a material within the continuum framework. This theory is applicable for the analysis of phenomena where the material microstructure has a strong influence upon the response of a structure to external load factors. This is likely to occur in granular or fibrous materials near areas of large stress gradients; for example, occurrence is frequent in the near proximity of holes or cracks. The widespread use of various types of composite materials, in which the microstructure is known to control mechanical properties, has stimulated interest in this theory. Accordingly, Eringen [3,4] presented the linear theory of micropolar elasticity.

In linear theory, a micropolar continuum may be regarded as a classical continuum, each point of which, in addition to translation, is assigned a second continuum with an added rotational degree of freedom. Thus, the deformation of a body is described by the displacement vector u_k and an independent microrotation vector ϕ_k. In addition, micropolar materials experience the couple stress m_{lk} as well as the force stress t_{lk}, resulting in nonsymmetric stress and strain tensors. In general, the additional degree of freedom makes the performance of stress analysis on structures composed of micropolar materials more difficult than for classical elastic materials. Frequently, only approximate solutions can be obtained for the micropolar case, where closed form solutions are available in the case of classical elasticity.

Stress concentrations around circular holes in plates have been analyzed by Mindlin [5], who developed the indeterminate couple-stress theory, a special case in general micropolar theory. Based upon micropolar elasticity, Kaloni and Ariman [6] investigated same problem and compared their results to those obtained by Mindlin

[5]. In turn, Kim and Eringen [7] presented an analytical solution for the stress concentration around elliptical holes. In addition, a number of studies have involved the analysis of cracks in micropolar materials. Through numerical solution of integral equations, based upon application of indeterminate couple stress [5], Sternberg and Muki [8] computed the stress intensity factors around cracks. Atkinson and Leppington [9] presented limited numerical results for stress intensity factors and energy release rates for semi-infinite cracks in micropolar materials. By solving a Fredholm integral equation, Paul and Sridharan [10] determined the effects of couple stresses upon the stress field around a penny-shaped crack. Sladec and Sladec [11] then developed an approximate solution for the penny-shaped crack. In each of these studies, the response of the micropolar materials was considered only in static terms.

The development of finite element analysis for micropolar materials has been limited in extent. Malcolm [12] developed a finite element procedure for micromorphic materials and used it to compute the stress field around holes in plates under tension. Hermann [13] used mixed variational equations to investigate and compare four mixed finite elements for plane couple stress elasticity, considering the stress concentration problem for straight-sided isoparametric elements with either four or eight nodes. Nakamura et al. [14] used triangular elements to model stresses around holes in anisotropic micropolar materials, whereas Kennedy and Kim [15] used quadrilateral elements to study fractures in micropolar materials. Nakamura and Lakes [16] addressed a similar problem, but for the case of blunt-edged notches with elliptic contours. Using first order stress functions, Wood [17] developed a finite element procedure for plane linear elastic couple-stress theory, solving for stress concentrations around circular holes in plates. For each of these finite element analyses, again only the static responses of the materials were considered.

The dynamic response of materials containing defects to impulse loading has been of interest in a variety of technological circumstances. In recent years, numerous studies have been performed in the area of classical dynamic fracture mechanics, many of which have been summarized in comprehensive review articles by Sih [18], Williams and Knauss [19], Kanninen and Popelar [20], and Parton and Boriskovsky [21,22]. However, due to the complexities of micropolar elastodynamic problems, to date the extent of this research has been limited. Some of the fundamental problems in micropolar elastodynamics were summarized by Nowacki [23]. Iesan [24] examined dynamic energy release rates for micropolar elastodynamic crack propagation, while Rao [25] investigated the problem of longitudinal wave propagation in micropolar wave guides. Vukobrat [26] derived path-independent integrals, originally introduced by Rice [27], for micropolar elastodynamics, using the Noether theorem to study the case of steady-state crack propagation. Recently, through the numerical solution of singular integral equations, Han et al. [28] developed a solution for the diffraction of plane dilatational waves in the proximity of moving cracks in unbounded micropolar materials. However, this solution proved to be valid only for small values of time and the peak values of responses could not be calculated.

For the past two decades, investigative efforts have been undertaken in the area of dynamic finite element methods within the classical continuum framework, and it has become common practice for the structural analyst to calculate the response of structural systems to transient loads. The prediction of displacement, velocity, acceleration, and stress-time histories at nodes and elements of the finite element model has been among the results achieved in this research direction. In addition, it has been noted that the use of direct time integration as a solution procedure for finite element semidiscretizations may be advantageous for linear systems.

The characteristics of the time integration procedure can have a critical impact on the feasibility of the calculation. The wrong choice of time integrator may result in an impractical methodology, or may lead to excessive errors in simulations. For this reason, direct time integration has continued to be an active area of research.

The fundamental characteristic of any direct time integration algorithm is that it is either explicit or implicit. Belytschko et al. [29] provided an elegant summary of the stability criteria and the solution properties for explicit central difference integration. Implicit schemes possess stability characteristics superior to those for explicit schemes, which because of the stability problem often require very small time-steps. Initially, Houbolt [30] presented a three-step, second-order implicit scheme, but from the viewpoint of both the damping ratios and the period errors, the method seems to have had too great an effect upon the low modes. In turn, Newmark [31] proposed an unconditionally stable second-order time integration scheme, if $\gamma \geq 1/2$ and $\beta \geq (\gamma + 1/2)^2/4$. The θ-method of Wilson et al. [32] is a modification of Newmark's algorithm in which a linear variation of acceleration is assumed within a time-step. By combining aspects of the Newmark method and the Wilson θ-method, Hilber et al. [33] introduced the α-method to improve the numerical damping properties of the Newmark method without degrading the order of accuracy, followed by development of the collocation method [34]. In addition, the ρ-method of Bazzi and Anderheggen [35] can be viewed as an extension of the Newmark method.

Among more recent developments, particularly for nonlinear problems, the algorithm proposed by Park [36] was based on a combination of the mathematical approximations contained in the Gear two-step and three-step methods [37]. The shortcoming of this method is that it requires special starting procedures. Zienkiewicz et al. [38] presented a unified formulation of single-step methods, enabling the

implementation of different methods within a single program. In addition, so-called implicit-explicit procedures, which were an attempt to apply different operators to different parts of a structure, dependent upon the range of frequencies excited, were investigated by Belytschko and Mullen [39], Hughes and Liu [40], and Liu and Belytschko [41]. Zienkiewicz [42] and Wood [43] developed the weighted residual method, which used a Galerkin form of discretization in the time domain. In addition to the development of these essential algoritms, considerable effort has been concentrated in this area to improve both the accuracy and the stability criteria for integration schemes. In the end, the choices of method are strongly problem-dependent and must be based on experience. For this area of interest, comprehensive reviews and guidelines may be found in Belytschko [42], Bathe [43], Cook [44], Hughes [45], Bickford [46], and Zienkiewicz [47].

In dynamic finite element analysis, a mass matrix accounting for inertia, is an important factor affecting solutions. It is generally acknowledged that Archer [48,49] was the first to point out the correctness of a consistent mass which at certain points, when compared to the physical lumping of the structural mass, can be generated with shape functions that are identical to those used for an element stiffness matrix. When a central difference algorithm is concerned, a diagonal mass matrix obtained by a lumping technique is preferred since it does not require solution of a set of algebraic equations for each time-step. For higher order elements or those of irregular shape, systematic lumping schemes are necessary. Hinton et al. [50] developed a special lumping technique which always produces positive-diagonal lumped masses. Fried and Malkus [51] developed rules of optimal quadrature for triangular elements, in which the mass matrix may contain zero or negative diagonal quantities and often requires special solution treatments. Malkus and Plesha [52], and then Malkus et al. [53], discussed the zero or negative masses of optimally

lumped mass matrices. In the row-sum technique [45], the elements in each row of a consistent mass matrix are summed and lumped on the diagonal. However, among the various methods of generating mass matrices, there is no single solution which will satisfy every problem. The choice of mass is solely problem-dependent, and matched methods are generally recommended [44,45]. For example, for central differences and a lumped mass, the Newmark method [31] in conjunction with a consistent mass would be an appropriate match.

For application of finite element methods to dynamic fracture mechanics, there are two distinct types of problems for which the forces of inertia must be included in the equations of motion for the cracked body: 1) The initiation of crack growth under impact loading and 2) rapid crack propagation under fixed loading. Kanninen [54] subjected the application of numerical methods to dynamic fracture mechanics to a critical appraisal in 1978. At that time, since the relevant singularities could be modeled for the crack tip elements, the finite element method was believed to be the most suitable method for the analysis of stationary cracks under dynamic loads, whereas it was believed to be unsuitable for the analysis of dynamic crack propagation because of the numerical difficulties involved in advancing the crack in a discrete manner. However, in the intervening period the state of the art for the application of finite element methods to dynamic fracture mechanics has greatly advanced.

Recent advances in the application of finite element methods to dynamic fracture mechanics were considered by Atluri and Nishioka [55] and by Liebowitz and Moyer [56], and may be summarized as follows. Henshell and Shaw [57] and Barsoum [58] noted that by the displacement of the midside node of an eight-node quadrilateral element to a quarter-point position, the element strain field naturally exhibited a square root singularity. In addition, Barsoum [59] observed that when the ele-

ment was collapsed into a triangular shape, predicted angular strain variations were increasingly accurate. Mall [60] demonstrated that extensions of the quarter-point element to transient dynamic analysis were automatic, and Murti and Valliappan [61] investigated the application of the quarter-point element to dynamic crack analysis. Morgan et al. [62] conducted one of the initial attempts to implement a special dynamic cracked element, but neglected incompatibilities along the boundary with conventional elements.

The first attempts at developing finite element methods for the calculation of stress intensity factors for propagating cracks were conducted by Aoki et al. [63], Bazant et al. [64], and King and Malluck [65]. Special singular elements were proposed for modeling crack growth, and successive applications were formulated by Atluri and Nishioka [55,66], Nishioka and Atluri [67,68,70,71], and by Nioshioka et al. [69,72]. For the hybrid elements developed for these investigations, more than a single eigenfunction for the propagation of cracks was included as a displacement basis function and in the least-squares sense, displacement compatibility between the singular element and its surrounding conventional elements was achieved. These methods were based upon a moving mesh procedure, in which the singular element containing the crack tip was translated for each time-step in the direction of crack growth, while the regular elements surrounding the moving singular element were continuously distorted. Insofar as these approaches encompassed the development of path-independent integrals for elastodynamically propagating cracks, Kishimoto et al. [73] derived a path-independent integral $\hat{J}$ for spatially fixed paths, which is equivalent to the energy release rate for only stationary cracks in solids under dynamic motion. Overall, these methods have been successfully applied to a number of dynamic problems, but the problem they pose lies in the complexity of the formula-

tion for each implementation as well as the necessity of remeshing without any evidence of computational improvement.

In addition, based upon the employment of only conventional elements, a great deal of work has been accomplished in the area of elastodynamic fractures, primarily directed at the prediction of dynamic stress intensity factors or dynamic energy release rates for running cracks. For consideration of crack propagation in double cantilever beam and pipeline problems, Owen and Shantaram [74] used standard isoparametric elements for dynamic transient stress analysis, changing the location of the crack-tip from one node to the next node along the crack axis in a time-step employed within a time integration scheme. Sudden increases in crack length, accompanied by the release of displacement constraints, induced spurious high frequency oscillations in finite element solutions. Keegstra et al. [75] overcame this difficulty by releasing the nodes gradually over a period of time, using non-zero hold-back forces for more than a single node behind the advancing crack-tip. For conventional elements, the use of non-zero hold-back (i.e., node releasing) force for a single node behind the advancing crack-tip and gradual release techniques were developed by Malluck and King [76], Rydholm et al. [77], and Kobayashi et al. [78]. In the first two studies, relationships between the releasing force and the original reaction force at same node were nonlinear, while linear relaxation was proposed in the third study. Malluck and King [79] compared two releasing mechanisms. Linear relaxation, investigated by Kobayashi et al. [78] and Hodulak et al. [80], was subsequently considered for an eight-node element by Atluri and Nioshioka [55]. Mall and Luz [81] investigated the simultaneous release of both the corner and the midside nodes for eight-node isoparametric elements.

The crack closure integral for calculation of strain energy release rates, based upon infinitesimal and virtual crack length increments, was originally derived by

Irwin [82]. Subsequently, Sih and Hartranft [83] provided an equivalent relationship for three dimensional crack-front configurations and a modified crack closure integral, enabling computation of strain energy release rates from nodal forces and displacements obtained from finite element solutions, was presented by Rybicki and Kanninen [84]. Finally, Jih and Sun [85] extended the crack closure method for the calculation of dynamic strain energy release rates, comparing their results to those obtained for path independent integrals as well as a number of other methods.

1.2 Objective of the Investigation

From the evidence presented in section 1.1, considerable progress has been achieved in the application of dynamic finite element as well as finite element methods to the solution of problems of classical dynamic fracture mechanics. However, there are no indications that dynamic finite element methods have been applied to micropolar elastodynamic theory. In addition, stationary cracks under impact loads and the dynamic propagation of a finite cracks in micropolar elastic media have not been subject to numerical solutions based upon finite element methodology.

Thus, the objective of the current investigation is to develop the dynamic finite element method in accordance with micropolar elastodynamic theory, analyzing problems of stress concentration in micropolar elastic materials. Based upon the work of Eringen [4] and Nowacki [23], micropolar elastodynamic theory is considered in Chapter 2. In Chapter 3, based upon a virtual work principle, the formulation of a dynamic finite element method for the solution of crack problems in micropolar elastodynamics is presented. To verify the solution, the problem of a half-space whose surface is subject to a shear stress uniform in space and harmonic in time is solved and compared to the analytical solution proposed by Nowacki [23]. In

Chapter 4, a method for the calculation of dynamic energy release rates for both stationary and propagating cracks is developed and node release techniques are discussed. Chapter 5 describes the results of numerical example problems, as follows: 1) Stress concentration around a circular holes in a plate subject to a plane-strain condition; 2) stress concentration around an elliptical hole within a plate; 3) a stationary crack in a finite plate subject to mode-I impact load and a plane-strain condition; and 4) a crack propagating at a constant velocity in a body subject to static tension load. For each example problem, classical solutions are obtained when the micropolar moduli are set to zero; therefore, this investigation confirms that with the suppression of micropolar moduli, classical elasticity is a special case of micropolar elasticity. Compared to classical media, as the effect of micropolar properties is increased, dynamic stress concentration and the dynamic energy release rate become smaller. The findings of this investigation are summarized and discussed in Chapter 6.

2. MICROPOLAR ELASTICITY THEORY

The basic equations for micropolar elasticity theory are presented in this chapter. Homogeneous, isotropic, and centrally symmetric elastic bodies, the characteristics of which are known from classical elasticity, are considered, and the tensor equations from micropolar elasticity theory [1-4] are developed in terms of the individual components for a rectangular coordinate system. The notation used is identical to that provided by Eringen [1-4].

2.1 Equations of Equilibrium and Motion

The equations of motion used in micropolar elastodynamics theory can be derived from the laws of conservation of linear momentum and angular momentum. In the absence of body force and body couple, the component form of these equations are:

$$\rho \ddot{u}_k = t_{lk,l} \tag{2.1}$$

and

$$\rho j \ddot{\phi}_k = m_{lk,l} + e_{kmn} t_{mn} , \tag{2.2}$$

where t_{lk} is the force stress tensor, m_{lk} is the couple stress tensor, ρ is the mass density, j is the microinertia density, e_{kmn} is the permutation symbol, u_k is the displacement vector, and ϕ_k represents three microrotation components. These equations are the Cauchy first and second laws of motion; whereas the first is

identical to the case for classical elastodynamics, the second differs from the classical case.

In rectangular coordinates, and under two-dimensional plane-strain conditions, equations (2.1) and (2.2) can be expanded as

$$\rho \ddot{u}_x = \frac{\partial t_{xx}}{\partial x} + \frac{\partial t_{yx}}{\partial y} , \tag{2.3}$$

$$\rho \ddot{u}_y = \frac{\partial t_{xy}}{\partial x} + \frac{\partial t_{yy}}{\partial y} , \tag{2.4}$$

and

$$\rho \ddot{\phi}_z = \frac{\partial m_{xz}}{\partial x} + \frac{\partial m_{yz}}{\partial y} + t_{xy} - t_{yx} . \tag{2.5}$$

When the time derivative terms of equations (2.3)—(2.5) are dropped, the static case for balance equations (i.e., equilibrium equations) may be obtained as

$$\frac{\partial t_{xx}}{\partial x} + \frac{\partial t_{yx}}{\partial y} = 0 , \tag{2.6}$$

$$\frac{\partial t_{xy}}{\partial x} + \frac{\partial t_{yy}}{\partial y} = 0 , \tag{2.7}$$

and

$$\frac{\partial m_{xz}}{\partial x} + \frac{\partial m_{yz}}{\partial y} + t_{xy} - t_{yx} = 0 . \tag{2.8}$$

From equation (2.8), it is apparent that for the shear stresses t_{xy} and t_{yx} , classical balance is eliminated by the effect of couple stresses. Consequently, the stress tensors are not symmetric in micropolar elasticity.

2.2 Constitutive Equations

The constitutive equations for linear, isotropic, homogeneous, and centrosymmetric elastic bodies can be formulated on the basis of such principles of thermodynamics as the energy balance and inequality equations [86]. Thus, defining the elastic properties of micropolar materials, the constitutive equations consist of a stress constitutive equation, involving both displacements and microrotations, and a couple stress constitutive equation, involving the gradients of microrotation.

The stress constitutive equation is written as

$$t_{kl} = \lambda \epsilon_{rr} \delta_{kl} + (\mu + \kappa) \epsilon_{kl} + \mu \epsilon_{lk} , \tag{2.9}$$

where λ, μ, and κ are micropolar moduli and δ_{kl} is the Kronecker delta. The asymmetric strain tensor ϵ_{kl} is defined as

$$\epsilon_{kl} = u_{l,k} - e_{klm} \phi_m , \tag{2.10}$$

where the comma denotes partial differentiation. Once again, it should be noted that equation (2.10) reflects both displacement and microrotation schemes, differing from classical elasticity in that the latter contains only the displacement component. The microrotation vector ϕ_m is independent of the displacement vector u_k; that is, ϕ_m differs from the classical elasticity macrorotation vector ω_m, defined as

$$\omega_m = \frac{1}{2} e_{mlk} u_{k,l} . \tag{2.11}$$

Of a possible total of nine equations, equation (2.9), when placed within a rectangular coordinate system, leads to four constitutive stress equations under two-dimensional plane-strain condition,

$$t_{xx} = (\lambda+2\mu+\kappa)\,\epsilon_{xx} + \lambda\epsilon_{yy} , \tag{2.12}$$

$$t_{yy} = \lambda\epsilon_{xx} + (\lambda+2\mu+\kappa)\,\epsilon_{yy} , \tag{2.13}$$

$$t_{xy} = (\mu+\kappa)\,\epsilon_{xy} + \mu\epsilon_{yx} , \tag{2.14}$$

and

$$t_{yx} = \mu\epsilon_{xy} + (\mu+\kappa)\,\epsilon_{yx} . \tag{2.15}$$

Equation (2.10) may then be rewritten for a two-dimensional plane-strain condition in rectangular coordinates as

$$\epsilon_{xx} = \frac{\partial u_x}{\partial x} , \tag{2.16}$$

$$\epsilon_{yy} = \frac{\partial u_y}{\partial y} , \tag{2.17}$$

$$\epsilon_{xy} = \frac{\partial u_y}{\partial x} - \phi_z, \tag{2.18}$$

and

$$\epsilon_{yx} = \frac{\partial u_x}{\partial y} + \phi_z . \tag{2.19}$$

The couple stress constitutive equations, which have no counterpart in classical elasticity, may be written in two forms:

$$m_{kl} = \alpha\phi_{r,r}\delta_{kl} + \beta\phi_{k,l} + \gamma\phi_{l,k} \tag{2.20}$$

or

$$m_{kl} = \alpha \chi_{rr} \delta_{kl} + \beta \chi_{lk} + \gamma \chi_{kl} , \tag{2.21}$$

where α, β, and γ are additional micropolar moduli, and χ_{kl} is a torsion tensor, defined as

$$\chi_{kl} = \phi_{l,k} . \tag{2.22}$$

For rectangular coordinates, subject to the two-dimensional plane-strain condition, equations (2.20) and (2.22) may be represented as:

$$m_{xz} = \gamma \frac{\partial \phi_z}{\partial x} , \tag{2.23}$$

$$m_{yz} = \gamma \frac{\partial \phi_z}{\partial y} , \tag{2.24}$$

$$\chi_{xz} = \frac{\partial \phi_z}{\partial x} , \tag{2.25}$$

and

$$\chi_{yz} = \frac{\partial \phi_z}{\partial y} . \tag{2.26}$$

The difference between isotropic micropolar elasticity and classical elasticity is noted by the presence of four extra moduli, in addition to the Lamé constants λ and μ from classical elasticity; that is, κ, α, β, and γ. When these moduli are set to zero, equations (2.9) and (2.20) revert to Hooke's law of linear isotropic elastic solids. For two-dimensional plane-strain micropolar elasticity, four of a total of six micropolar moduli must be considered; that is, λ, μ, κ, and γ. Six components of force and couple stresses, from equations (2.12)—(2.15) and (2.23)—(2.24), are shown for two-dimensional Cartesian coordinates in Figure 2.1.

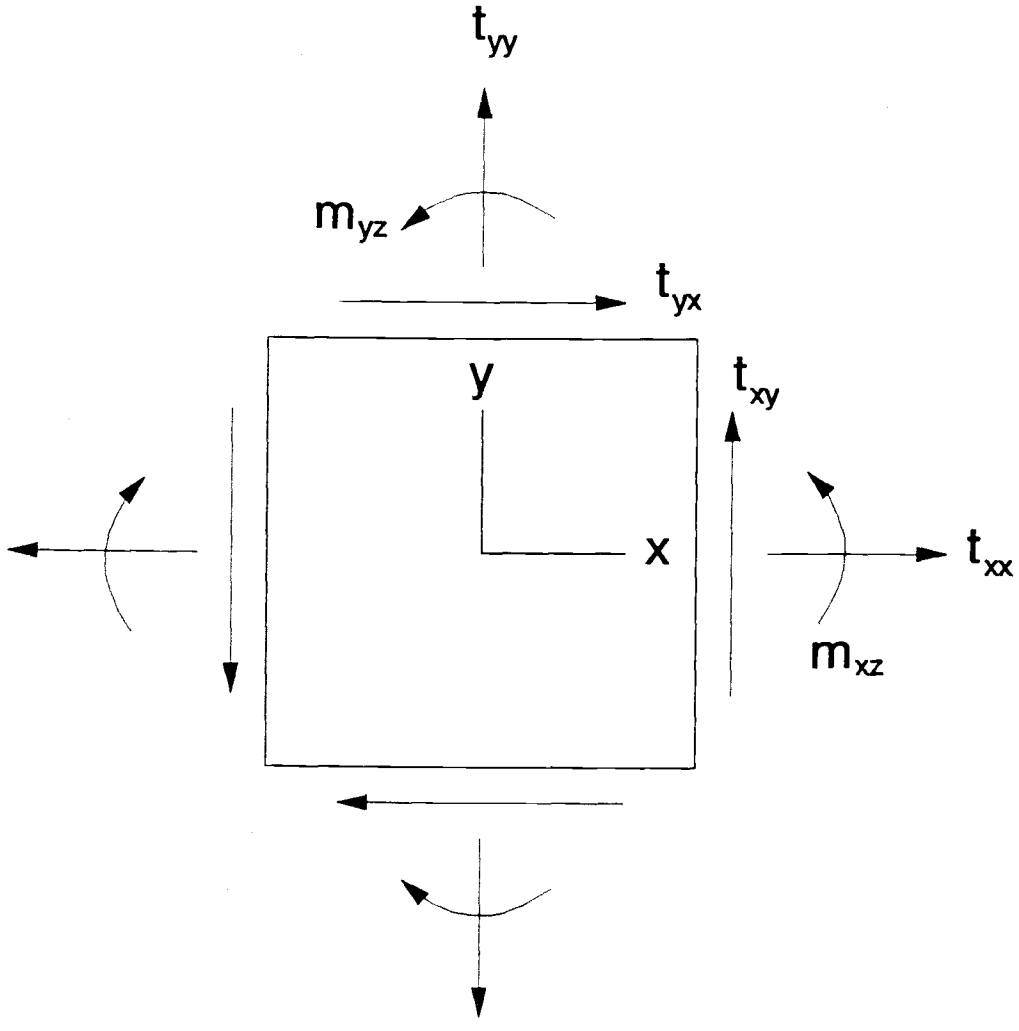

Figure 2.1 Force stress and couple stress orientations.

2.3 Equations of Motion for Displacement and Microrotation

The field equations for linear micropolar elasticity are obtained by combining the constitutive equations with the balance laws. Substituting equations (2.9) and (2.20) into equations (2.1) and (2.2), using equation (2.10), yields:

$$(\lambda+\mu)u_{l,lk} + (\mu+\kappa)u_{k,ll} + \kappa e_{klm}\phi_{m,l} = \rho\ddot{u}_k \tag{2.27}$$

and

$$(\alpha+\beta)\phi_{l,lk} + \gamma\phi_{k,ll} + \kappa e_{klm}u_{m,l} - 2\kappa\phi_k = \rho j\ddot{\phi}_k \ . \tag{2.28}$$

Equations (2.27) and (2.28) result in six partial differential equations for six unknown quantities: three displacements for u_k and three microrotations for ϕ_k.

For plane-strain problems (i.e., $u_z = \phi_x = \phi_y = 0$), equations (2.27) and (2.28) can be written as

$$(\lambda+\mu)\frac{\partial}{\partial x}\left[\frac{\partial u_x}{\partial x} + \frac{\partial u_y}{\partial y}\right] + (\mu+\kappa)\left[\frac{\partial^2 u_x}{\partial x^2} + \frac{\partial^2 u_x}{\partial y^2}\right] + \kappa\frac{\partial \phi_z}{\partial y} = \rho\frac{\partial^2 u_x}{\partial t^2} \ , \tag{2.29}$$

$$(\lambda+\mu)\frac{\partial}{\partial y}\left[\frac{\partial u_x}{\partial x} + \frac{\partial u_y}{\partial y}\right] + (\mu+\kappa)\left[\frac{\partial^2 u_y}{\partial x^2} + \frac{\partial^2 u_y}{\partial y^2}\right] - \kappa\frac{\partial \phi_z}{\partial x} = \rho\frac{\partial^2 u_y}{\partial t^2} \ , \tag{2.30}$$

and

$$\gamma\left[\frac{\partial^2\phi_z}{\partial x^2}+\frac{\partial^2\phi_z}{\partial y^2}\right]+\kappa\left[\frac{\partial u_y}{\partial x}-\frac{\partial u_x}{\partial y}\right]-2\kappa\phi_z=\rho j\frac{\partial^2\phi_z}{\partial t^2}\,. \tag{2.31}$$

2.4 Compatibility Conditions and Restrictions on Micropolar Elastic Moduli

Compatibility equations are used to assure compatibility among displacements and microrotations within specific micropolar elastic solutions. Following the prescription of the six quantities, u_k and ϕ_k , the microstrain field is uniquely determined from equation (2.10) by substitution. Nonetheless, since the system is overdetermined, specifications of ϵ_{kl} are not sufficient to determine displacement and microrotation uniquely. To assure maintenance of single values and continuity within the displacement and microrotation fields, constraints must be applied to ϵ_{kl} and $\phi_{k,l}$. These constraints, known as the compatibility conditions, are given by

$$\epsilon_{ik,r}-\epsilon_{rk,i}+e_{ikm}\phi_{m,r}-e_{rkm}\phi_{m,i}=0 \tag{2.32}$$

and

$$\phi_{i,mn}=\phi_{i,nm}\,. \tag{2.33}$$

For rectangular coordinates under two-dimensional plane-strain conditions, equations (2.32) and (2.33) may be expanded into three equations, as follows:

$$\frac{\partial\epsilon_{xx}}{\partial y}-\frac{\partial\epsilon_{yx}}{\partial x}+\frac{\partial\phi_z}{\partial x}=0\,, \tag{2.34}$$

$$\frac{\partial \epsilon_{xy}}{\partial y} - \frac{\partial \epsilon_{yy}}{\partial x} + \frac{\partial \phi_z}{\partial y} = 0 \ , \tag{2.35}$$

and

$$\frac{\partial^2 \phi_z}{\partial x \partial y} = \frac{\partial^2 \phi_z}{\partial y \partial x} \ . \tag{2.36}$$

Additional compatibility equations may be obtained for plane-strain problems by the examination of equations (2.23) and (2.24). The differentiation of equation (2.23) with respect to y and the differentiation of equation (2.24) with respect to x yields

$$\frac{\partial m_{xz}}{\partial y} = \frac{\partial m_{yz}}{\partial x} \ . \tag{2.37}$$

The stability of the material requires that stored elastic energy be nonnegative. This condition has important implications with regard to stability problems, wave propagations, and the uniqueness of solutions. Thus, it is necessary and sufficient that the material moduli satisfy the following restrictions:

$$\begin{aligned} &0 \leq 3\lambda + 2\mu + \kappa \ , \quad 0 \leq 2\mu + \kappa \ , \quad 0 \leq \kappa \ , \\ &0 \leq 3\alpha + \beta + \gamma \ , \quad -\gamma \leq \beta \leq \gamma \ , \quad 0 \leq \gamma \ . \end{aligned} \tag{2.38}$$

Among the restriction in equation (2.38), Eringen [3] presented an incorrect inequality

$$0 \leq \mu \ , \tag{2.39}$$

which was subsequently corrected in 1968 [4]. Cowin [87] corrected the thermodynamic restrictions for Eringen's incorrect inequality, equation (2.39), and stated that the modulus μ differed from the classical Lamé shear modulus. If the classical Lamé

shear modulus is denoted by G, then the use of the symbol μ [3] can be denoted as follows:

$$G = \mu + \frac{1}{2}\kappa \ . \tag{2.40}$$

The thermodynamic restrictions require that

$$G \geq 0 \ , \tag{2.41}$$

or $2\mu + \kappa \geq 0$, which is included in equation (2.38).

It is convenient to define additional quantities for the micropolar moduli as follows:

$$\begin{aligned} E &= \frac{(2\mu+\kappa)(3\lambda+2\mu+\kappa)}{2\lambda+2\mu+\kappa} \ , \quad \nu = \frac{\lambda}{2\lambda+2\mu+\kappa} \ , \\ b^2 &= \frac{\gamma}{2(2\mu+\kappa)} \ , \quad c^2 = \frac{\gamma(\mu+\kappa)}{\kappa(2\mu+\kappa)} \ , \end{aligned} \tag{2.42}$$

where E is Young's modulus, ν is Poisson's ratio, and b and c, the material properties associated with the scale of the microstructure, are characteristic lengths [4]. If the ratio of the smallest dimension of a body to these characteristic lengths is large, then in accordance with micropolar elasticity theory, the effect of couple stresses is negligible. However, when high strain gradients exist, and when the body dimensions approach the characteristics lengths, the micropolar effects may be of appreciable magnitude. For the sake of convenience in numerical experimentation, the coupling factor N is defined as follows [87]:

$$N = \sqrt{\frac{\kappa}{2(\mu+\kappa)}} \qquad \left[\text{or } N = \frac{b}{c}\right] \ , \tag{2.43}$$

and $0 \leq N \leq 1$. When $N = 0$, the classical case is recovered, and when $N = 1$, the result is the same as that for indeterminate couple stress theory [5].

Since the incorrect inequality equation (2.39) was used, rather than the inequality equation given in equation (2.38), Han et al. [28] used an unnecessarily limited range, $0 \leq N \leq 1/\sqrt{2}$, as the coupling factor.

3. FINITE ELEMENT ANALYSIS

The essential feature of the finite element method is the ability to represent a given structure at interest by a number of elements, such that each element covers a relatively small piece of the structure. A single type of element has been developed for this study; that is, the two-dimensional, eight-node isoparametric quadrilateral element. For dynamic, plane-strain micropolar elasticity analysis, the dynamic finite element method, which accounts for both inertia and a time integration effects, is formulated upon the basis of virtual work principles.

3.1 Virtual Work Principle for Micropolar Elasticity

In this section, a principle of virtual work for micropolar elastic materials is developed for application to the finite element method. First, the body at issue is subjected to the virtual displacement δu_k and virtual microrotation $\delta\phi_k$, respectively, the virtual increments of the diplacement u_k and the microrotation ϕ_k. It is assumed that the quantities δu_k, $\delta\phi_k$ are infinitesimal and arbitrary, are continuous functions, and are compatible with the geometric boundary conditions. Multiplying equation (2.1) by δu_k and equation (2.2) by $\delta\phi_k$, adding the products of the multiplication, and then integrating over the volume gives

$$\begin{aligned}\int\int\int_V (\rho\ddot{u}_k\delta u_k + \rho j\ddot{\phi}_k\delta\phi_k)\,dV \\ - \int\int\int_V (t_{lk,l}\delta u_k + m_{lk,l}\delta\phi_k + e_{kmn}t_{mn}\delta\phi_k)\,dV = 0\ .\end{aligned} \tag{3.1}$$

Once again, note that the body force and body couple were ignored. Applying the Green-Gauss divergence theorem to the first two terms in the second integral of equation (3.1) results in

$$\int\int\int_V t_{lk,l}\delta u_k \, dV = \int\int_A P_k \delta u_k \, dA - \int\int\int_V t_{lk}\delta u_{k,l} \, dV \tag{3.2}$$

and

$$\int\int\int_V m_{lk,l}\delta\phi_k \, dV = \int\int_A M_k \delta\phi_k - \int\int\int_V m_{lk}\delta\phi_{k,l} \, dV \, , \tag{3.3}$$

where the applied surface force P_k and surface couple M_k are defined as

$$P_k = t_{lk} n_l \tag{3.4}$$

and

$$M_k = m_{lk} n_l \, . \tag{3.5}$$

Then, substituting equations (3.2) and (3.3) into equation (3.1), and recalling equation (2.10),

$$\begin{aligned} \int\int\int_V \left[\rho\ddot{u}_k \delta u_k + \rho j\ddot{\phi}_k \delta\phi_k\right] dV + \int\int\int_V \left[t_{lk}\delta\epsilon_{lk} + m_{lk}\delta\phi_{k,l}\right] dV \\ = \int\int_A \left[P_k \delta u_k + M_k \delta\phi_k\right] dA \, . \end{aligned} \tag{3.6}$$

In the absence of couple stresses and microinertia density, equation (3.6) constitutes the principle of virtual work for classical dynamic elasticity.

If equation (3.6) is specialized for the case of plane-strain $(\epsilon_z = \phi_x = \phi_z = 0)$, then

$$\int\int\int_V \left[\rho\ddot{u}_x \delta u_x + \rho\ddot{u}_y \delta u_y + \rho j\ddot{\phi}_z \delta\phi_z\right] dV$$
$$+ \int\int\int_V \left[t_{xx}\delta\epsilon_{xx} + t_{yy}\delta\epsilon_{yy} + t_{xy}\delta\epsilon_{xy} + t_{yx}\delta\epsilon_{yx} \right.$$
$$\left. + m_{xz}\frac{\partial\phi_z}{\partial x} + m_{yz}\frac{\partial\phi_z}{\partial y} \right] dV \qquad (3.7)$$
$$= \int_A \int \left[P_x \delta u_x + P_y \delta u_y + M_z \delta\phi_z\right] dA \ ,$$

in which u_x and u_y are displacements in the x and y directions, and ϕ_z is microrotation perpendicular to the x—y plane.

3.2 Finite Element Formulation

For dynamic, plane-strain micropolar elasticity analysis, an eight-node isoparametric, quadrilateral element is developed, with three degrees of freedom at each node, as shown in Figure 3.1. This element is similar to those used for classical theory, with the exception that there is an additional rotational degree of freedom ϕ_z (i.e., microrotation) at each node. A set of functions is chosen to define the state of displacement within each element with respect to nodal displacement and rotation. Thus,

$$\{u\} = [N]\{q\} \ , \qquad (3.8)$$

where $[N]$ is a set of interpolation functions, called the shape functions, $\{u\}$ is the displacement vector, and $\{q\}$ is the vector for nodal displacement and rotation of the element. The isoparametric family consists of a group of elements in which the same shape functions are used to define both the geometric and displacement fields. Similar to the classical case, the natural coordinates ξ and η, in the range $+1$ to

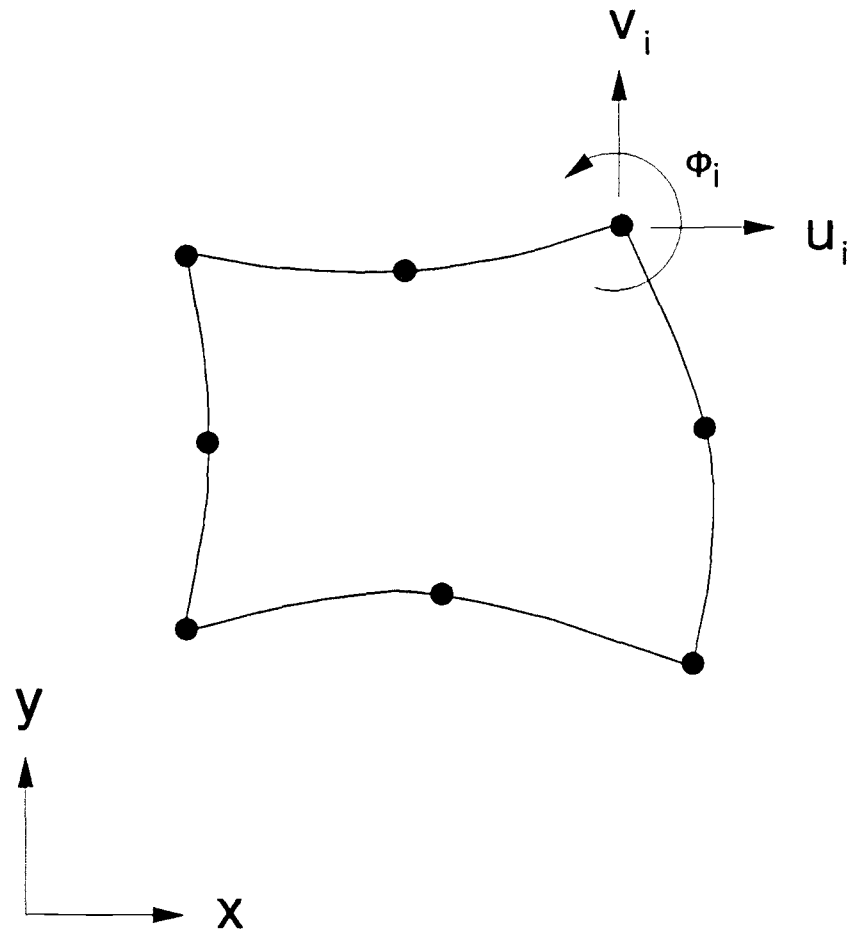

Figure 3.1 Two-dimensional eight-node isoparametric quadrilaterial element.

-1, are introduced. The x and y coordinates, which define the location of any point within the element, may be written as

$$x(\xi,\eta) = \sum_{i=1}^{8} N_i(\xi,\eta)x_i \ ,$$
$$y(\xi,\eta) = \sum_{i=1}^{8} N_i(\xi,\eta)y_i \ , \tag{3.9}$$

where x_i and y_i represent the various nodal coordinates, and the two-dimensional quadratic shape functions, $N_i(\xi,\eta)$, are defined as:

$$\begin{aligned}
N_1(\xi,\eta) &= -\frac{1}{4}(1-\xi)(1-\eta)(1+\xi+\eta) \\
N_2(\xi,\eta) &= \frac{1}{2}(1-\xi^2)(1-\eta) \\
N_3(\xi,\eta) &= \frac{1}{4}(1+\xi)(1-\eta)(\xi-\eta-1) \\
N_4(\xi,\eta) &= \frac{1}{2}(1+\xi)(1-\eta^2) \\
N_5(\xi,\eta) &= \frac{1}{4}(1+\xi)(1+\eta)(\xi+\eta-1) \\
N_6(\xi,\eta) &= \frac{1}{2}(1-\xi^2)(1+\eta) \\
N_7(\xi,\eta) &= \frac{1}{4}(1-\xi)(1+\eta)(-\xi+\eta-1) \\
N_8(\xi,\eta) &= \frac{1}{2}(1-\xi)(1-\eta^2) \ .
\end{aligned} \tag{3.10}$$

Similar functions are introduced to represent the displacements $u_x(\xi,\eta)$ and $u_y(\xi,\eta)$, and the microrotation $\phi_z(\xi,\eta)$ within the element as

$$
\begin{aligned}
u_x(\xi,\eta) &= \sum_{i=1}^{8} N_i(\xi,\eta)(u_x)_i \ , \\
u_y(\xi,\eta) &= \sum_{i=1}^{8} N_i(\xi,\eta)(u_y)_i \ , \\
\phi_z(\xi,\eta) &= \sum_{i=1}^{8} N_i(\xi,\eta)(\phi_z)_i \ ,
\end{aligned}
\tag{3.11}
$$

where $(u_x)_i$ and $(u_y)_i$ are the nodal displacements, and $(\phi_z)_i$ is the nodal microrotation at node i. These relations can be expressed in matrix form as

$$
\{u\} = \sum_{i=1}^{8} [N]_i \{q\}_i \ , \tag{3.12}
$$

where

$$
[N]_i = \begin{bmatrix} N_i(\xi,\eta) & 0 & 0 \\ 0 & N_i(\xi,\eta) & 0 \\ 0 & 0 & N_i(\xi,\eta) \end{bmatrix} \tag{3.13}
$$

and

$$
\{q\}_i = \begin{Bmatrix} (u_x)_i \\ (u_y)_i \\ (\phi_z)_i \end{Bmatrix} \ . \tag{3.14}
$$

The basic equations for micropolar theory are then rewritten for the case of plane-strain in matrix form. Thus, the kinematic equations (2.16)—(2.19) and (2.25)—(2.26) become

$$\{\epsilon\} = \begin{Bmatrix} \epsilon_{xx} \\ \epsilon_{yy} \\ \epsilon_{xy} \\ \epsilon_{yx} \\ \phi_{z,x} \\ \phi_{z,y} \end{Bmatrix} = \begin{Bmatrix} \dfrac{\partial u_x}{\partial x} \\ \dfrac{\partial u_y}{\partial y} \\ \dfrac{\partial u_y}{\partial x} - \phi_z \\ \dfrac{\partial u_x}{\partial z} + \phi_z \\ \dfrac{\partial \phi_z}{\partial x} \\ \dfrac{\partial \phi_z}{\partial y} \end{Bmatrix} . \tag{3.15}$$

The constitutive equations (2.12)—(2.15) and (2.23)—(2.24) are then written as

$$\{\sigma\} = \begin{Bmatrix} t_{xx} \\ t_{yy} \\ t_{xy} \\ t_{yx} \\ m_{xz} \\ m_{yz} \end{Bmatrix} = [\boldsymbol{D}]\{\epsilon\} , \tag{3.16}$$

where $[\boldsymbol{D}]$ is the matrix of micropolar elastic constants given by

$$[D] = \begin{bmatrix} \lambda+2\mu+\kappa & \lambda & 0 & 0 & 0 & 0 \\ \lambda & \lambda+2\mu+\kappa & 0 & 0 & 0 & 0 \\ 0 & 0 & \mu+\kappa & \mu & 0 & 0 \\ 0 & 0 & \mu & \mu+\kappa & 0 & 0 \\ 0 & 0 & 0 & 0 & \gamma & 0 \\ 0 & 0 & 0 & 0 & 0 & \gamma \end{bmatrix} . \tag{3.17}$$

The virtual work expression for plane-strain, equation (3.7), may then be written in matrix form:

$$\int\int\int_V \{\delta u\}^T [\rho] \{\ddot{u}\} dV + \int\int\int_V \{\delta \epsilon\}^T \{\sigma\} dV = \int\int_A \{\delta u\}^T \{F\} dA , \tag{3.18}$$

where

$$\{u\} = \begin{Bmatrix} u_x \\ u_y \\ \phi_z \end{Bmatrix} , \tag{3.19}$$

$$[\rho] = \begin{bmatrix} \rho & 0 & 0 \\ 0 & \rho & 0 \\ 0 & 0 & \rho j \end{bmatrix} , \tag{3.20}$$

and

$$\{F\} = \begin{Bmatrix} P_x \\ P_y \\ M_z \end{Bmatrix} . \tag{3.21}$$

Thus, equation (3.18) is similar in form to the virtual work principle adopted for use in classical theory.

To obtain strains from the nodal displacements, equation (3.12) is substituted into equation (3.15), resulting in

$$\{\epsilon\} = \sum_{i=1}^{8} [B]_i \{q\}_i , \tag{3.22}$$

where

$$[B]_i = \begin{bmatrix} \frac{\partial N_i}{\partial x} & 0 & 0 \\ 0 & \frac{\partial N_i}{\partial y} & 0 \\ 0 & \frac{\partial N_i}{\partial x} & -N_i \\ \frac{\partial N_i}{\partial y} & 0 & -N_i \\ 0 & 0 & \frac{\partial N_i}{\partial x} \\ 0 & 0 & \frac{\partial N_i}{\partial y} \end{bmatrix} . \tag{3.23}$$

Just as for the case of classical elasticity, N_i are expressed in terms of ξ and η rather than x and y. This requires the introduction of the Jacobian matrix $J(\xi,\eta)$ as:

$$[J] = \begin{bmatrix} \frac{\partial x}{\partial \xi} & \frac{\partial y}{\partial \xi} \\ \frac{\partial x}{\partial \eta} & \frac{\partial y}{\partial \eta} \end{bmatrix} = \sum_{i=1}^{8} \begin{bmatrix} \frac{\partial N_i}{\partial \xi} x_i & \frac{\partial N_i}{\partial \xi} y_i \\ \frac{\partial N_i}{\partial \eta} x_i & \frac{\partial N_i}{\partial \eta} y_i \end{bmatrix} . \tag{3.24}$$

The inverse of the Jacobian matrix can be readily obtained by application of a standard matrix inversion technique:

$$[J]^{-1} = \begin{bmatrix} \frac{\partial \xi}{\partial x} & \frac{\partial \eta}{\partial x} \\ \frac{\partial \xi}{\partial y} & \frac{\partial \eta}{\partial y} \end{bmatrix} = \frac{1}{\det J} \begin{bmatrix} \frac{\partial y}{\partial \eta} & -\frac{\partial y}{\partial \xi} \\ -\frac{\partial x}{\partial \eta} & \frac{\partial x}{\partial \xi} \end{bmatrix} . \tag{3.25}$$

The chain rule of differentiation is then used to calculate the derivatives of $N_i(\xi,\eta)$,

$$\begin{aligned} \frac{\partial N_i}{\partial x} &= \frac{\partial N_i}{\partial \xi}\frac{\partial \xi}{\partial x} + \frac{\partial N_i}{\partial \eta}\frac{\partial \eta}{\partial x} \\ \frac{\partial N_i}{\partial y} &= \frac{\partial N_i}{\partial \xi}\frac{\partial \xi}{\partial y} + \frac{\partial N_i}{\partial \eta}\frac{\partial \eta}{\partial y} \end{aligned} . \tag{3.26}$$

Substituting equations (3.12), (3.16), and (3.22) into equation (3.18) results in the familiar form of the finite element equation

$$[M]\{\ddot{q}\} + [K]\{q\} = \{F_e\} , \tag{3.27}$$

where $[M]$ is the mass matrix, $[K]$ is the stiffness matrix, and $\{F_e\}$ are applied nodal forces or couples

$$[M] = \int\int\int_V [N]^T [\rho][N]\, dV , \tag{3.28}$$

$$[K] = \int \int_V \int [B]^T [D][B]\, dV \ , \tag{3.29}$$

and

$$\{F_e\} = \int_A \int [N]^T \{F\}\, dA \ . \tag{3.30}$$

and the integration equations (3.28)—(3.29) are carried out in natural coordinates, using nine-point Gauss quadrature (Appendix A). It follows that equation (3.27) is the system of second-order differential equations governing the linear dynamic response of a system of finite elements.

3.3 Solution Procedure

For equation (3.27), which is called the semidiscrete equation of motion, there are a number of implicit and explicit time-integration techniques available for solution. Explicit methods are most efficient when a lumped (i.e., a diagonal) mass matrix is used, but these methods are only conditionally stable and often require very small time-steps. A number of implicit methods are unconditionally stable, but at the same time may require more computational effort per time-step than explicit methods. With respect to each other, each method has its strengths and weaknesses. Therefore, selection of a method should be based upon the physical problem to be solved, the degree of accuracy required, and the stability criterion. For this investigation, the central different method (i.e., an explicit method) and the Newmark method (i.e., an implicit method), combined with either a lumped or a consistent mass, were compared.

3.3.1 Time-Integration Methods

For wave propagation problems, in which it is known that a large number of frequencies are excited in the system, such explicit methods as the central difference method have been subjected to wide usage. The central difference method approximates velocity and acceleration by

$$\{\dot{q}\}_n = \frac{1}{2\Delta t}\left(\{q\}_{n+1} - \{q\}_{n-1}\right) \tag{3.31}$$

and

$$\{\ddot{q}\}_n = \frac{1}{\Delta t^2}\left(\{q\}_{n+1} - 2\{q\}_n + \{q\}_{n-1}\right), \tag{3.32}$$

where the subscript n denotes the n^{th} time-step. Substituting equation (3.32) into equation (3.27) results in

$$\left[\frac{M}{\Delta t^2}\right]\{q\}_{n+1} = \{F_e\}_n - [K]\{q\}_n + \left[\frac{M}{\Delta t^2}\right]\left(2\{q\}_n - \{q\}_{n-1}\right), \tag{3.33}$$

which may be solved for $\{q\}_{n+1}$. To solve equation (3.33), special starting procedures are required, that is,

$$\{q\}_{-1} = \{q\}_0 - \Delta t\{\dot{q}\}_0 + \frac{\Delta t^2}{2}\{\ddot{q}\}_0 \tag{3.34}$$

and

$$\{\ddot{q}\}_0 = [M]^{-1}\left(\{F_e\}_0 - [K]\{q\}_0\right), \tag{3.35}$$

in which $\{q\}_0$ and $\{\dot{q}\}_0$ are, respectively, initial displacements and velocities. It is noteworthy that a matrix solver for the solution of equation (3.33) is not required if there is a diagonal mass matrix. In addition, this advantage may reduce the time required to reach a solution. However, this method poses several shortcomings.

First, the method is conditionally stable, thus the time-step Δt should be smaller than the critical time-step Δt_{cr} [29],

$$\Delta t_{cr} = \frac{2}{\lambda_{\max}} , \tag{3.36}$$

where $\lambda_{\max}$ is the highest frequency of the discrete mesh. Second, this method is effective only when used with a diagonal mass matrix. Third, the method does not provide useful algorithmic damping effect properties to suppress undesired high frequency oscillations. In the current investigation for certain types of wave problems (Appendix B), it was observed that the central difference method produced results which were less accurate, when used with either lumped mass (i.e., HRZ special lumped mass) or consistent mass matrices, than the Newmark method.

The Newmark method is based upon an extension of the average acceleration method (i.e., the Trapezoidal rule), which is unconditionally stable. In this method, displacement and velocity are assumed to be

$$\{q\}_{n+1} = \{q\}_n + \Delta t\{\dot{q}\}_n + \frac{\Delta t^2}{2}\left((1-2\beta)\{\ddot{q}\}_n + 2\beta\{\ddot{q}\}_{n+1}\right) \tag{3.37}$$

and

$$\{\dot{q}\}_{n+1} = \{\dot{q}\}_n + \Delta t\left((1-\gamma)\{\ddot{q}\}_n + \gamma\{\ddot{q}\}_{n+1}\right) , \tag{3.38}$$

where β and γ are parameters for the determination of the stability and accuracy characteristics of the algorithm under consideration. This method will remain unconditionally stable so long as the parameters β and γ are chosen to satisfy $\gamma \geq 0.5$ and $\beta = (\gamma+0.5)^2/4$, and these values provide characteristics of maximal high-frequency numerical dissipation [45]. If $\gamma = 0.5$ and $\beta = 0.25$, then the algorithm is in correspondence to the average acceleration method originally proposed by Newmark [31]. The use of this method provides second-order accuracy and uncondi-

tional stability, but at the same time it does not reflect algorithmic damping properties for the suppression of spurious oscillations. Though wave propagation problems may include a number of frequencies, the higher modes may reflect significant errors due to spatial discretization. Therefore, unconditionally stable methods with appropriate numerical damping properties are to be preferred. By selecting $\gamma > 1/2$ to accommodate high-frequency dissipation, the order of accuracy of this method is degraded to first-order. For the current study, several values for the damping parameters have been tried and analyzed (Appendix C). From a series of numerical experiments, it was observed that the Newmark method, with the use of the parameters $\beta = 0.36$ and $\gamma = 0.7$ in conjunction with a consistent mass matrix, provided the closest agreement with the analytical solution for the problem of the diffraction of a plane wave by a cylindrical cavity [99] (Appendix C).

For the solution of displacements at the time $(n+1)\Delta t$, equation (3.27), in addition to equations (3.37) and (3.38), is rewritten as

$$[M]\{\ddot{q}\}_{n+1} + [K]\{q\}_{n+1} = \{F_e\}_{n+1} , \tag{3.39}$$

where $n+1$ denotes the $(n+1)^{\text{th}}$ time-step. Then, substituting equations (3.37) and (3.38) into equation (3.39), and rearranging,

$$\left[\frac{1}{\beta\Delta t^2}[M] + [K]\right]\{q\}_{n+1} = \{F_e\}_{n+1} + [M]\left[\frac{1}{\beta\Delta t^2}\{q\}_n + \frac{1}{\beta\Delta t}\{\dot{q}\}_n + \frac{1/2 - \beta}{\beta}\{\ddot{q}\}_n\right] . \tag{3.40}$$

Solving for $\{q\}_{n+1}$ from equation (3.40), then substituting for $\{\ddot{q}\}_{n+1}$ in equation (3.37), $\{\ddot{q}\}_{n+1}$ is obtained; similarly, $\{\dot{q}\}_{n+1}$ may be obtained from equation (3.38) with $\{\ddot{q}\}_{n+1}$. These procedures are repeated for each time-step.

For the current investigation, the Newmark method was selected and applied for reason of the simplicity of its computer implementation, as well as the unconditional stability and favorable properties of accuracy for linear systems. In the Newmark method, it is noteworthy that the explicit central difference scheme may be recovered by setting $\gamma = 1/2$ and $\beta = 0$.

3.3.2 Mass Matrices and Time-Step Estimates

For wave propagation problems, several studies have examined methods of estimating time-step size, the effect of mesh sizes, and the influence of the mass matrices in use [89-98]. However, these studies have not been in agreement on the best method of approach, and it is apparent that optimal selection tends to be problem-dependent.

A uniform grid is recommended for use in wave problems, unless spurious wave reflection occur between element interfaces which are nonexistent in the continuum [92]. However, for certain types of physical problems, such as stress concentrations around a circular hole or a crack, the use of variably sized finite elements cannot be avoided. The consequence is that sudden changes in the mesh sizes of neighboring elements can lead to severe spurious oscillations. Thus, gradually changing element sizes should be used to reduce these undesired oscillations. Spurious wave reflections are less pronounced among higher order elements (e.g., eight-node quadrilateral elements) and for consistent rather than lumped masses [7,17,18]. If the largest element size in the domain is larger than the smallest desired wave length, then the element size will act as a low pass filter which prevents the passage of the desired wave length through the larger element. Therefore, the size of the largest element must be smaller than the largest desired frequency component [89,90,98], and it is recommended that

$$H \leq 1/8\,\Omega_{small} \tag{3.41}$$

be used, where Ω_{small} is the smallest desired wave length for the slowest body wave and H is the largest element size.

In the present study, it was observed, contrary to the arguement presented by Bazant [91], that the consistent mass produced slightly better results than the lumped mass. Mullen [93] demonstrated that the lumped mass matrix introduces severe dispersion for directions which do not coincide with the mesh lines. Laturelle [97] presented a thorough discussion of this issue for problems of two-dimensional wave propagation.

Appropriate selection of the time-step size was considered in a number of the studies cited, but without determination of a singular general approach. When the unconditionally stable Newmark method for time integration is adopted, then only the Courant condition [100] need be considered:

$$\rho_c = \frac{\Delta t \cdot C_d}{h} \leq 1 \,, \tag{3.42}$$

where h is the smallest element dimension, C_d is the dilatation wave velocity, and ρ_c is the Courant number. The time-step h/C_d, called the characteristic time-step, is equal to the transit time for a wave moving at unit speed to traverse one element of size h. The range of ρ_c used for the current investigation is $0.3 \leq \rho_c \leq 0.9$. Though both Tedesco [96] and Bathe [43] provided a time-step wave propagation criterion for the eight-node quadrilateral element as

$$\Delta t = \frac{L_e}{C_d} \,, \tag{3.43}$$

where L_e is the distance between element integration points in the direction of wave propagation, with ρ_c close to 0.38 when three-point Gauss integration is used, such

larger sized time-steps as $\rho_c = 0.7 \sim 0.8$, produced better results, including fewer spurious oscillations (Appendix D). However, the use of smaller time-steps does not always contribute to more accurate results. It is possible for smaller time-steps to violate the discrete maximum principle [101], thus leading to physically unreasonable results. Moreover, smaller time-steps could reduce the desired damping algorithms, thus increasing spurious oscillations [97]. For problems of wave propagation, the use of an optimal time-step is known to yield the best results and the optimization process is dependent upon experience.

A list of programs which include the use of a consistent mass and the Newmark integration technique is provided in Appendix F.

3.4 Verification Problem

To verify that the micropolar effects were correctly modeled in the finite element program developed for the current study, the results obtained were compared to those from an independent solution method for a dynamic problem in micropolar elasticity. The problem selected is presented in Figure 3.2, showing a half-space, the surface of which is subject to a shear stress that is uniform in space and harmonic in time. This case was selected for reason of its relative simplicity and the fact that solutions for both microrotation and couple stress are developed. By applying $u_x = 0$ and $\partial/\partial y = 0$ (i.e., u_y and ϕ_z are dependent only upon the x-coordinate), the governing equations for this case may be obtained from equations (2.29)— (2.31):

$$(\mu + \kappa)\frac{\partial^2 v}{\partial x^2} - \kappa\frac{\partial \phi}{\partial x} = \rho\frac{\partial^2 v}{\partial t^2} \tag{3.44}$$

and

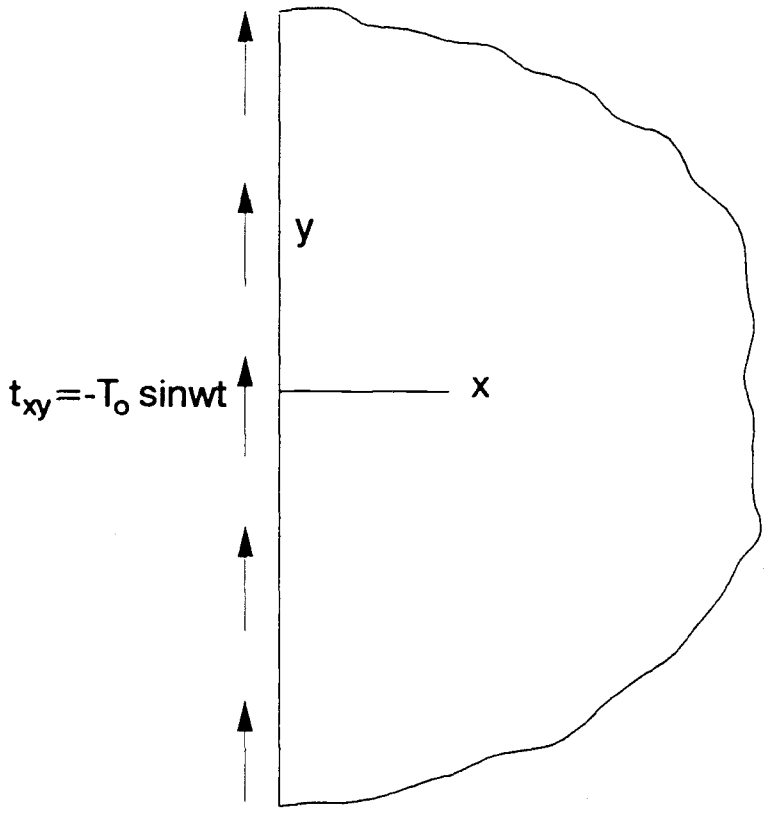

Figure 3.2 Shear loading of a micropolar half-space.

$$\gamma \frac{\partial^2 \phi}{\partial x^2} + \kappa \frac{\partial v}{\partial x} - 2\kappa\phi = \rho j \frac{\partial^2 \phi}{\partial t^2} , \tag{3.45}$$

where v denotes u_y and ϕ denotes ϕ_z. The boundary and initial conditions are

$$t_{xy} = (\mu+\kappa) \frac{\partial v}{\partial x} - \kappa\phi = -T_0 \sin wt , \qquad \text{at } x=0 \tag{3.46}$$

and

$$m_{xz} = \gamma \frac{\partial \phi}{\partial x} = 0 , \qquad \text{at } x=0 \tag{3.47}$$

$$v = \frac{\partial v}{\partial t} = \phi = \frac{\partial \phi}{\partial t} = 0 . \qquad \text{for } t=0 \tag{3.48}$$

Nowacki [23] provided a steady-state solution for this problem (Appendix E). However, an analytical solution for the transient case has not been developed and, due to the complexity of the solution required, the generation of an analytical solution would not appear to be an easy process. To generate a transient solution for the current study, a numerical approach independent of the finite-element analysis was developed. Using the second-order central difference method in both space and time, equations (3.44) and (3.45) may be readily written in the difference form:

$$(\mu+\kappa) \frac{\left(v_{i+1}^n - 2v_i^n + v_{i-1}^n\right)}{\Delta x^2} - \kappa \frac{\left(\phi_{i+1}^n - \phi_{i-1}^n\right)}{2\Delta x} = \rho \frac{\left(v_i^{n+1} - 2v_i^n + v_i^{n-1}\right)}{\Delta t^2} \tag{3.49}$$

and

$$\gamma \frac{\left(\phi_{i+1}^{n} - 2\phi_{i}^{n} + \phi_{i-1}^{n}\right)}{\Delta x^2} + \kappa \frac{\left(v_{i+1}^{n} - v_{i-1}^{n}\right)}{2\Delta x} - 2\kappa\phi_{i}^{n} = \rho j \frac{\left(\phi_{i}^{n+1} - 2\phi_{i}^{n} + \phi_{i}^{n-1}\right)}{\Delta t^2} , \tag{3.50}$$

where index i refers to space discretization in the x-direction and n refers to discretization in the time domain. Equations (3.46)—(3.48) may then be expressed as

$$(\mu+\kappa) \frac{\left(v_{i}^{n} - v_{-1}^{n}\right)}{2\Delta x} - \kappa\phi_{0}^{n} = -T_o \sin wt_n , \tag{3.51}$$

$$\gamma \frac{\left(\phi_{1}^{n} - \phi_{-1}^{n}\right)}{2\Delta x} = 0 , \tag{3.52}$$

$$v_{i}^{0} = \phi_{i}^{0} = 0 , \tag{3.53}$$

$$\frac{\left(v_{i}^{1} - v_{i}^{-1}\right)}{2\Delta t} = 0 , \tag{3.54}$$

and

$$\frac{\left(\phi_{i}^{1} - \phi_{i}^{-1}\right)}{2\Delta t} = 0 , \tag{3.55}$$

where subscript "0" refers to $x = 0$, and superscript "0" refers to the initial time-step. These equations were thus solved and their long-time solution was found to be in agreement with the steady-state solution presented by Nowacki [23]. Using dimensions of sufficient length in the x-direction, the steady-state response was

obtained at $x = 0$ (i.e., at the surface) following approximately 2,900 time-steps at $\Delta t = 0.5$ μsec. Due to the physical properties of the micropolar continuum, a considerable length of time was required to reach steady-state.

From Nakamura et al. [14] and Gauthier [102], the following values were used: $\lambda = 14.29$ MPa; $\mu = 6.9$ MPa; $\kappa = 6.9$ MPa; $\gamma = 1.71$ N; $\rho = 2192$ Kg/m^3; $j = 1.935 \times 10^{-7}$ m^2; $\nu = 0.29$; $b = 2.032 \times 10^{-4}$ m; and $N = 0.5$; in addition, $\Delta x = 6.35 \times 10^{-5}$ m; $T_0 = 4.45$ N; and $w = 5 \times 10^5$ sec^{-1} were used for the finite difference calculations. The finite difference program is listed in Appendix G.

As indicated in Figures 3.3 and 3.4, the displacement and microrotation values obtained from use of the finite difference method were in good agreement with the steady-state analytical solution (Appendix E). It should be noted that in comparison to the finite difference solution, the displacement v from the analytical solution shifted vertically by 9.13×10^{-8} meter. This discrepancy existed since the steady-state harmonic solution presented by Nowacki [23] was based upon the assumption that v was a harmonic function; for the solution proposed in this investigation, v was expressed only in terms of derivatives and thus the constant term in v could not be obtained.

A two-dimensional finite element mesh for the problem given in Figure 3.5, with the boundaries of the mesh sufficiently far from the point of origin (i.e., point A, Fig. 3.5) that wave effects from the boundaries were not a factor during the time period of interest, was also constructed. For the finite element calculations, 300 elements and 981 nodes were used, with an element size of 1.27×10^{-4} m for the uniform mesh. The two phase velocities for the coupled transverse shear wave were, respectively, 64.57 and 83.59 m/sec. Again, to satisfy the Courant condition, it should be reiterated that the time-step Δt was chosen to adequately represent the

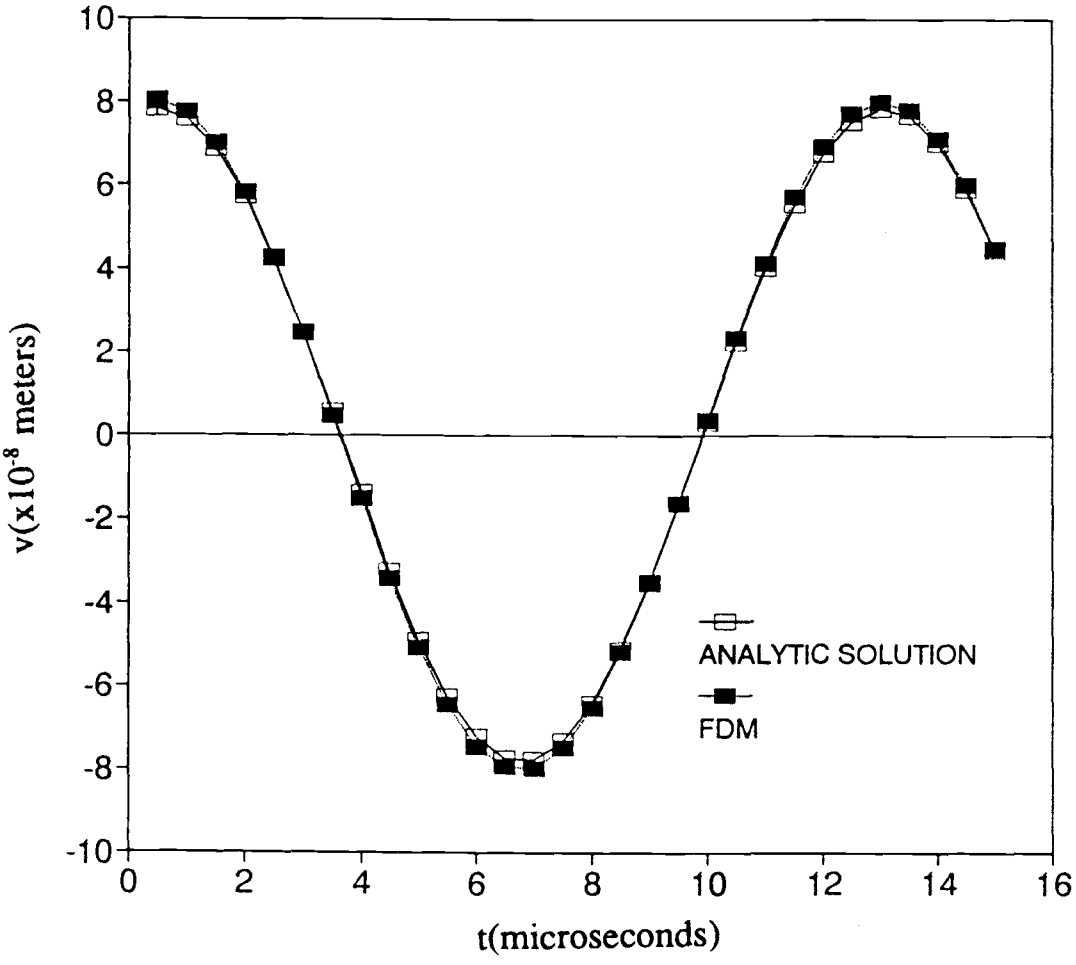

Figure 3.3 Surface displacement versus time for a micropolar half-space (steady-state solution).

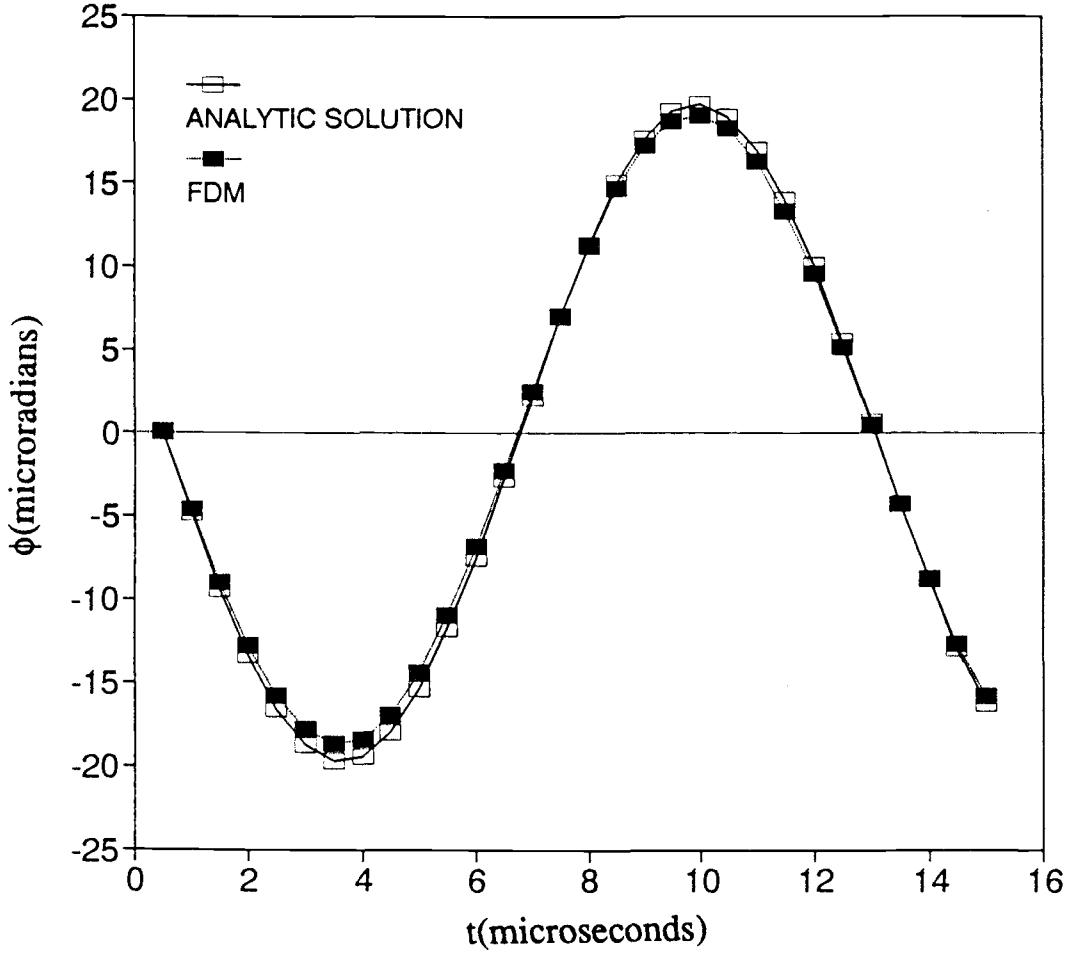

Figure 3.4 Surface microrotation versus time for a micropolar half-space (steady-state solution).

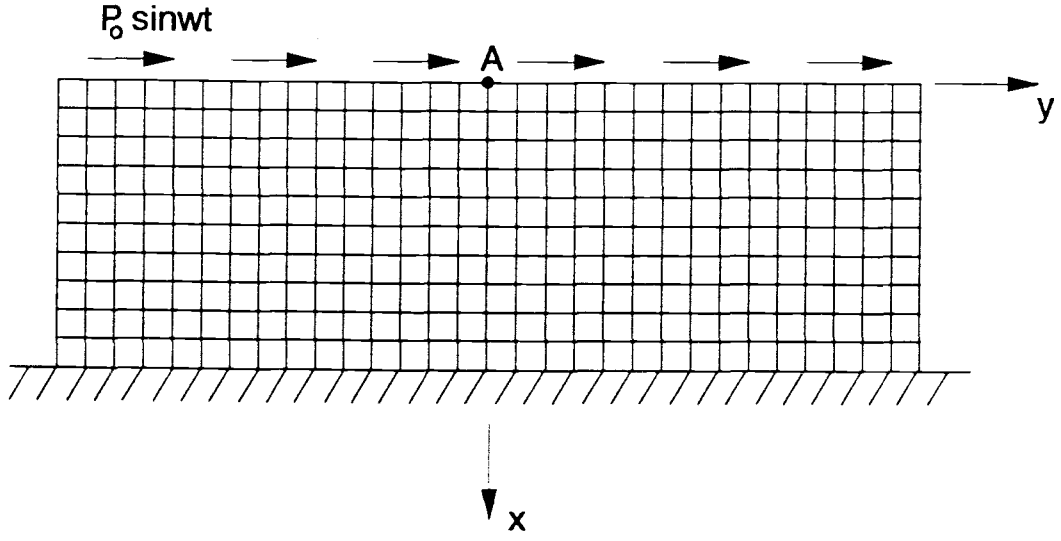

Figure 3.5 Finite element mesh for a micropolar half-space.

input frequency (i.e., more than 20 points per cycle) and to travel approximately $\frac{1}{3}\ell$ (where ℓ = element length) per time-step. A comparison of the transient solutions from the finite element calculations and from the finite difference calculations is given in Figures 3.6 and 3.7, indicating displacements and microrotation at the origin as functions of time. It may be seen that these two solutions are in close agreement; that is, they were within 5 percent.

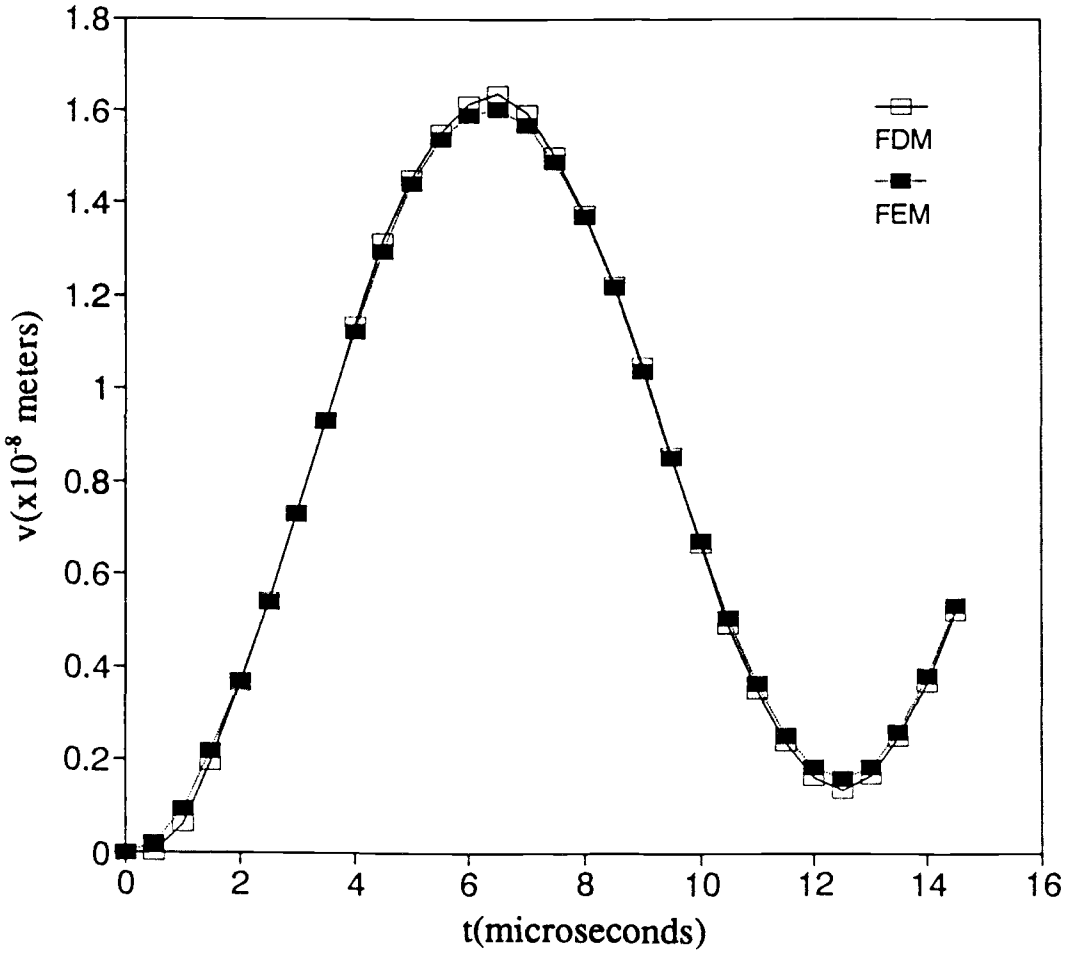

Figure 3.6 Surface displacement versus time for a micropolar half-space (transient solution).

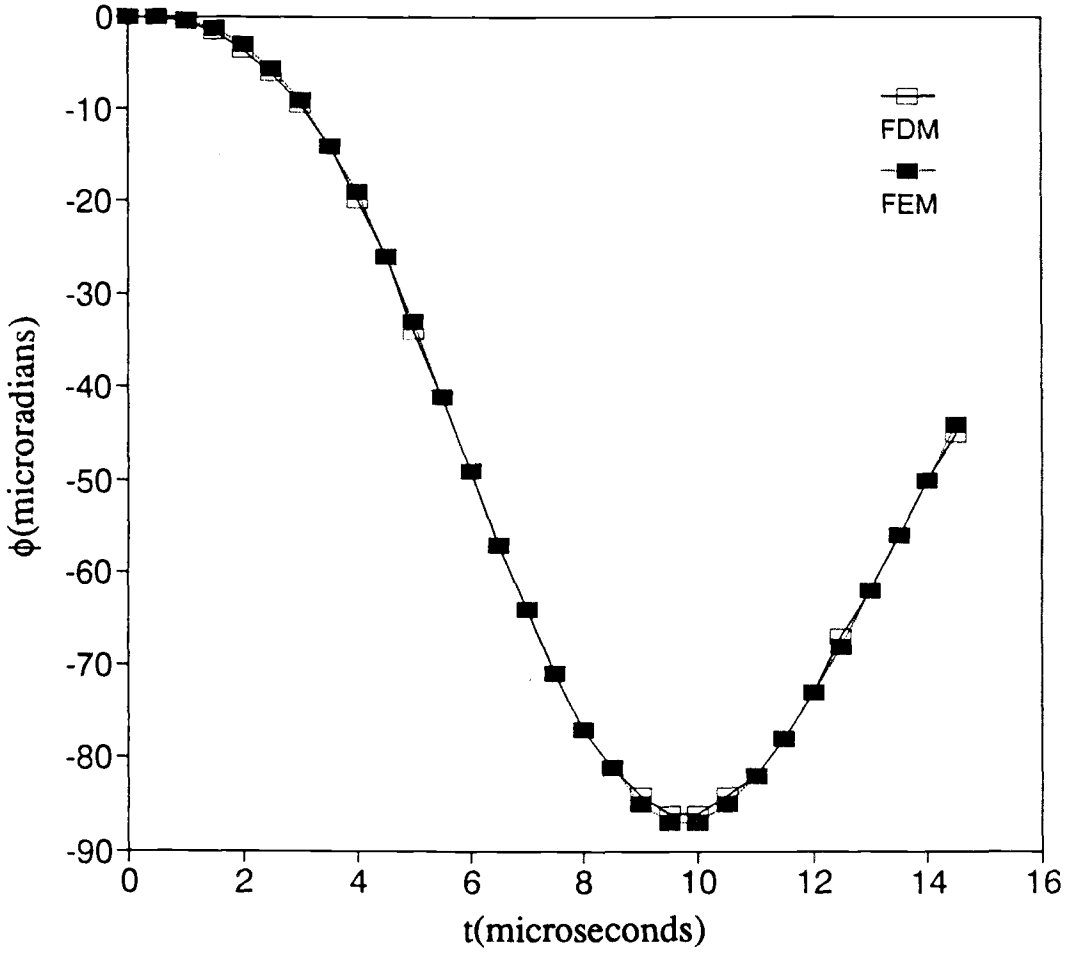

Figure 3.7 Surface microrotation versus time for a micropolar half-space (transient solution).

4. CALCULATION OF DYNAMIC ENERGY RELEASE RATE

The parameters most commonly used for the fracture analysis of brittle materials are either the energy release rate G or the stress intensity factor K. For classical elastic materials, there is a simple relationship between these two parameters. However, their relationships has not been determined for micropolar elastic materials. From the viewpoint of computation requirements, it is simpler to perform an accurate calculation of the energy-based criterion G than it is to determine the stress-based parameter K for reason of the difficulty of accurately modeling stress near the crack tip. Thus, for the current investigation, G has been calculated for crack problems.

In this chapter, two dynamic fracture problems are considered, whereas problems of stress concentration are considered in the following chapter. The first dynamic fracture problem is concerned with a stationary crack in a body subject to dynamic, mode-I loading. The second problem is concerned with a statically loaded body containing a crack that is subject to sudden propagation at a constant velocity. Techniques for the calculation of the dynamic energy release rates for these two cases are presented in the following two sections.

4.1 Dynamic Energy Release Rate for a Stationary Crack

To calculate the energy release rate for the case of a stationary crack under dynamic load, the method proposed by Jih and Sun [85] for the case of classical elasticity is extended to the case of micropolar elasticity. This approach is based upon the crack-closure integral presented by Irwin [82], which followed from the concept

that when a crack is extended by a small amount, δa , the energy released in the process is equal to the work required to close the crack to its original length. For the case of classical elasticity with mode-I loading, the energy release rate is then given as

$$G = \lim_{\delta a \to 0} \frac{1}{\delta a} \int_0^{\delta a} t_{yy}(x,0)\, u_y(x,0)\, dx \ , \qquad (4.1)$$

where the x,y-coordinate system has its origin at the crack tip prior to the virtual crack extension, $t_{yy}(x,0)$ is the normal stress just ahead of the crack tip prior to extension, and $u_y(x,0)$ is the vertical displacement just behind the crack tip following extension. For the plane-strain case of micropolar elasticity, the couple stress m_{yz}, in addition to the force stress t_{yy}, must also be taken into account; that is

$$G = \lim_{\delta a \to 0} \frac{1}{\delta a} \int_0^{\delta a} \left[t_{yy}(x,0)\, u_y(x,0) + m_{yz}(x,0)\, \phi_z(x,0) \right] dx \ . \qquad (4.2)$$

The implementation of this procedure for calculating G for a finite element analysis with eight-node quadrilateral elements employs the original concept of determining the amount of work required to close the crack by the small amount δa . Ordinarily, this would require two complete finite element analyses: one prior to virtual crack extension and one following virtual crack extension. In Figure 4.1, the region near the crack tip is illustrated, modeling only the upper part of the body due to symmetric requirements. It is convenient to maintain an identical element size along the plane of the crack. The vertical force F_y and the moment M on nodes C and D are calculated prior to the virtual crack extension (Fig. 4.1a). The vertical displacement u_y and the microrotation ϕ_z for nodes C and D are then calculated following virtual crack extension (Fig. 4.1b). With respect to finite element representation, the energy release rate can then be expressed by

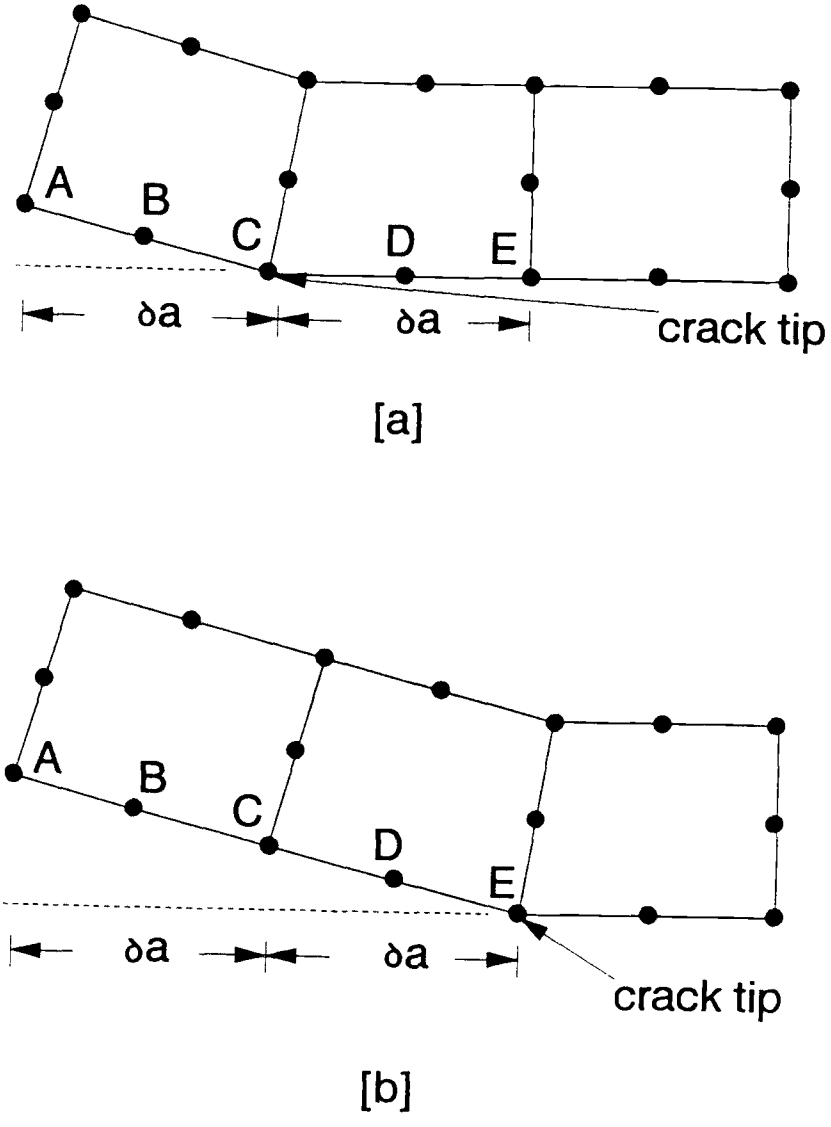

Figure 4.1 Finite element model near the crack tip: a) before virtual crack extension; b) after virtual crack extension.

$$G = \frac{F_{yC}\, u_{yC} + M_C\, \phi_{zC} + F_{yD}\, u_{yD} + M_D\, \phi_{zD}}{\delta a} \,. \tag{4.3}$$

As suggested by Jih and Sun [85], advantage may be drawn from the fact that the displacements and microtations of nodes A and B, given in Figure 4.1a, are approximately equal to the displacements and microtations of nodes C and D, given in Figure 4.1b, and can be written as

$$G = \frac{F_{yC}\, u_{yA} + M_C\, \phi_{zA} + F_{yD}\, u_{yB} + M_D\, \phi_{zB}}{\delta a} \,. \tag{4.4}$$

This formulation provides the advantage that it requires only a single finite element analysis to determine G, while at the same time providing acceptably accurate results. Moreover, this approach offers particular convenience for cases of dynamic crack propagation since the crack closure operation can be performed continuously, trailing the propagating crack tip.

4.2 Dynamic Energy Release Rate for a Propagating Crack

Modeling a propagating crack using finite elements requires the sequential release of nodes along the plane of the crack. In the first applications of the finite element method to dynamic crack propagation, conducted prior to 1978, crack tip motion was modeled by discontinuous jumps. This was accomplished by changing the location of the crack tip from one node to the next along the crack axis at time intervals Δt employed in the time integration scheme. In general, since crack propagation velocity is significantly smaller than wave velocity, the crack tip could take positions between any two successive nodal points. If the finite element mesh was not subject to change with time (i.e., a stationary mesh), then the kinematic boundary conditions in front of the crack tip would be violated, unless the tip was at one

of the nodal points. This approach induced spurious high-frequency oscillations and inaccuracies in finite element solutions.

To overcome these problems, over a period of time several attempts at the gradual release of the nodes were undertaken [75—80]. As the crack tip was moved from one node to the next, the condition of the released node was smoothly relaxed from zero displacement to the zero external nodal force normal to the crack plane over a period of time. This negative work was accomplished by diminishing the force at the released node assumed to represent the energy release mechanism of a propagating crack. This process is modeled in Figure 4.2. Again, for reasons of symmetry, only the upper portion of the body for opening mode (i.e., mode-I) fracture problems can be modeled. During the time interval in which the crack tip passed the node A location and proceeded to the node B location, the releasing force F and the releasing moment M were prescribed as the decay, respectively, from the reactions F_0 and M_0, computed at the instant prior to the release of node A, to zero at the point the crack tip reached node B.

To accomplish this procedure, several different mathematical forms have been proposed. Rydholm et al. [77] proposed the relation

$$\frac{F}{F_0} = \left[1 - \frac{b}{d} \right]^{1/2}, \tag{4.5}$$

where F is the value of the nodal force at the current time step, F_0 is the original value of the nodal force when the crack tip was at that node, b is the distance that the crack tip has propagated along the element, and d is the length of nodal distance. Malluck and King [76] used the relation

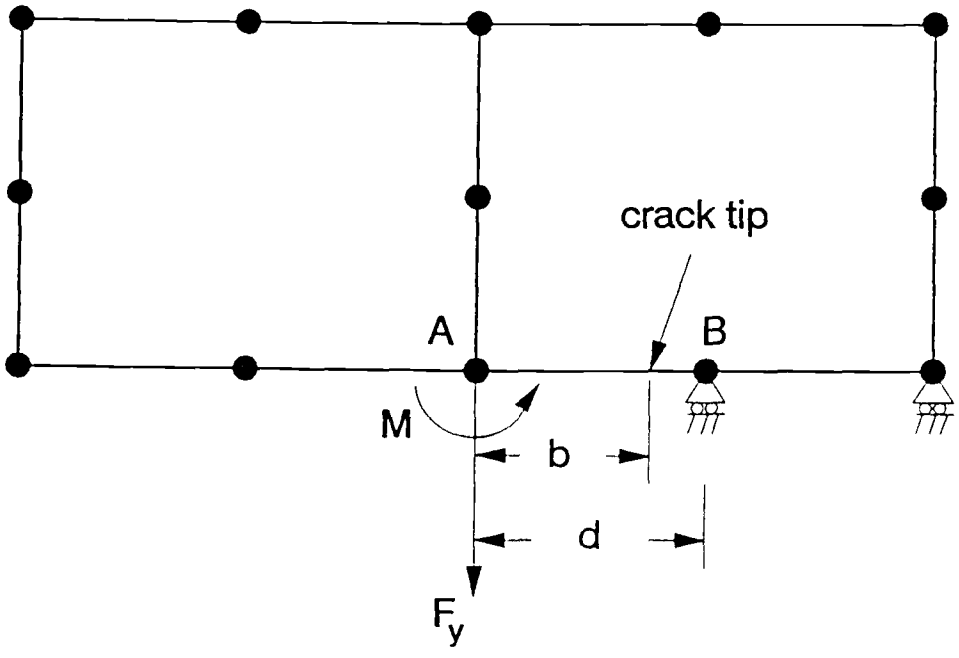

Figure 4.2 Finite element model near the tip of a propagating crack.

$$\frac{F}{F_0} = \left[1 - \frac{b}{d} \right]^{3/2} . \tag{4.6}$$

For the current study, the linear release of nodal force proposed by Kobayashi et al. [78], together with the linear release of nodal torque for the case of micropolar elasticity, is used:

$$\frac{F}{F_0} = \left[1 - \frac{b}{d} \right] \tag{4.7}$$

and

$$\frac{M}{M_0} = \left[1 - \frac{b}{d} \right] , \tag{4.8}$$

where M is the value of the nodal torque at the current time step and M_0 is the original value of the nodal torque when the crack tip was at that node. Equations (4.7) and (4.8) provide the intermediate characteristics of two nonlinear relations, equations (4.5) and (4.6). Investigation of the differences obtained from the use of the three models, equations (4.5)—(4.7), indicated only slight variations for opening mode crack propagation in linearly elastic isotropic bodies [79,80].

The values for the dynamic energy release rates for a running crack problem are calculated as prescribed in section 4.1. For finite element implementations, it may be noted that the total number of unknown variables determined changes as the crack tip is released successively. Thus, though recomputation of element stiffness and the mass matrices is unnecessary, the advantage of the equation resolution facility implied from use of the frontal technique, which is the matrix solver used for this investigation, is lost.

5. RESULTS OF THE NUMERICAL COMPUTATIONS

In this chapter, the dynamic finite element procedure developed for this investigation is applied to the following problems:

- A suddenly applied normal stress σ_0 on the surface of a plate containing a circular hole;
- A suddenly applied normal stress σ_0 on the surface of a plate containing an elliptical hole;
- A stationary crack in a body subject to dynamic mode-I loading; and
- A statically loaded body containing a crack that suddenly begins to propagate at a constant velocity.

5.1 Circular Holes

As shown in Figure 5.1, an analytical solution to the case of a dynamic stress concentration around a circular hole, with radius a, in an infinite body of classical material was presented by Baron and Matthews [99]. This solution serves as a base case for assessment of the accuracy of the finite element model developed for the current study.

The effect of a dynamic load is to generate elastic waves, which are propagated throughout the body and diffracted when passed through geometric discontinuities, such as cavities, resulting in the amplification of the dynamic signal. This wave diffraction constitutes the plane-strain problem, which requires the determination of the

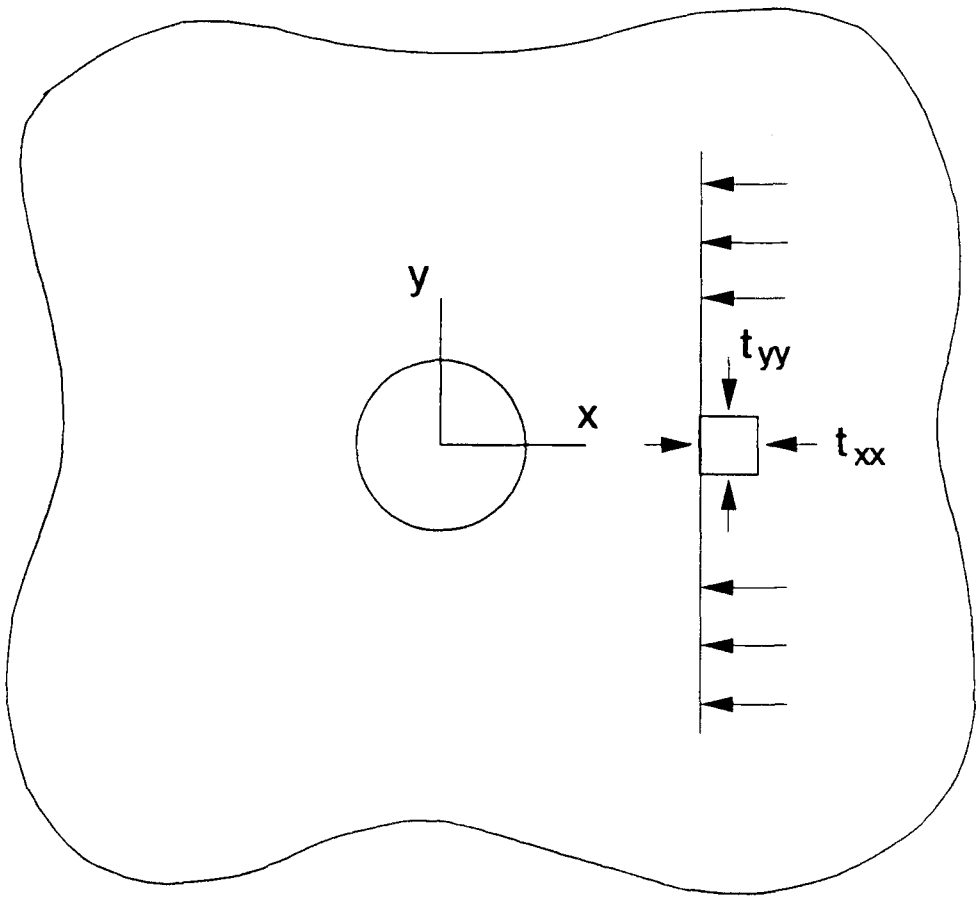

Figure 5.1 Circular hole in an infinite medium subject to suddenly applied pressure waves.

state of stress around a circular hole in a plate loaded dynamically by a wave pulse, resulting in the suddenly applied load tensor

$$t_{xx} = \sigma_0 \tag{5.1}$$

and

$$t_{yy} = \frac{\nu}{1-\nu}\sigma_0 \ , \tag{5.2}$$

where σ_0 is the applied load and ν is the Poisson's ratio. Equations (5.1) and (5.2) include the components of incoming waves with plane-wave fronts (i.e., $\epsilon_{yy} = 0$), as shown in Figure 5.1.

The finite element mesh proposed for the problem under consideration is shown in Figure 5.2, in which only one-half of the body needs to be considered due to symmetric requirements. Eight-node quadrilateral isoparametric elements, each node with three degrees of freedom (i.e., two displacements, u_x, u_y and the micro-rotation ϕ_z), were used, employing a total of 128 elements and 433 nodes. The upper half of the body was restrained against motion in the y-direction, resulting in the lateral normal stress $t_{yy} = \nu/(1-\nu)\,\sigma_0$ in the wave, where σ_0 is the applied load. The two cases considered by Baron and Mathews [99], ($t_{yy} = \sigma_0/3$ and $t_{yy} = 0$), can be duplicated by setting $\nu = 0.25$ and $\nu = 0$, respectively. The size of the body, 3.566×10^{-3} meters in width by 1.778×10^{-3} meters in length, was selected to eliminate the effects of wave reflection from the boundaries during the time period of interest. The size of the hole radius was 2.54×10^{-4} meters. The time period selected was the time required for the stress at the edge of the hole (at $x = 0$, $y = a$) to reach peak value. Thus, maximum stress concentration was not affected by the boundaries of the body, and the suddenly applied tensile loading σ_0 was 6.8966×10^3 Pa.

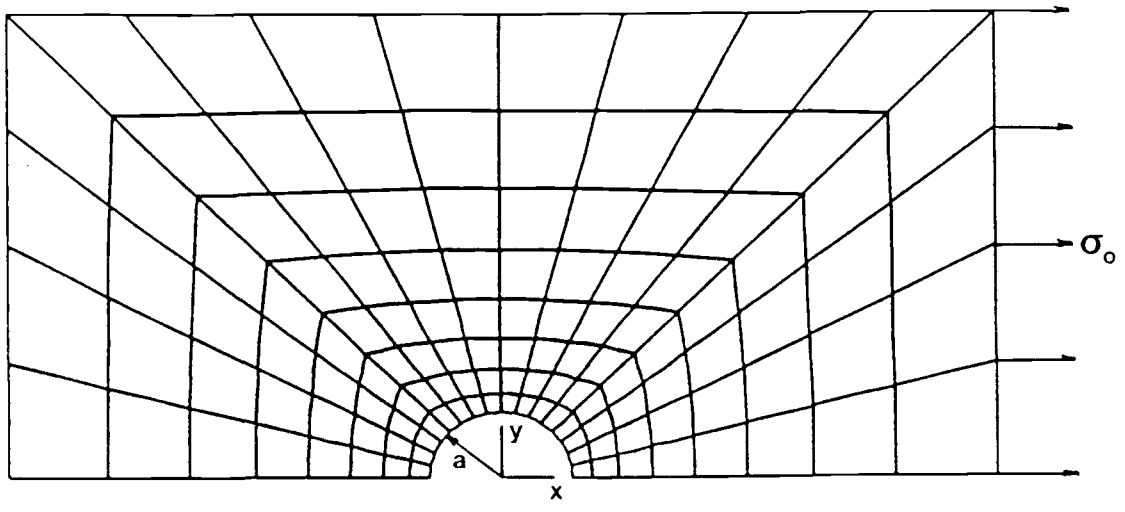

Figure 5.2 Finite element mesh for a circular hole with $a/c = 0.25$ and $\nu = 0.25$.

In Figure 5.3, the nondimensionalized normal stress t_{xx}/σ_0 at the edge of the hole (x = 0, y = a) is shown as a function of nondimensionalized time, $(C_d t)/2a$ (where C_d is the dilatational wave speed), for $a/c = 0.25$ (where c is a micropolar characteristic length, as defined in Chapter 2) and for $\nu = 0.25$. The micropolar material properties for these cases are listed in Table 5.1. The mass density (ρ) and the microinertia density (j) of the materials were, respectively, 2192 Kg/m^3 and 1.935×10^{-7} m^2, and the hole size was fixed at 2.54×10^{-4} meters. Results are given for several different coupling factor values, ranging from $N = 0$ to $N = 0.9$; that is, $N = 0.0$, 0.25, 0.5, 0.75, and 0.9. For the purpose of numerically comparing each case, the time step $\Delta t = (3.9077\,m)/C_d$ was selected, where C_d represents dilatational wave velocity. From Eringen [4], for micropolar elasticity, $C_d = \sqrt{(\lambda+2\mu+\kappa)/\rho}$. Then, substituting $\epsilon_{yy} = 0$ into equations (2.12) and (2.13),

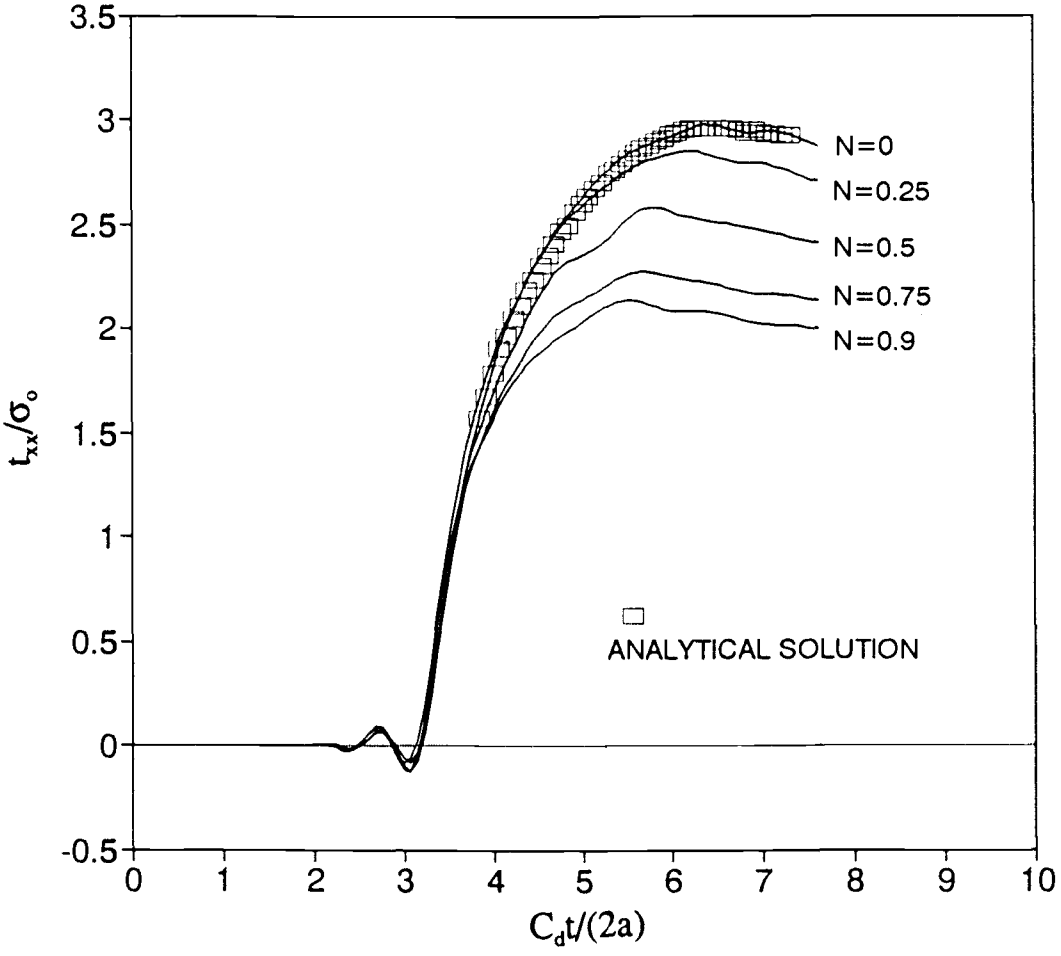

Figure 5.3 Stress versus time at the edge of a circular hole, $a/c = 0.25$ and $\nu = 0.25$.

Table 5.1 Material properties used for the analysis of a circular hole in a micropolar body ($a/c = 0.25$, $\nu = 0.25$, $a = 2.54 \times 10^{-4}$ m).

N	λ (N/m^2)	μ (N/m^2)	κ (N/m^2)	γ (N)	E (N/m^2)
0	10.345×10^6	10.345×10^6	0.0	0.0	3.231×10^7
0.25	51.725×10^6	48.276×10^6	6.897×10^6	13.350	7.225×10^7
0.5	10.345×10^6	6.897×10^6	6.897×10^6	10.680	3.231×10^7
0.75	2.682×10^6	-0.766×10^6	6.897×10^6	6.230	1.645×10^7
0.9	0.809×10^6	-2.639×10^6	6.897×10^6	2.715	0.904×10^7

$$t_{yy} = \frac{\lambda}{\lambda + 2\mu + \kappa} t_{xx} \ . \tag{5.3}$$

From equation (2.42), equation (5.3) may then be expressed as

$$t_{yy} = \frac{\nu}{1-\nu} t_{xx} \ , \tag{5.4}$$

corresponding to a wave with a plane wave front identical to that for the classical case (equation (5.2)).

For $N = 0$, behavior is identical to that for classical elastic material, and the finite element calculations are close to those for the analytical solution [99] (i.e., in Fig. 5.3, peak stresses are within one percent). As N is increased, the micropolar properties of the material become more pronounced and a significant reduction in peak stress occurs (i.e., when $N = 0.9$, peak stress is reduced by 30 percent), an apparent indication that the micropolar properties of the material assist in the alleviation of stress concentrations. For this reason, the coupling factor N is designated as a measure of the influential strength of the micropolar effects.

These finite element calculations were repeated for $a/c = 1.0$ and $a/c = 4.0$, and the results are shown in Figures 5.4 and 5.5. For both cases, the Poisson's ratio was 0.25. For $a/c = 1.0$, there was a significant reducation in stress concentration (i.e., for $N = 0.9$, an approximate 25 percent reduction), whereas for $a/c = 4.0$, the micropolar effects were slight (i.e., for $N = 0$ through $N = 0.9$, reductions were within 10 percent). This indicates that micropolar effects are important only for those holes whose size is not significantly larger than the micropolar characteristic length c, which in turn is related to the microstructural dimensions; that is, to grain or particle size. If the ratio of the smallest dimension of the body to c is large, then the effect of couple stress is in theory negligible.

The numerical results for $a/c = 0.25$, 1.0, and 4.0, when $\nu = 0.0$, are shown in Figures 5.6—5.8, respectively, and are provided only for purposes of comparison. Substituting $\nu = 0$ into equation (5.4) results in $t_{yy} = 0$, indicating that the incoming stress wave has only a component of $t_{xx} = \sigma_0$, where σ_0 is the suddenly applied tensile load. The case of $N = 0$ is then reduced to the case of classical elasticity, and the maximum stress concentration factors for the finite element calculations and the results provided by Baron and Matthews [99] are in agreement within a range of one percent, as shown in Figure 5.6. The micropolar material properties for $a/c = 0.25$, with $\nu = 0.25$ are provided in Table 5.2. The results indicated in Figure 5.6 show that as the micropolar coupling factor N increased from 0.0 to 0.9, the maximum stress concentration factor declined by 45 percent. Similarly, 38 and 10 percent reductions in the stress intensity factor are shown, respectively, in Figures 5.7 and 5.8. These trends were identical to those observed for $\nu = 0.25$.

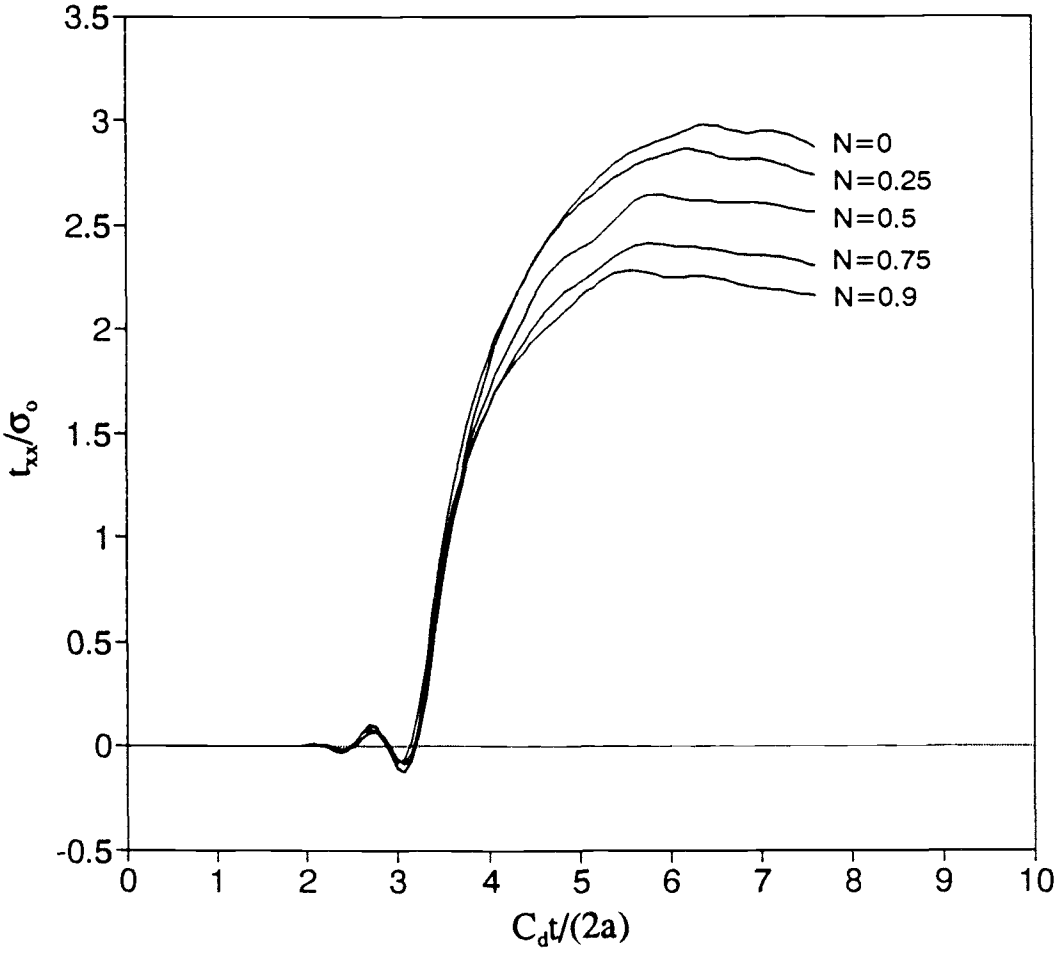

Figure 5.4 Stress versus time at the edge of a circular hole, $a/c = 1$ and $\nu = 0.25$.

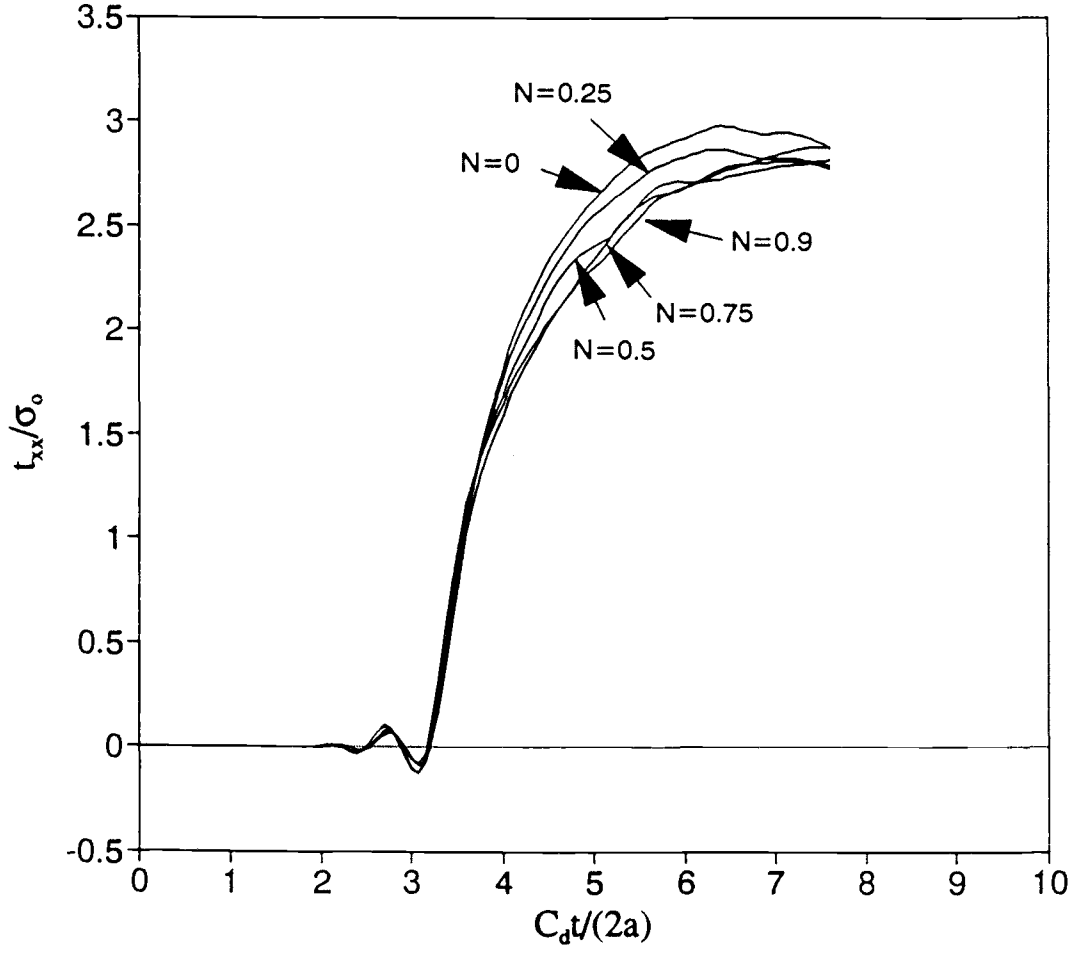

Figure 5.5 Stress versus time at the edge of a circular hole, $a/c = 4$ and $\nu = 0.25$.

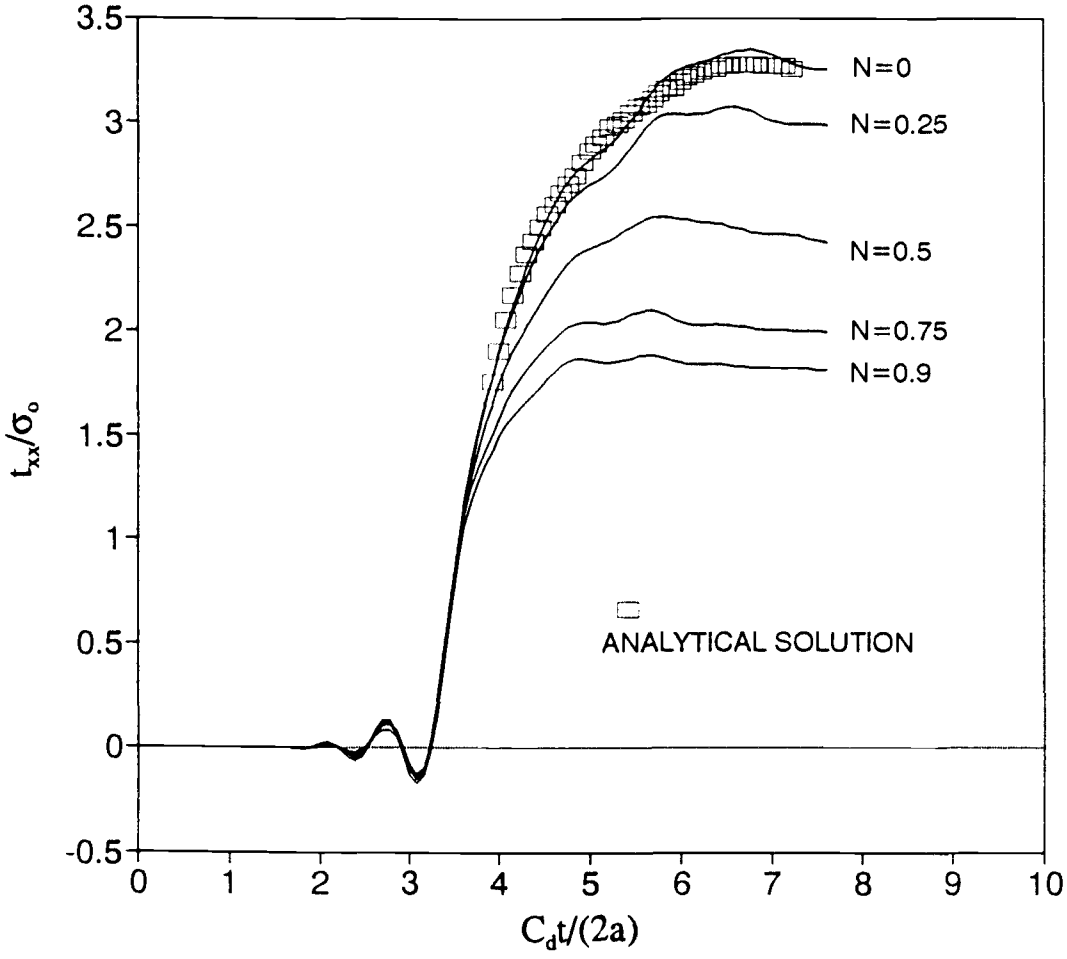

Figure 5.6 Stress versus time at the edge of a circular hole, $a/c = 0.25$ and $\nu = 0$.

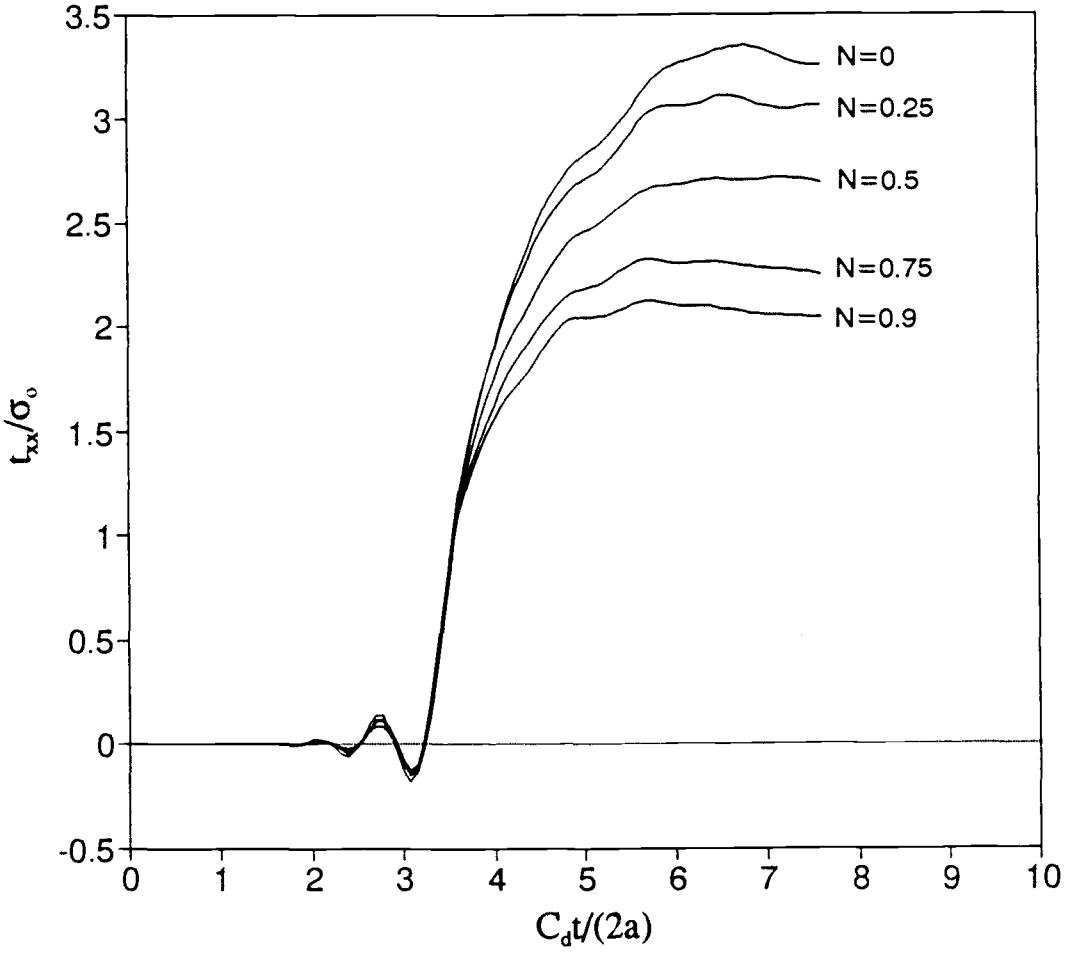

Figure 5.7 Stress versus time at the edge of a circular hole, $a/c = 1$ and $\nu = 0$.

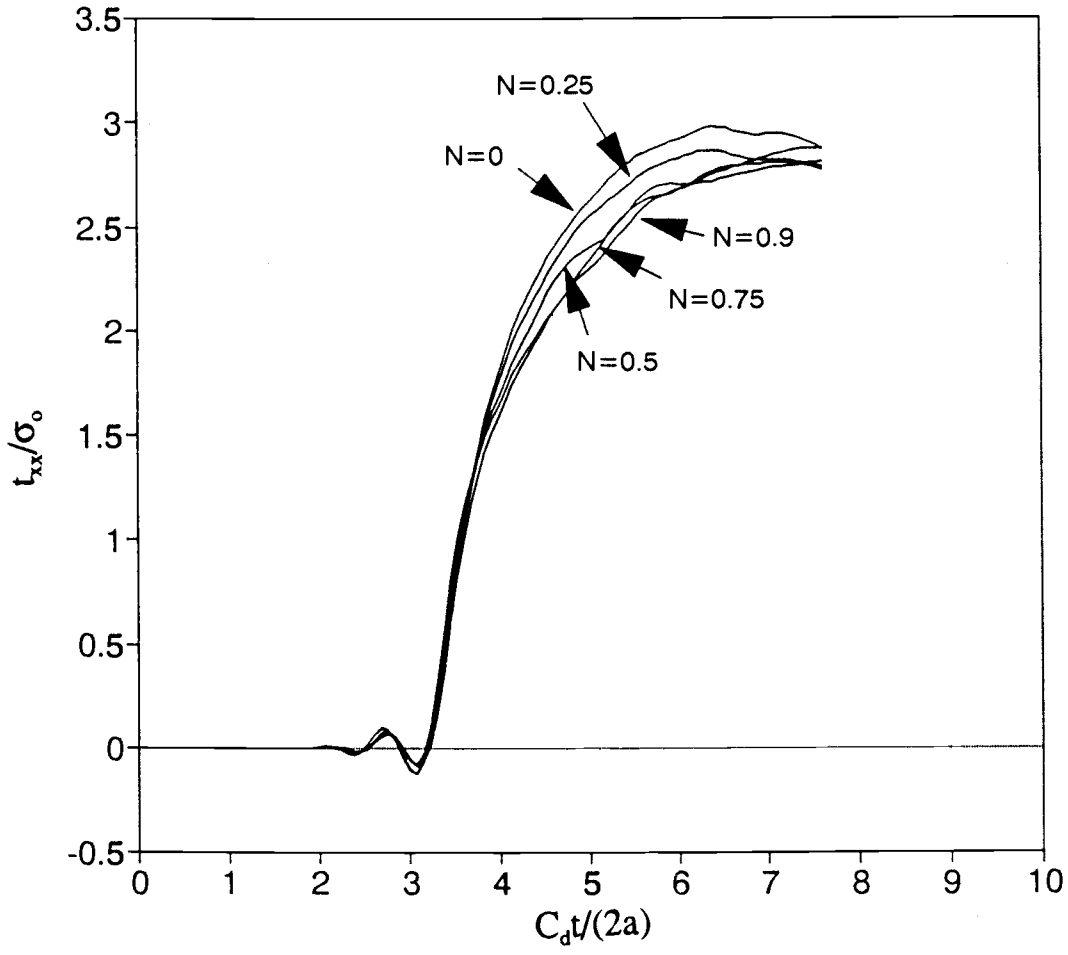

Figure 5.8 Stress versus time at the edge of a circular hole, $a/c = 4$ and $\nu = 0$.

Table 5.2 Material properties used for the analysis of a circular hole in a micropolar body ($a/c = 0.25$, $\nu = 0$, $a = 2.54 \times 10^{-4}$ m).

N	λ (N/m^2)	μ (N/m^2)	κ (N/m^2)	γ (N)	E (N/m^2)
0	0.0	10.345×10^6	0.0	0.0	2.638×10^7
0.25	0.0	48.276×10^6	6.897×10^6	13.350	5.899×10^7
0.5	0.0	6.897×10^6	6.897×10^6	10.680	2.638×10^7
0.75	0.0	-0.766×10^6	6.897×10^6	6.230	1.343×10^7
0.9	0.0	-2.639×10^6	6.897×10^6	2.715	0.738×10^7

5.2 Elliptical Holes

The case where the hole is elliptical in shape, with a major axis of length a_1 and a minor axis of length a_2, is now considered. The analytical solution for a micropolar material with a static load for this case was presented by Kim and Eringen [7] for the parameters $\alpha_0 = \coth^{-1}(a_1/a_2)$ and $R = (a_1+a_2)/2$, where α_0 represents the shape of the ellipse and R is the radius of a circle from which the ellipse is considered to be generated by boundary perturbations. Moreover, R/c indicates the ratio of the size of the elliptic hole to the characteristic length of the micropolar material. Identical parameters were used for the current investigation.

For a numerical study of a micropolar material, a strip 3.556 mm in width by 3.556 mm in length was considered. In Figure 5.9, the finite element mesh subject to analysis, with dimensions $a_1 = 0.254$ mm and $a_2 = 0.193$ mm (i.e., $a_1/a_2 = 1.32$ and $\alpha_0 = 1.0$), which takes advantage of symmetry as in the circular hole case, is shown. The total number of elements was 162, and 541 nodes were employed. Similar to the generation of the t_{yy} component in the case of circular holes, the top plane of the mesh represents a restrained boundary condition

for y-direction movements. Two different values for R/c , 1.0 and 0.29, were compared, and the material properties for the case R/c = 1.0 are listed in Table 5.3. For the Poisson's ratio ν = 0.25, the time step Δt was selected to allow a dilatational wave to travel the distance of 5.08 m in 200 time steps. The mass density ρ was 2192 Kg/m^3 with a microinertia of 1.935 $\times$ 10^{-7} m^2. The numerical results for N = 0.0, 0.25, 0.5, 0.75, and 0.9 are shown in Figure 5.10, with the nondimensionalized normal stress t_{xx}/σ_0 at the edge of the hole (x = 0, y = a_1) shown as a function of nondimensionalized time $C_d t/2R$, where σ_0 is a suddenly applied tensile load and C_d is the dilatational wave speed.

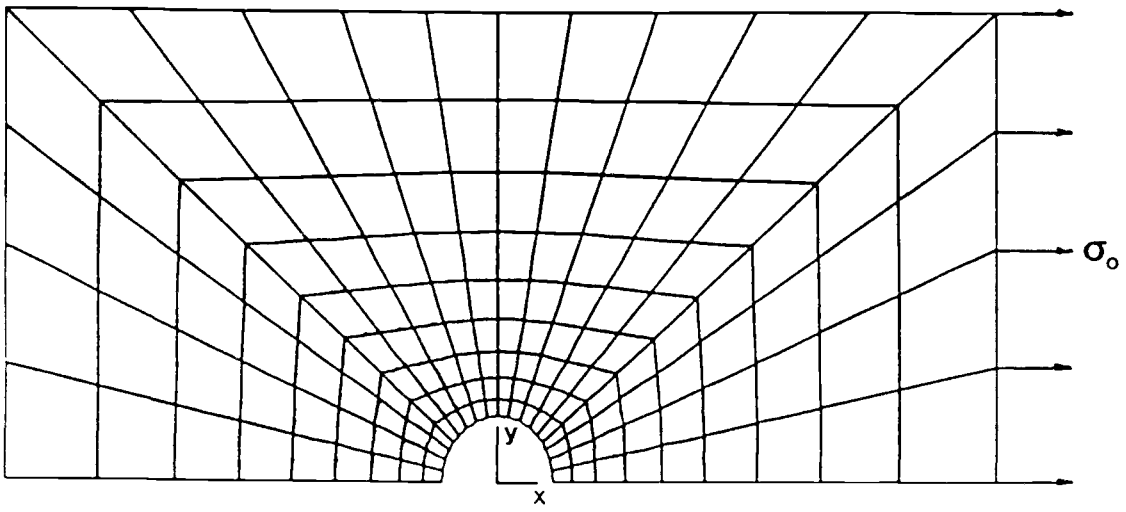

Figure 5.9 Finite element mesh for an elliptical hole in a micropolar body, α_0 = 1.

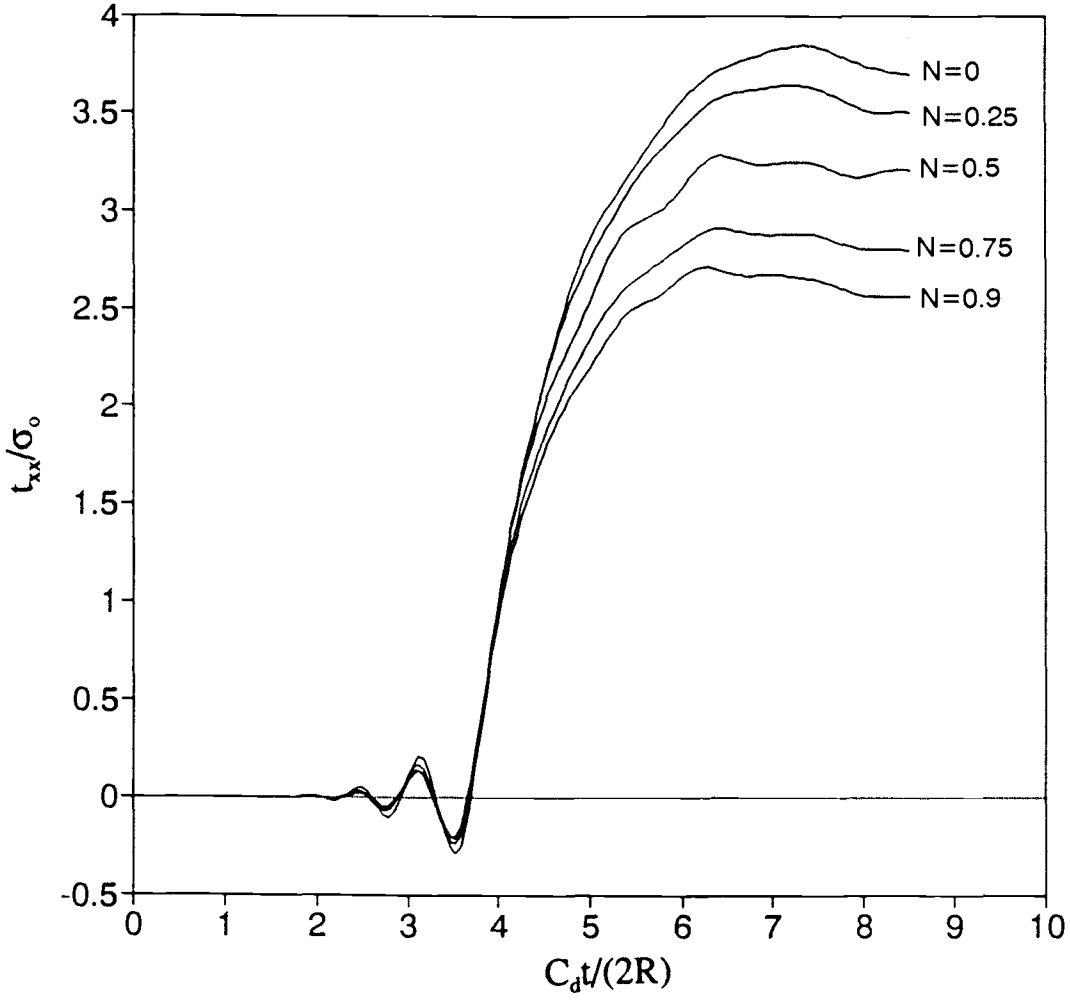

Figure 5.10 Stress versus time at the edge of an elliptic hole, $\alpha_0 = 1$, $R/c = 1$, and $\nu = 0.25$.

Table 5.3 Material properties used for the analysis of an elliptical hole in a micropolar body ($\alpha_0 = 1$, $\nu = 0.25$, $R/c = 1$, $R = 2.237 \times 10^{-4}$ m).

N	λ (N/m^2)	μ (N/m^2)	κ (N/m^2)	γ (N)	E (N/m^2)
0	10.345×10^6	10.345×10^6	0.0	0.0	3.231×10^7
0.25	51.725×10^6	48.276×10^6	6.897×10^6	6.475×10^{-1}	7.225×10^7
0.5	10.345×10^6	6.897×10^6	6.897×10^6	5.180×10^{-1}	3.231×10^7
0.75	2.682×10^6	-0.766×10^6	6.897×10^6	3.021×10^{-1}	1.645×10^7
0.9	0.809×10^6	-2.639×10^6	6.897×10^6	1.317×10^{-1}	0.904×10^7

Insofar as no prior investigations of dynamic stress concentrations around an elliptical hole in a micropolar elastic solid have been conducted, the results obtained from this investigation cannot be compared to a known analytical solution. However, similar to the case of circular holes, there was a substantial reduction in stress as the micropolar coupling factor was increased (i.e., from $N = 0.0$ to 0.9). For $N = 0.9$, the reduction in maximum stress was approximately 30 percent. To observe the effect of R/c, the case $R/c = 0.29$, (where $\alpha_0 = 1.0$ and $\nu = 0.25$) was analyzed with results as given in Figure 5.11. These results indicate that the micropolar effects were increasingly dominant in proportion to the decrease in the value of R/c. For $N = 0.9$ and $R/c = 0.29$, the reduction of maximum stress was approximately 35 percent, or larger than the results obtained for $R/c = 1.0$.

A secondary purpose of these numerical experiments was to determine the effect of α_0. When α_0 is reduced in size, the ellipse narrows and higher stress concentrations may be expected. The finite element mesh used for analysis of the case $\alpha_0 = 0.5$, where $a_1/a_2 = 2.16$, is shown in Figure 5.12, and the material properties for $\alpha_0 = 0.5$, $R/C = 1.0$ and $\nu = 0.25$ are listed in Table 5.4. Results for the various values of N are given in Figure 5.13. As expected, the narrower

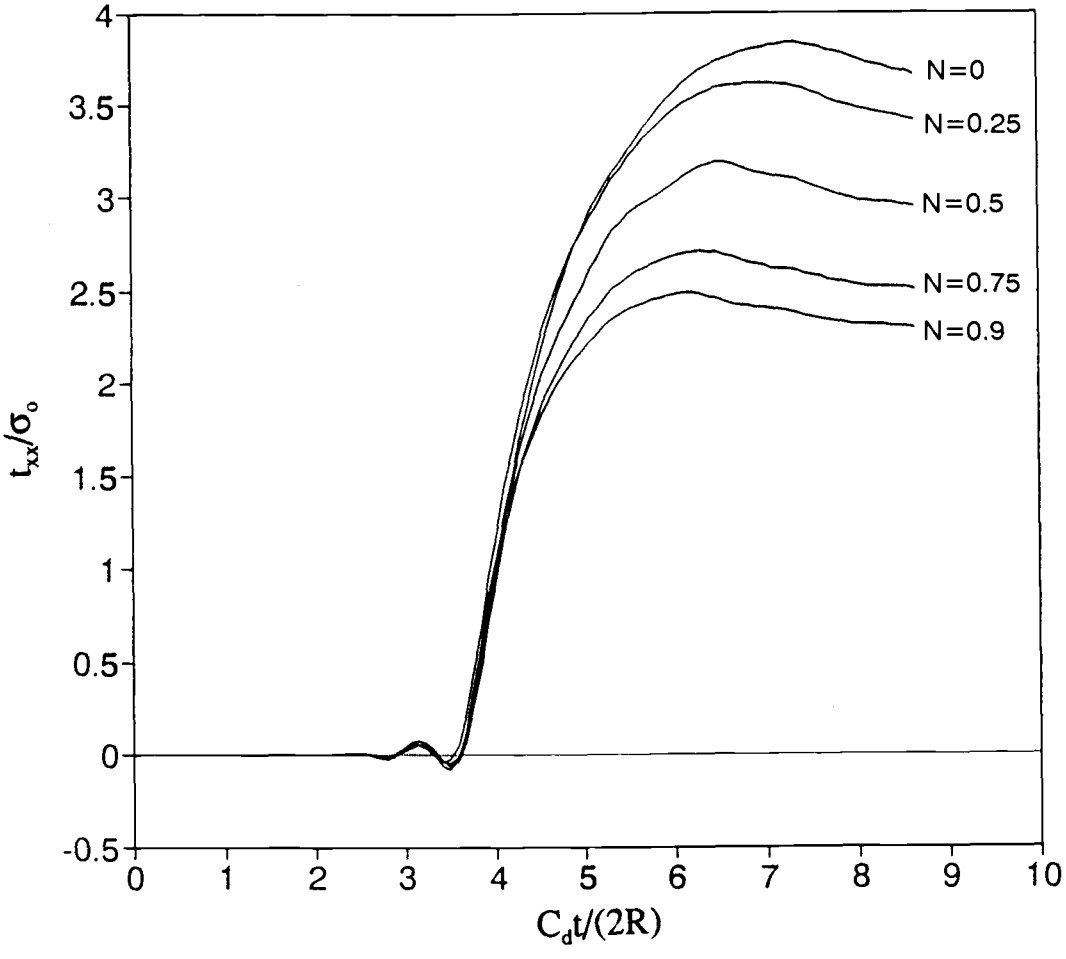

Figure 5.11 Stress versus time at the edge of an elliptic hole, $\alpha_0 = 1$, $R/c = 0.29$, and $\nu = 0.25$.

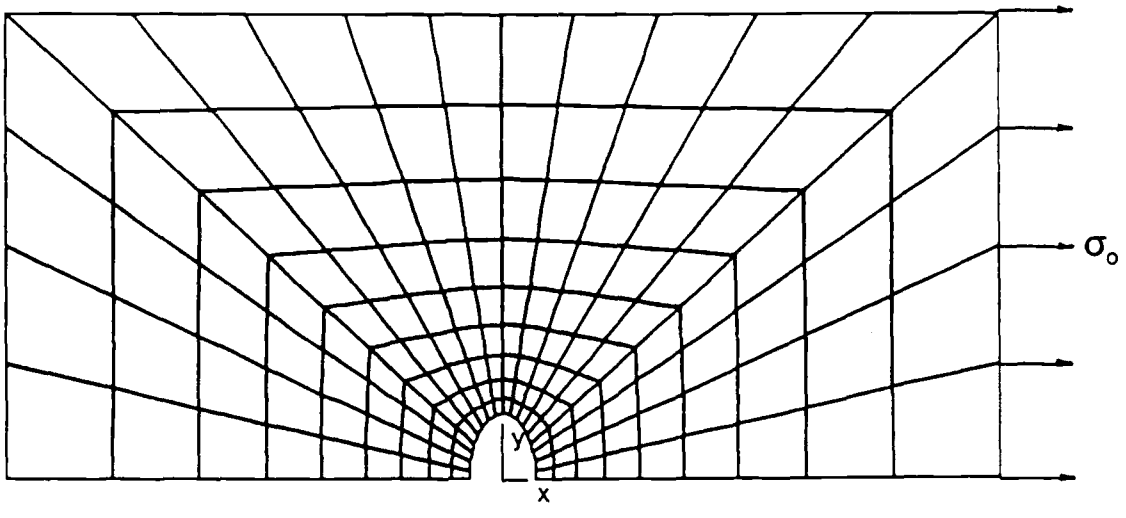

Figure 5.12 Finite element mesh for an elliptic hole in a micropolar body, for $\alpha_0 = 0.5$.

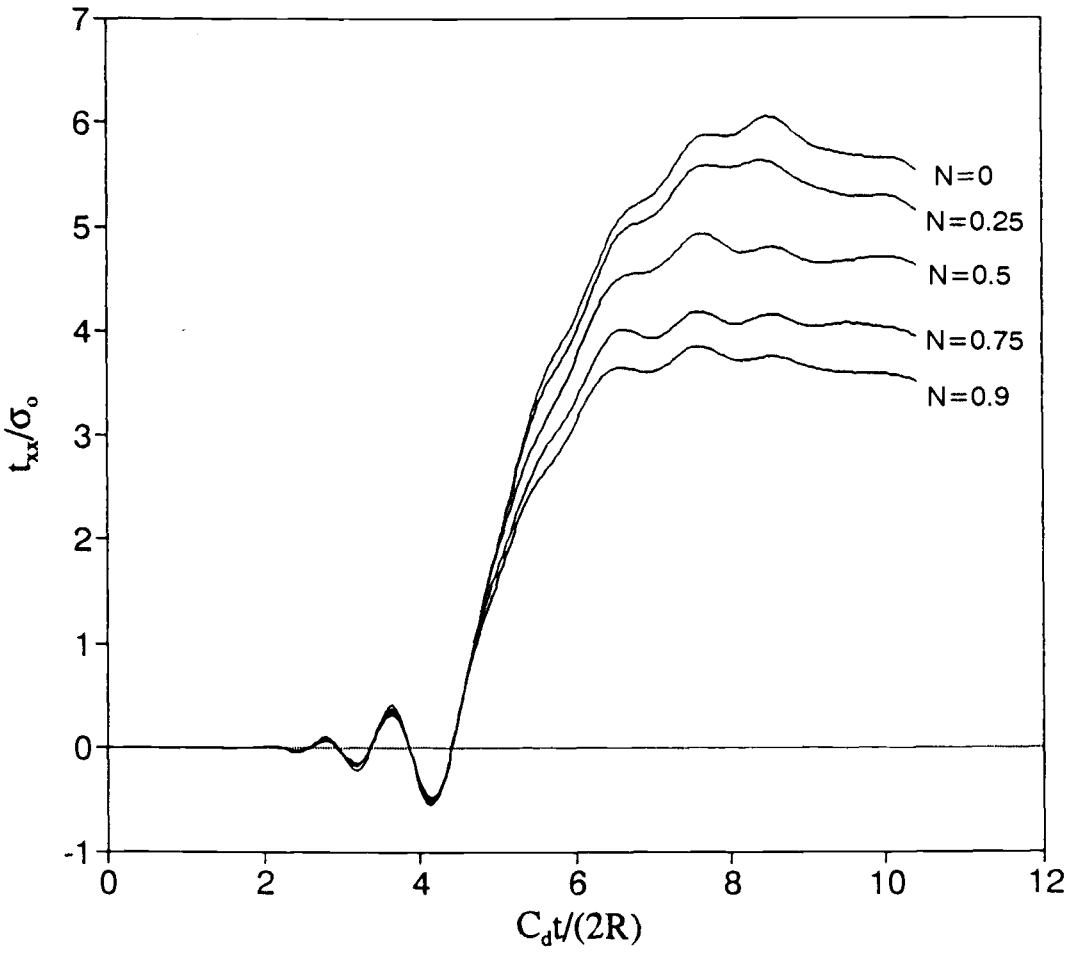

Figure 5.13 Stress versus time at the edge of an elliptic hole, $\alpha_0 = 0.5$, $R/c = 1$, and $\nu = 0.25$.

Table 5.4 Material properties used for the analysis of an elliptical hole in a micropolar body ($\alpha_0 = 0.5$, $\nu = 0.25$, $R/c = 1$, $R = 1.857 \times 10^{-4}$ m).

N	λ (N/m^2)	μ (N/m^2)	κ (N/m^2)	γ (N)	E (N/m^2)
0	10.345×10^6	10.345×10^6	0.0	0.0	3.231×10^7
0.25	51.725×10^6	48.276×10^6	6.897×10^6	4.461×10^{-1}	7.225×10^7
0.5	10.345×10^6	6.897×10^6	6.897×10^6	3.569×10^{-1}	3.231×10^7
0.75	2.682×10^6	-0.766×10^6	6.897×10^6	2.081×10^{-1}	1.645×10^7
0.9	0.809×10^6	-2.639×10^6	6.897×10^6	0.907×10^{-1}	0.904×10^7

ellipse (i.e., $\alpha_0 = 0.5$) produced higher stress concentrations than the previous case ($\alpha_0 = 1$). Once again, it may be observed that the micropolar properties resulted in a significant reduction of peak stress, in this case by approximately 40 percent for $N = 0.9$.

For purposes of comparison, identical procedures were repeated for $\nu = 0.0$. Similar to the case for circular holes at the same value, the incoming stress wave generated by the sudden application of a tensile load (σ_0) carried $t_{xx} = \sigma_0$ and $t_{yy} = 0$. Traction-free boundary conditions were applied to the top geometric plane for the finite element mesh. The material properties for $\alpha_0 = 1$, $R/c = 1$, and $\nu = 0.0$ are listed in Table 5.5. The trends observed were similar to those for $\nu = 0.25$, and the results for $\alpha_0 = 1$, $R/c = 1$, and $\nu = 0.0$ are shown in Figure 5.14, indicating that as N was varied from 0.0 to 0.9, there was an approximate 40 percent reduction in stress. In Figure 5.15, even more significant reductions in maximum stress concentration (i.e., approximately 50 percent) are indicated for $R/c = 0.29$, $\alpha_0 = 1$, and $\nu = 0$. In Figure 5.16, for comparison with the results indicated in Figure 5.14, the narrower ellipse ($\alpha_0 = 0.5$) was

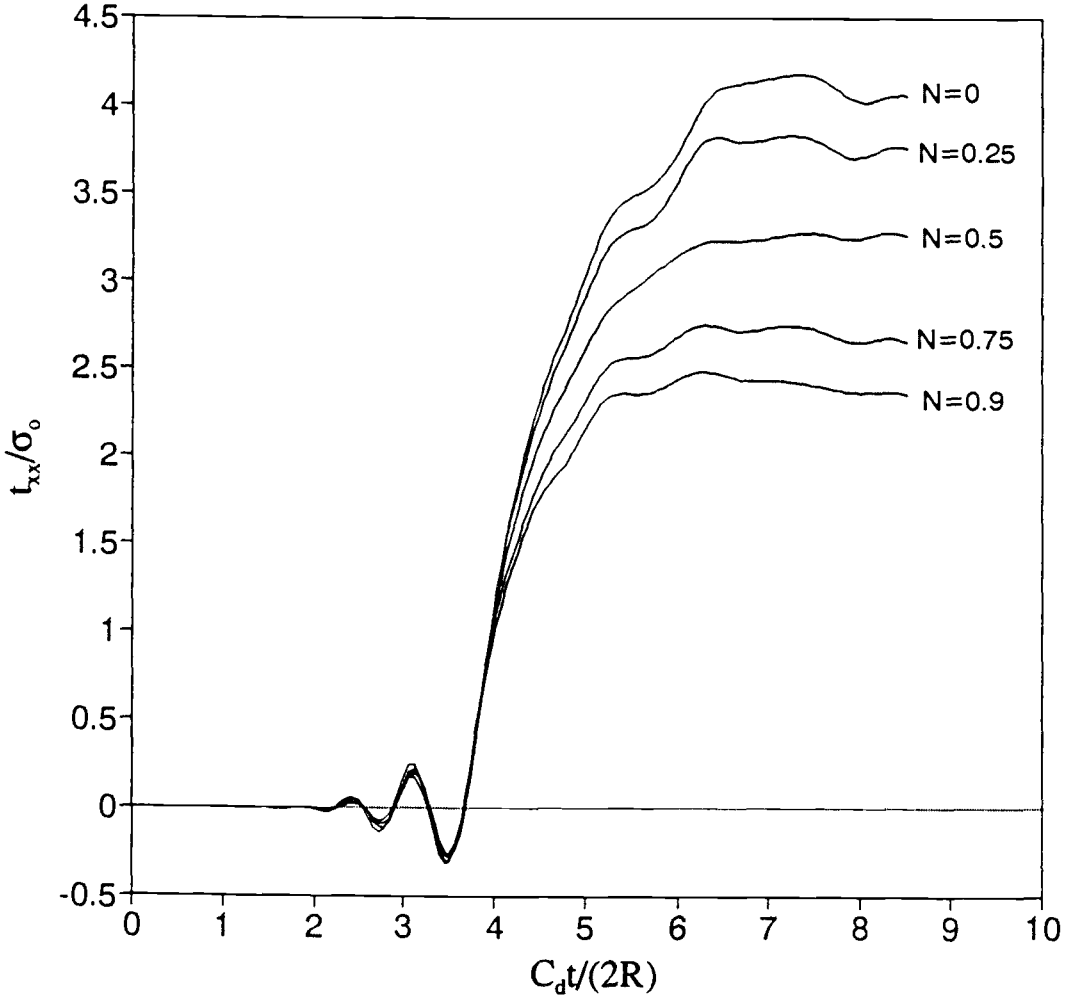

Figure 5.14 Stress versus time at the edge of an elliptic hole, $\alpha_0 = 1$, $R/c = 1$, and $\nu = 0$.

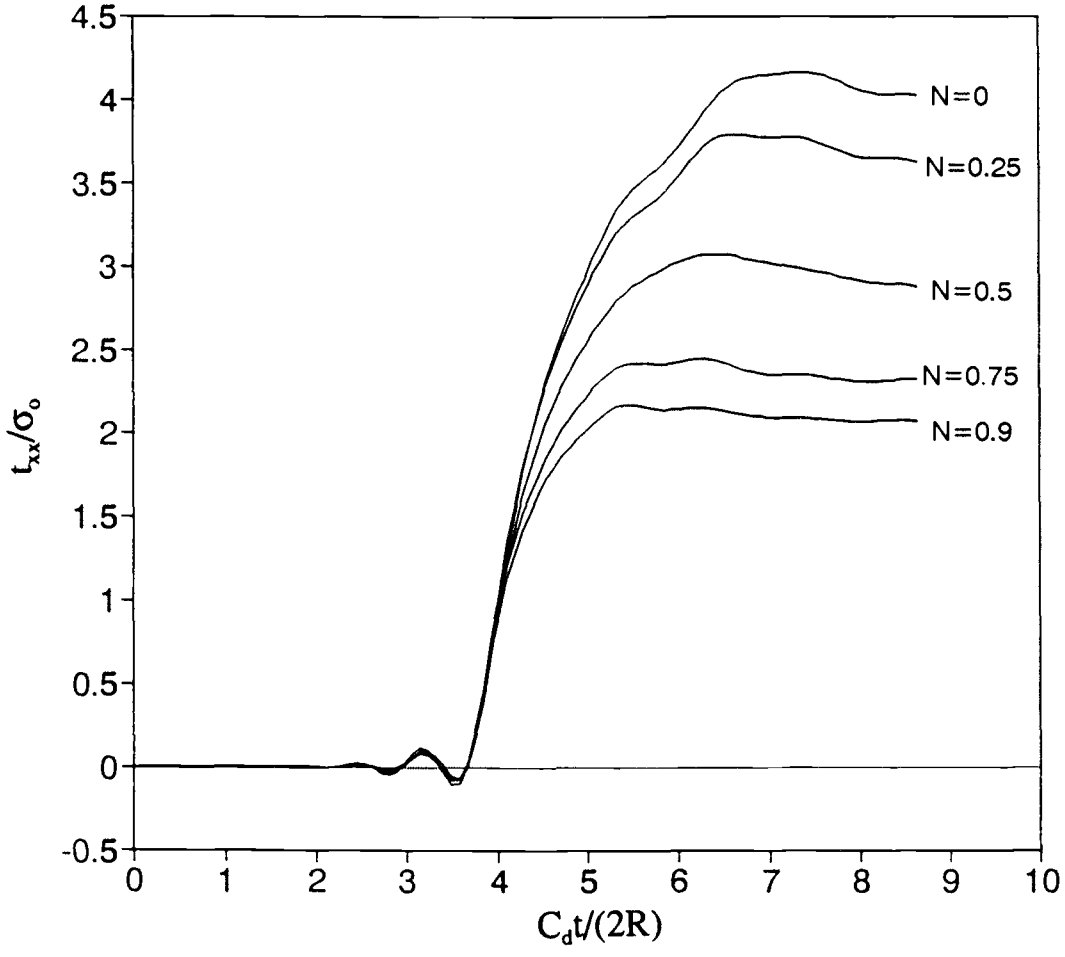

Figure 5.15 Stress versus time at the edge of an elliptic hole, $\alpha_0 = 1$, $R/c = 0.29$, and $\nu = 0$.

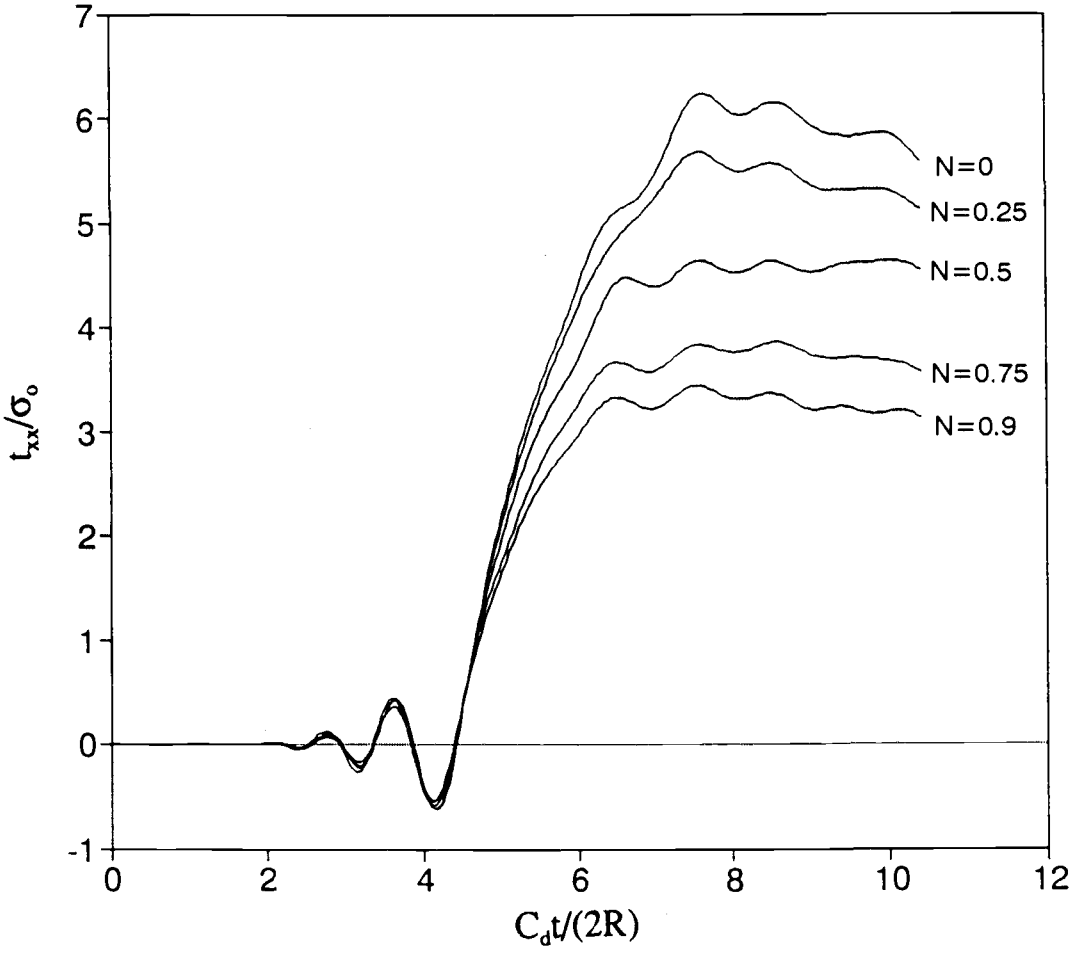

Figure 5.16 Stress versus time at the edge of an elliptic hole, $\alpha_0 = 0.5$, $R/c = 1$, and $\nu = 0$.

Table 5.5 Material properties used for the analysis of an elliptical hole in a micropolar body ($\alpha_0 = 1$, $\nu = 0$, $R/c = 1$, $R = 2.237 \times 10^{-4}$ m).

N	λ (N/m^2)	μ (N/m^2)	κ (N/m^2)	γ (N)	E (N/m^2)
0	0.0	10.345×10^6	0.0	0.0	2.638×10^7
0.25	0.0	48.276×10^6	6.897×10^6	6.475×10^{-1}	5.899×10^7
0.5	0.0	6.897×10^6	6.897×10^6	5.180×10^{-1}	2.638×10^7
0.75	0.0	-0.766×10^6	6.897×10^6	3.021×10^{-1}	1.343×10^7
0.9	0.0	-2.639×10^6	6.897×10^6	1.317×10^{-1}	0.738×10^7

employed for $R/c = 1.0$ and $\nu = 0.0$, and as N was varied from 0.0 to 0.9, the peak stress was reduced by approximately 45 percent.

From the results obtained, it may be concluded that micropolar properties serve to release stress concentrations in the direction along which stress is highly concentrated, while at the same time building stress in other directions. Similar to the results obtained for circular holes, maximum stress was reduced significantly when the micropolar effects were strong; that is, when N was increase in size or when R/c was reduced in size. As expected, higher stress concentrations were observed when a narrower ellipse was employed.

5.3 Stationary Cracks

The third case considered was that of a central stationary crack of length $2a$ in a body subject to dynamic loads. Sih and Embley [103] used classical elasticity theory and integral transforms to examine cracks in an infinite body where a uniform pressure σ was suddenly applied to the face of cracks. When this case is superposed with that for a plane dilatational wave of uniform tension σ passing through an uncracked body in a direction perpendicular to the plane of the crack, the case of a

plane dilatational wave diffracted by a crack is obtained. For the current investigation, this problem is considered for a micropolar elastic body. The finite element mesh for this case is shown in Figure 5.17, only one-quarter of the body of which needs to be modeled due to symmetry. It may be noted that the boundaries were removed a sufficient distance from the crack so that the wave reflection effects from the boundaries were minimized during the time period under consideration.

The finite element mesh was 52 mm in width by 44 mm in length, with a half-crack of length a at 12 mm, and employed 192 eight-node elements and 637 nodes (Fig. 5.17). Unform compressive loading of 1 Pa was applied to the crack surface, while the ratio of the crack element length to the crack length was 0.021. The mass density ρ was 2450 Kg/m^3, the microplar inertia j was 1.935×10^{-7} m^2, and the Poisson's ratio was 0.286. The micropolar properties used for the case $a/c = 0.25$, where c was a previously defined micropolar characteristic length, are listed in Table 5.6. Time step size was selected so that the dilatational wave traveled the distance $7.3a$ in 97 time steps. In the classical case presented by Sih and Embley [103], this distance corresponded to the elapsed time for the shear wave to travel the distance $4a$.

The numerical results for a/c at the values 0.25, 1.0, and 4.0 are shown, respectively, in Figures 5.18—5.20. In Figure 5.18, calculations for several different coupling factor values, in a range from $N = 0$ to $N = 0.9$, are given, and the results are plotted as a function of normalized time $C_d t/a$, where C_d is the dilatational wave speed and t is time. Energy release is normalized by dividing it by the energy release rate for the case of static-load classical elasticity,

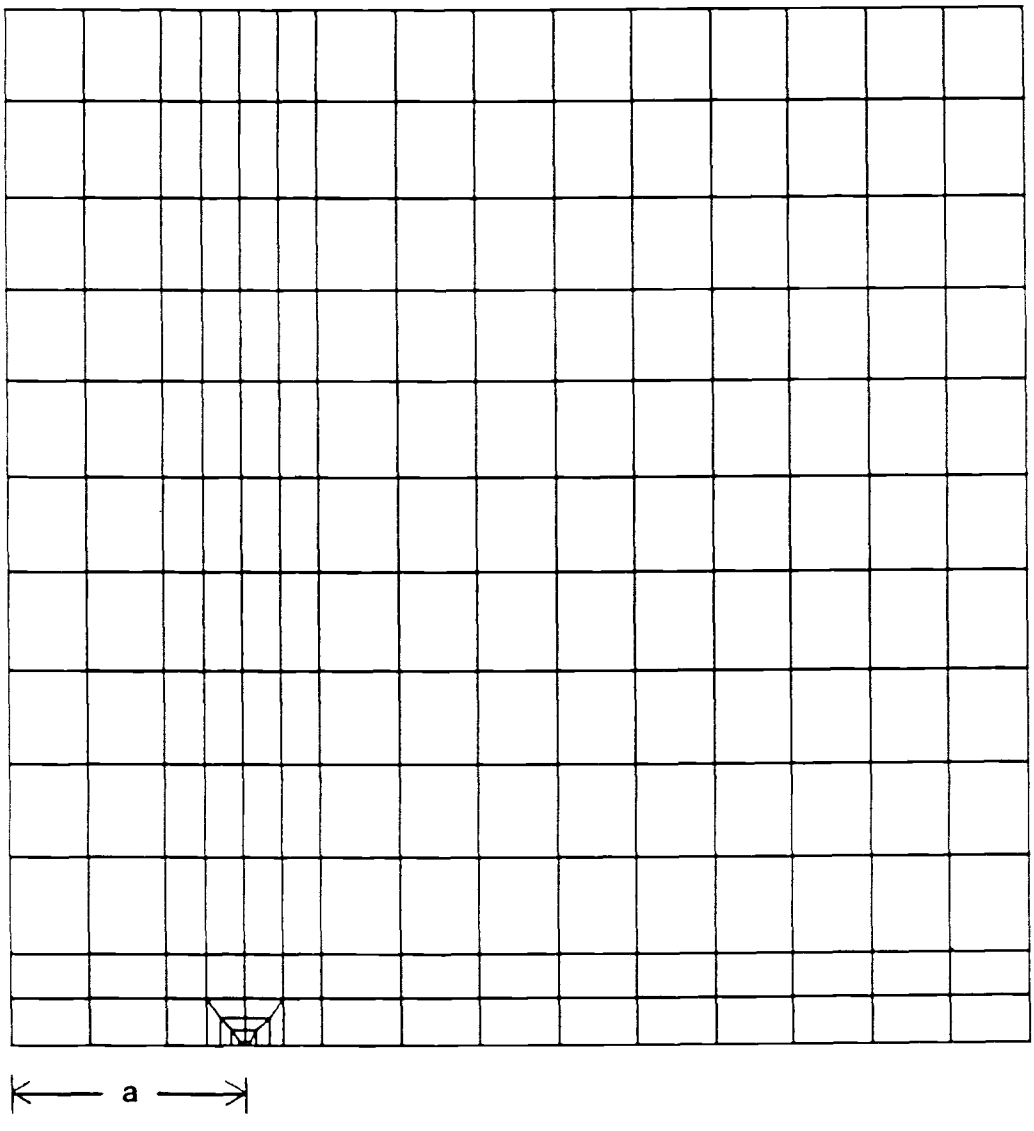

Figure 5.17 Finite element mesh for the stationary crack.

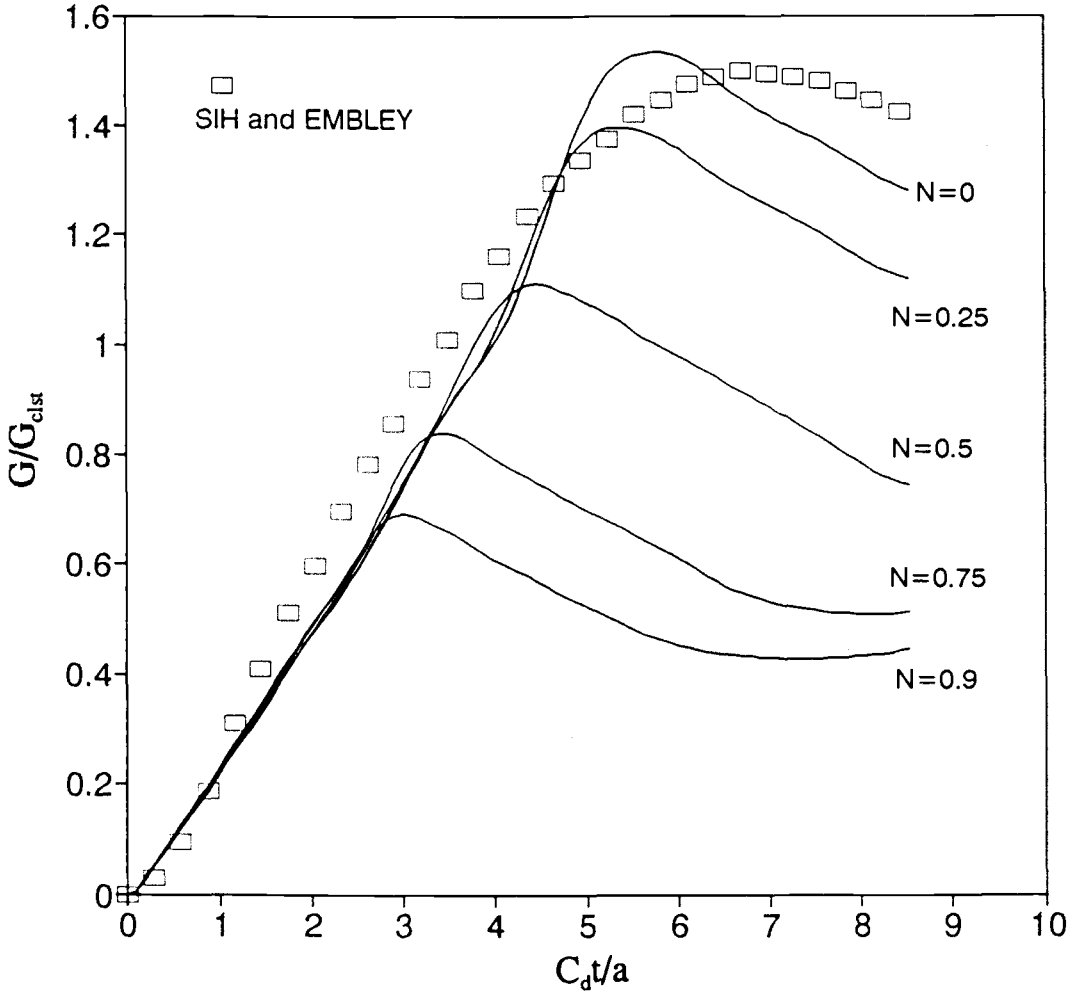

Figure 5.18 Energy release rate versus time for $a/c = 0.25$.

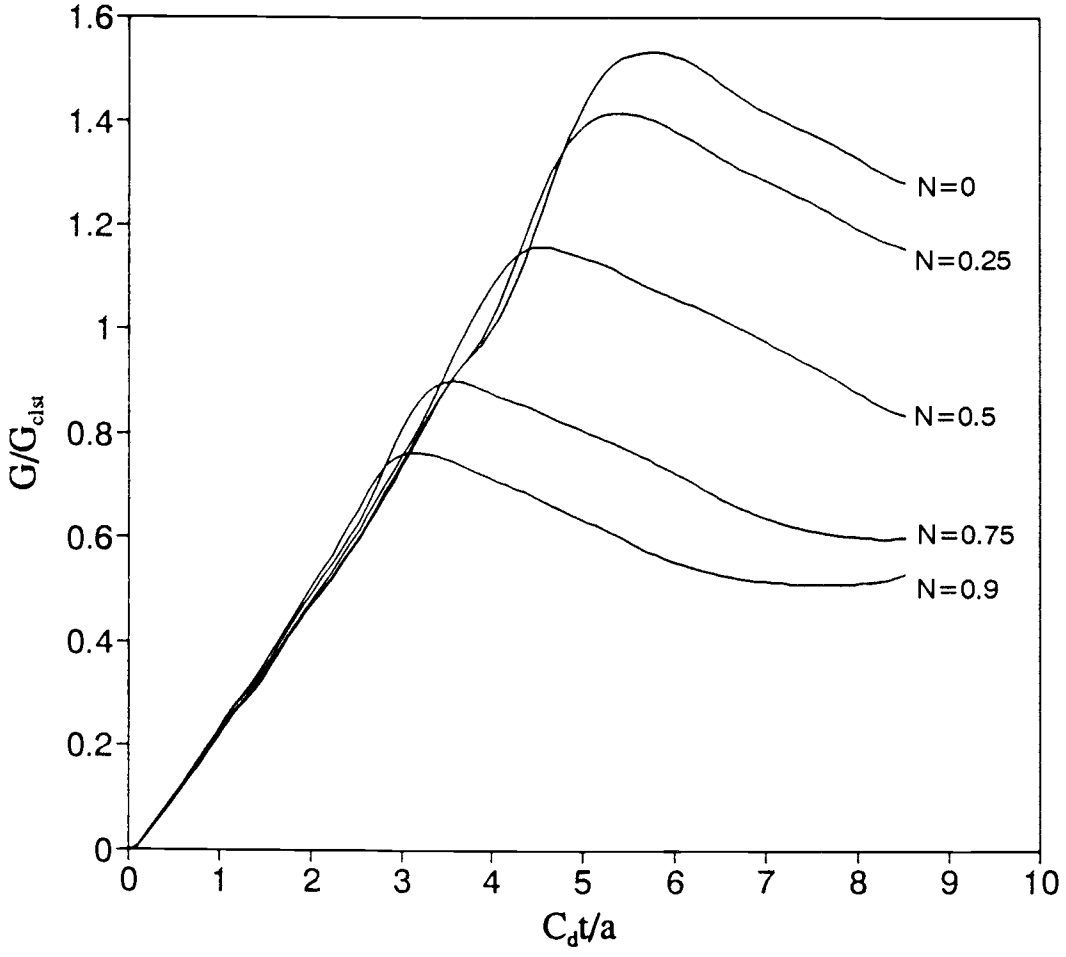

Figure 5.19 Energy release rate versus time for $a/c = 1$.

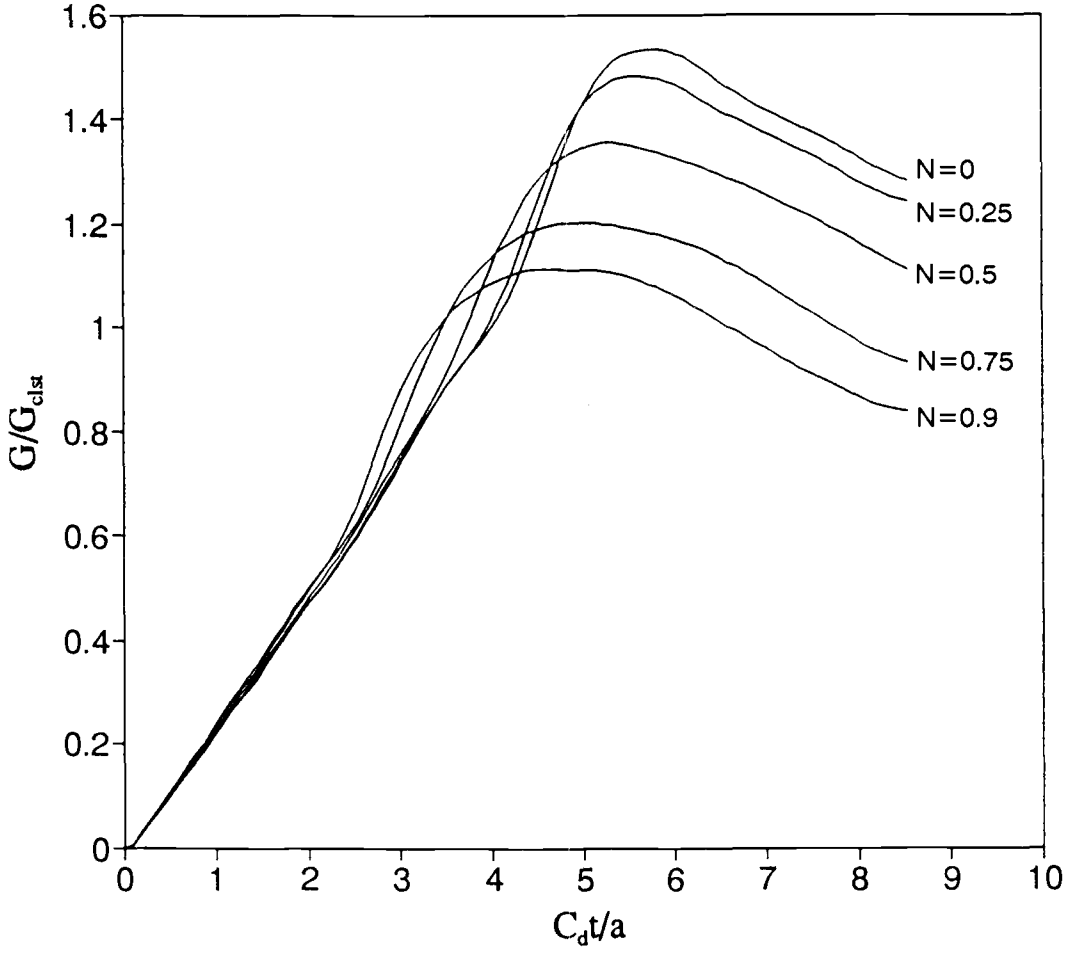

Figure 5.20 Energy release rate versus time for $a/c = 4$.

Table 5.6 Material properties used for the stationary crack ($a/c = 0.25$, $\nu = 0.286$).

N	λ (N/m^2)	μ (N/m^2)	κ (N/m^2)	γ (N)	E (N/m^2)
0	3.929×10^{10}	2.940×10^{10}	0.0	0.0	7.562×10^{10}
0.25	19.646×10^{10}	13.720×10^{10}	1.960×10^{10}	8.467×10^{7}	37.808×10^{10}
0.5	3.929×10^{10}	1.960×10^{10}	1.960×10^{10}	6.774×10^{7}	7.562×10^{10}
0.75	1.019×10^{10}	-0.218×10^{10}	1.960×10^{10}	3.951×10^{7}	1.960×10^{10}
0.9	0.307×10^{10}	-0.750×10^{10}	1.960×10^{10}	1.716×10^{7}	0.591×10^{10}

$$G_{\text{clst}} = \frac{\sigma^2 \pi a (1-\nu^2)}{E} , \tag{5.5}$$

where E is the Young's modulus. For purposes of comparison, the results of the stress intensity factors presented by Sih and Embley [103] were converted to corresponding energy release rates, using

$$G_I = \frac{(1-\nu^2)}{E} K_I^2 , \tag{5.6}$$

which is the known relationship between the mode-I stress intensity factor K_I and the mode-I energy relase rate. It should be noted that for dynamic fracture mechanics, equation (5.6) may be used as long as the crack is stationary.

For $N = 0$, the body behaves as a classical material. When the case $N = 0$ is compared to the results obtained by Sih and Embley [103], it may be observed that the peak values of the energy release rate are within approximately 2 percent of each other, as indicated in Figure 5.18. As N was increased, the micropolar effects of the material became more pronounced and a significant reduction in peak energy release rate was observed (i.e., approximately 55 percent at $N = 0.9$). This is an indication

that the classical theory of elasticity may overestimate the energy release rate for a crack in material in which the microstructure and the micropolar properties of the material contribute to a favorable distribution of stress around the crack.

The results for $a/c = 1.0$, given in Figure 5.19, indicate a significant reduction in peak energy rate (i.e., approximately 50 percent for $N = 0.9$), though not to the same extent as the reduction for $a/c = 0.25$. For $a/c = 4.0$, the micropolar effects had a significantly smaller influence upon the reduction of the peak value of the energy release rate (Fig. 5.20), approximately 27 percent as N was varied from 0.0 to 0.9. This finding was similar to that observed for a plane dilatational wave diffracted by a circular hole, indicating that micropolar effects are important primarily for those cracks which are not much larger than the characteristic length c. The latter length is related to the dimensions of the microstructure, that is, to grain or particle size.

To model crack problems with finite element methods, the use of very small elements near the crack tip, which serve to account for the singularity of the crack tip, is inevitable. To satisfy equation (3.42), this factor mandates the use of extremely small sized time steps (an issue discussed in Chapter 3). The time step Δt used for the cases shown in Figures 5.18—5.20 violated this condition for crack tip elements insofar as the dilatation wave passed the crack tip elements within the stated time step. To date, no investigations have been conducted to provide useful rules for the analysis of dynamic crack problems. For the current study, a smaller time step, one-quarter of that indicated above for the satisfaction of equation (3.42), was employed. Figures 5.21—5.23, showing the results, respectively, for a/c at values of 0.25, 1.0, and 4.0, indicate that the energy release rate values are nearly identical

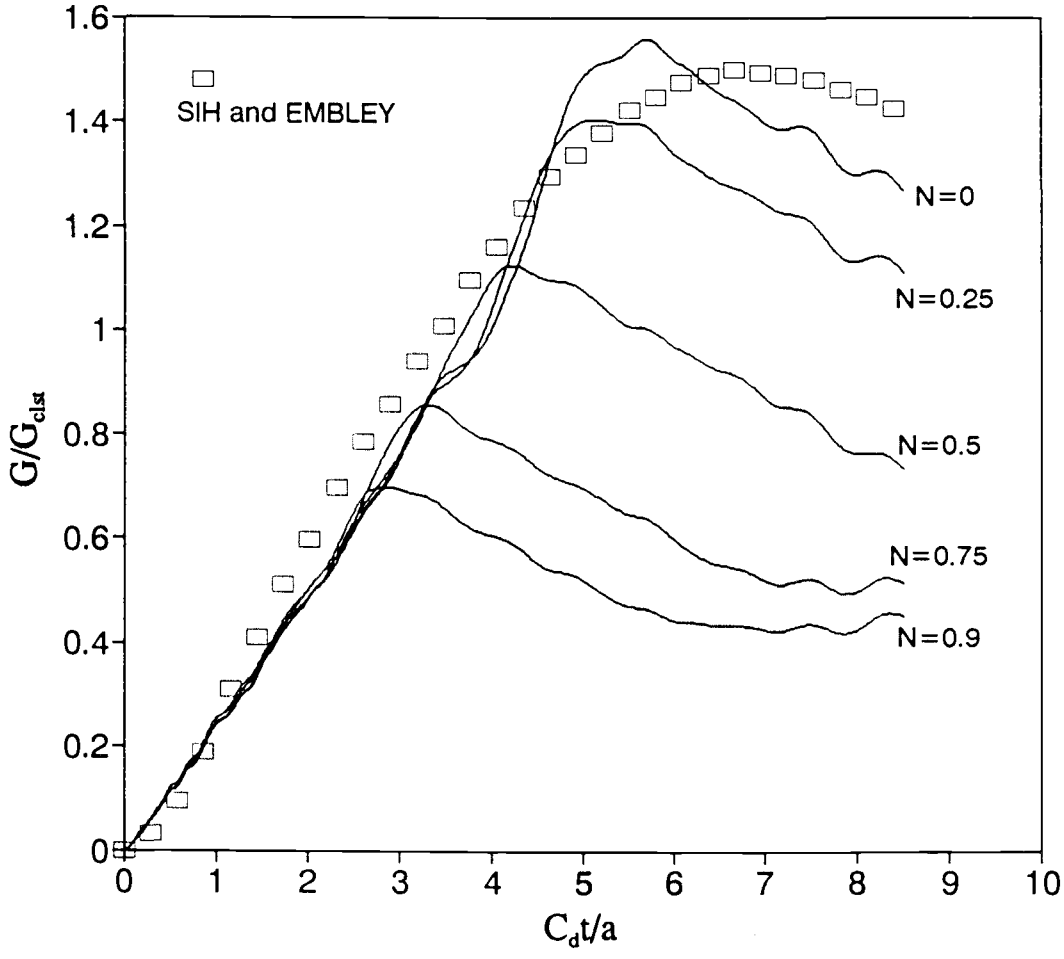

Figure 5.21 Energy release rate versus time for $a/c = 0.25$.

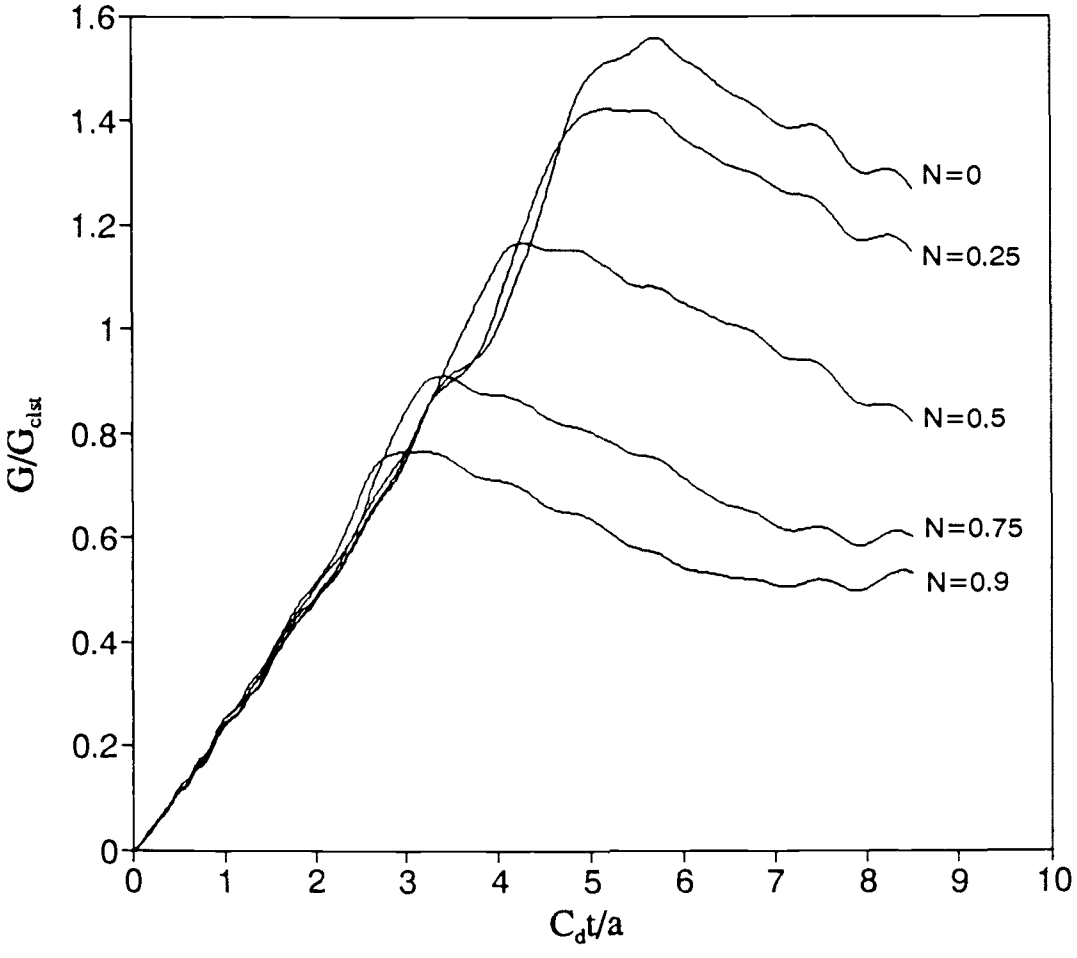

Figure 5.22 Energy release rate versus time for $a/c = 1$.

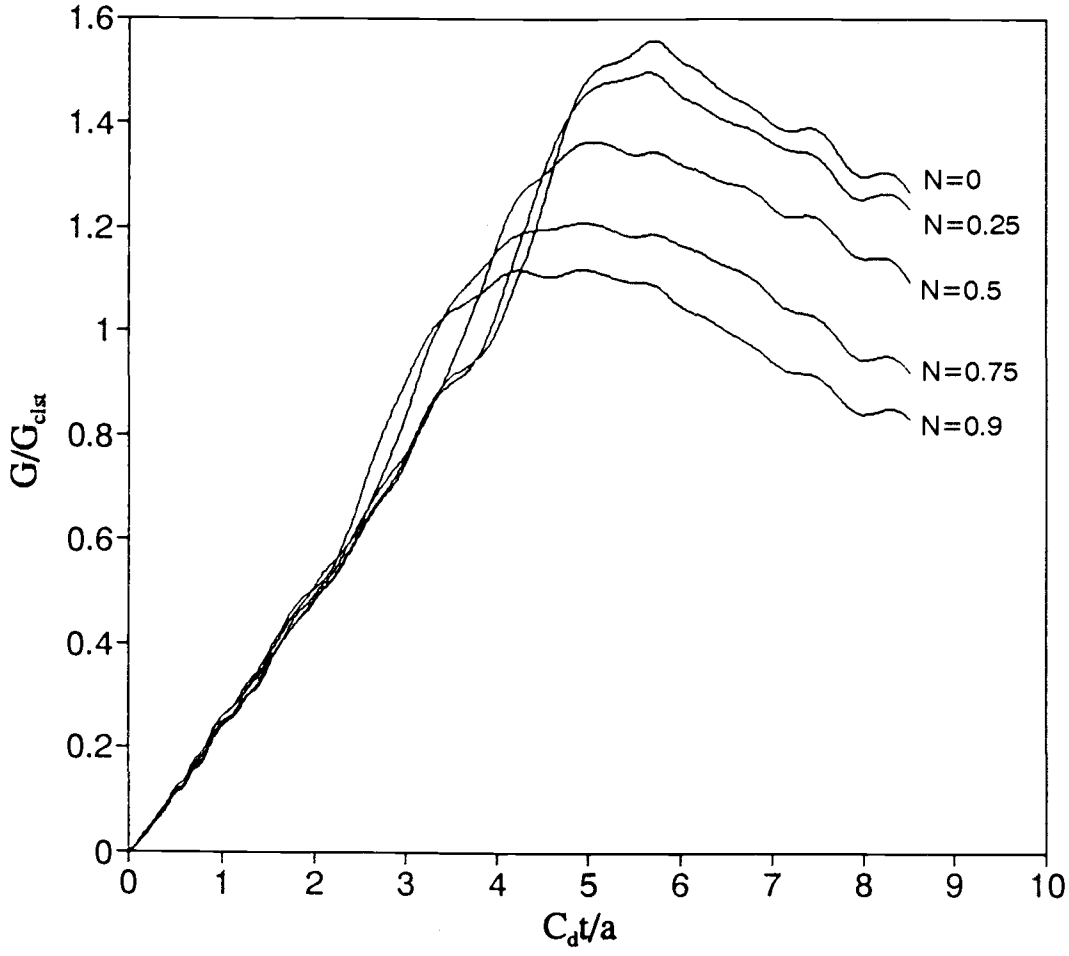

Figure 5.23 Energy release rate versus time for $a/c = 4$.

to those given in Figures 5.18—5.20, with the exception that the the results indicated in Figs. 5.21—5.23 include undesirable high-mode oscillations while requiring greater lengths of computation time (e.g., approximately 100 hours of 386-based PC time were required to yield the results shown in Fig. 5.21, which is nearly four times the requirement for calculation of the results shown in Fig. 5.18). From these results, it may be concluded that the selection of an optimal time step is strongly problem-dependent and should be based upon experience.

5.4 Propagating Cracks

The final problem considered for this study is the case of a center-cracked body with dimensions 80 mm by 80 mm under uniform tension, where the crack suddenly begins to propagate at a constant velocity. This problem is similar to that analyzed by Broberg [104], with the exception that the Broberg crack opened from an initial length of zero. For the case considered in the current study, the finite element mesh is shown in Figure 5.24 (once again, note that only one-quarter of the model is displayed due to symmetry). For this problem, the half-width L was 40 mm, the initial half-length of the crack was 8 mm, and 237 eight-node elements and 798 nodes were used. The mass density of the material was 2450 Kg/m^3, the microinertia j was 1.935×10^{-7} m^2, and the Poisson's ratio ν was 0.286. The micropolar material constant for the case $a/c = 0.25$ are listed in Table 5.7. It was assumed that a time-independent tensile stress acted along the edge of the panel parallel to the crack axis. To generate this load, displacement fields obtained from static finite element analysis and zero initial velocities were used as the initial conditions.

Table 5.7 Material properties used for the propagating crack ($a/c = 0.25$, $\nu = 0.286$).

N	λ (N/m^2)	μ (N/m^2)	κ (N/m^2)	γ (N)	E (N/m^2)
0	3.929×10^{10}	2.940×10^{10}	0.0	0.0	7.562×10^{10}
0.25	19.646×10^{10}	13.720×10^{10}	1.960×10^{10}	2.352×10^{6}	37.808×10^{10}
0.5	3.929×10^{10}	1.960×10^{10}	1.960×10^{10}	1.882×10^{6}	7.562×10^{10}
0.75	1.019×10^{10}	-0.218×10^{10}	1.960×10^{10}	1.098×10^{6}	1.960×10^{10}
0.9	0.307×10^{10}	-0.750×10^{10}	1.960×10^{10}	0.477×10^{6}	0.591×10^{10}

The linear node release technique (discussed in Chapter 4) was used to simulate the problem of a propagating crack. The time step Δt was selected so that the crack tip would pass one element at four time steps; that is, the crack tip node was released gradually. Three different crack speeds, C_d at 0.11, 0.219, and 0.328, and three micropolar values, a_0/c at 0.25, 1.0, and 4.0, were considered.

As the crack propagated from the original half-length $a = 0.2L$ to the final half-length $a = 0.3L$, where $2L$ is the width of the body, the energy release rate was calculated at the end of each incremental extension (Figures 5.24 and 5.25). This rate was normalized by dividing it by G_{clst}, given in equation (5.5), where the crack length given in equation (5.5) was used as the corresponding length for the propagating crack. In Figure 5.25, the normalized energy release rate is plotted as a function of the normalized crack half-length a/L for $a_0/c = 0.25$ at various values of N for a crack propagating velocity of $C_d = 0.11$. The Broberg [104] analysis of a classical elastic material is also given in this figure for the crack speed $C_d = 0.11$, which generated a result of 0.829. For $N = 0$ (i.e., a value identical to that for the case of classical elasticity), agreement between the finite element solution and the analytical solution was not quite as good as for the

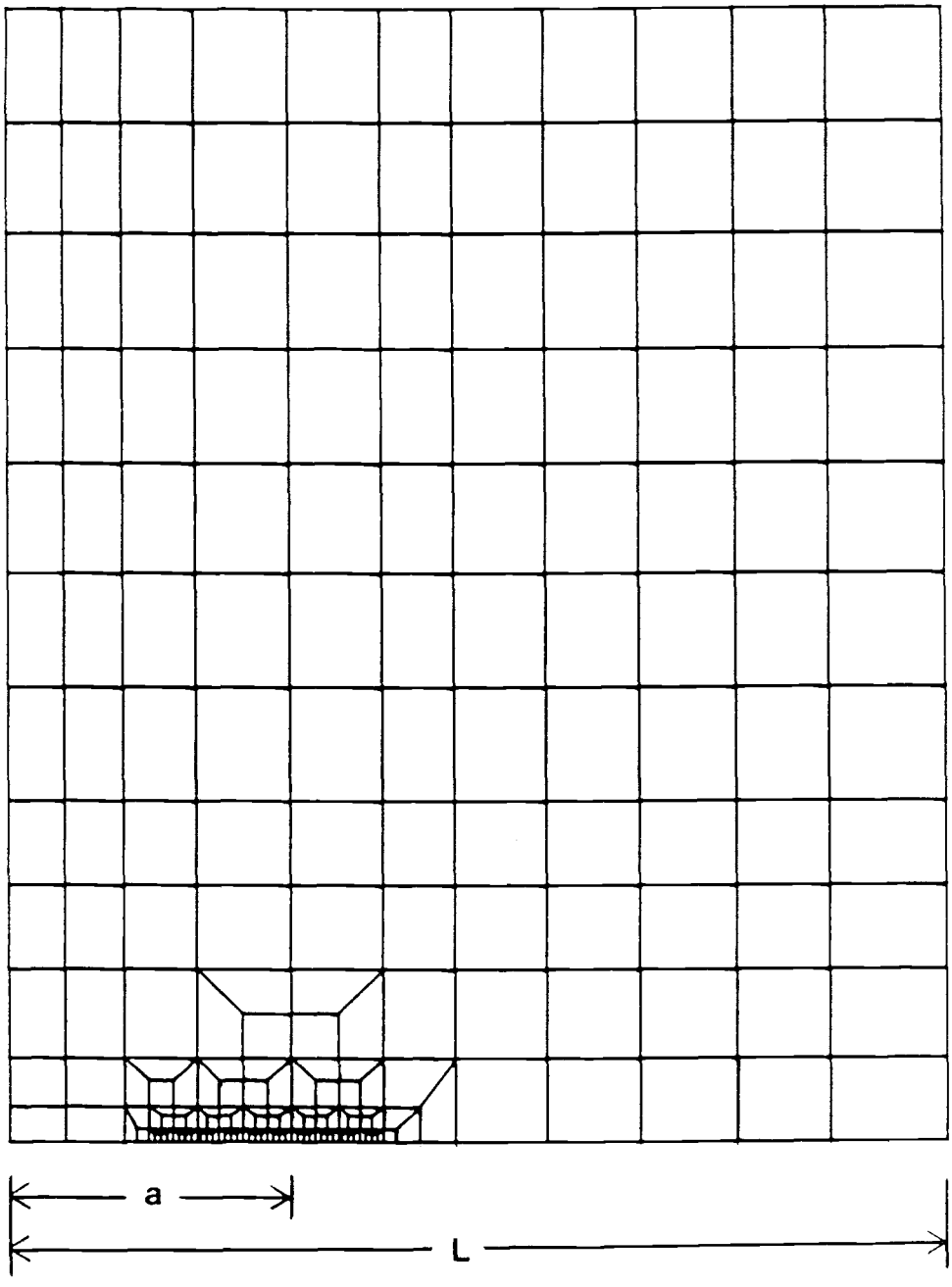

Figure 5.24 Finite element mesh for the propagating crack.

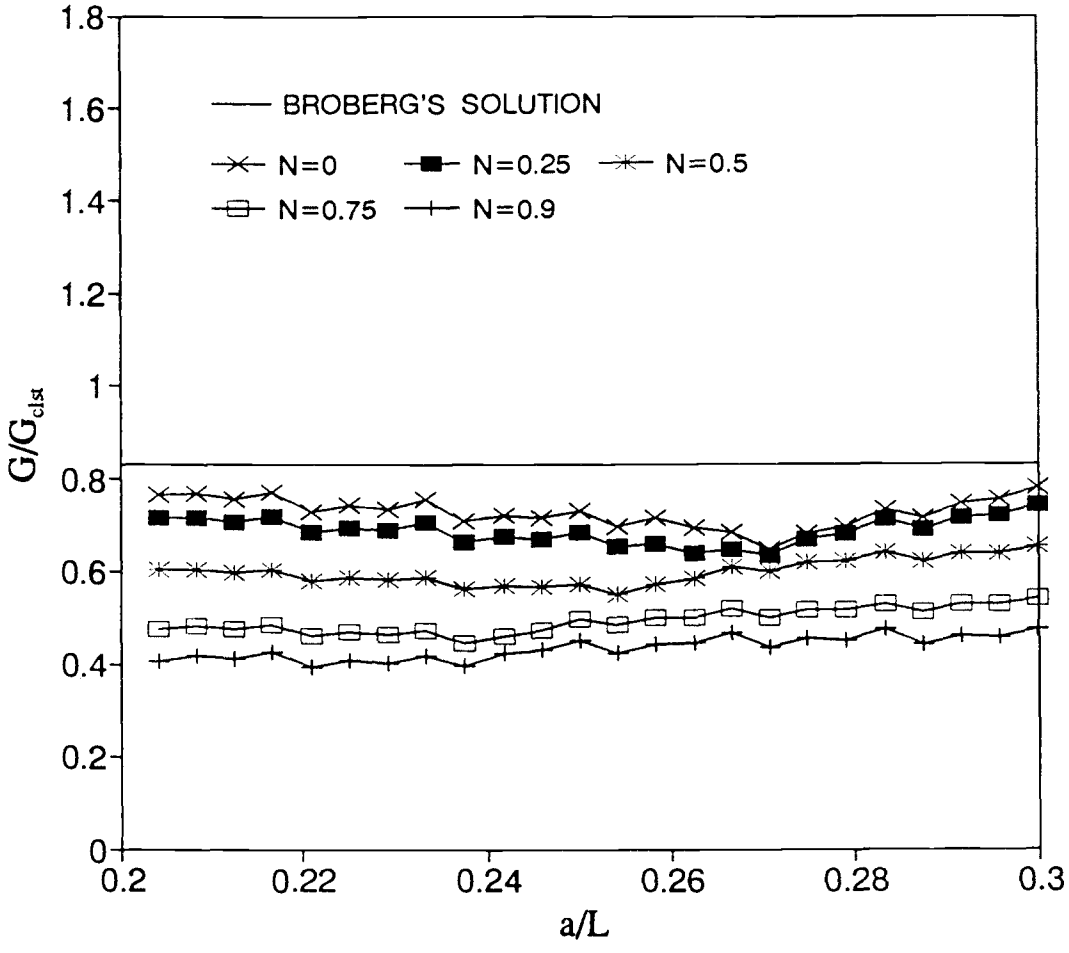

Figure 5.25 Energy release rate versus crack length for a crack propagating at the velocity 0.11 C_d, $a_0/c = 0.25$.

stationary crack considered in section 5.3. However, the level of accuracy of the solution was approximate to that obtained by Malluck and King [76] and by Jih and Sun [85]. Once again, the energy release rate became small in proportion to the degree that the micropolar properties were more pronounced (i.e., as N increased). These calculations were repeated for $a_0/c = 1$ and $a_0/c = 4$ and the results are given in Figure 5.26 and 5.27. As indicated in Figure 5.26, the micropolar effects maintained substantial influence in lowering the energy release rate for $a_0/c = 1$; for $a_0/c = 4$, the micropolar effects were slight (Fig. 5.27).

Identical calculation procedures were also completed for two additional crack propagation velocities, $0.219\ C_d$ and $0.328\ C_d$, for each case of a_0/c (i.e., 0.25, 1.0, and 4.0). Figures 5.28—5.30 show the results for each case at $C_d = 0.219$. Once again, it was observed that as N was enlarged from 0.0 to 0.9, the energy release rate was reduced, and as a_0/c was increased from 0.25 to 4.0, the micropolar effects decreased. Figures 5.31—5.33 show the results for a_0/c at, respectively, 0.25, 1.0, and 4.0 at the crack speed $0.328\ C_d$, indicating that the micropolar effects can scarcely be recognized.

From these numerical analyses, it may also be observed that the micropolar effects decrease in dominance in proportion to the increase in crack propagation velocity, or as the crack propagation approached its limiting velocity, which is generally recognized as the characteristic Rayleigh wave speed of the material at issue.

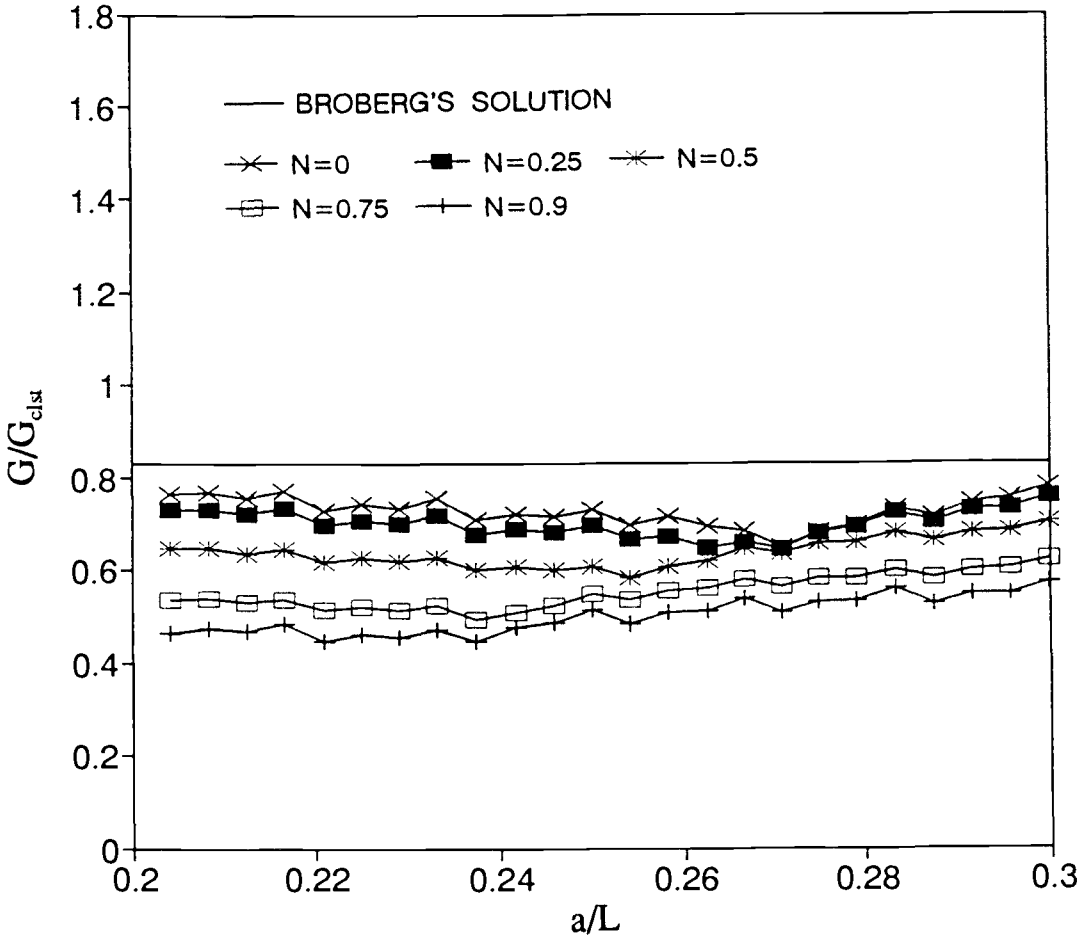

Figure 5.26 Energy release rate versus crack length for a crack propagating at the velocity 0.11 C_d, $a_0/c = 1$.

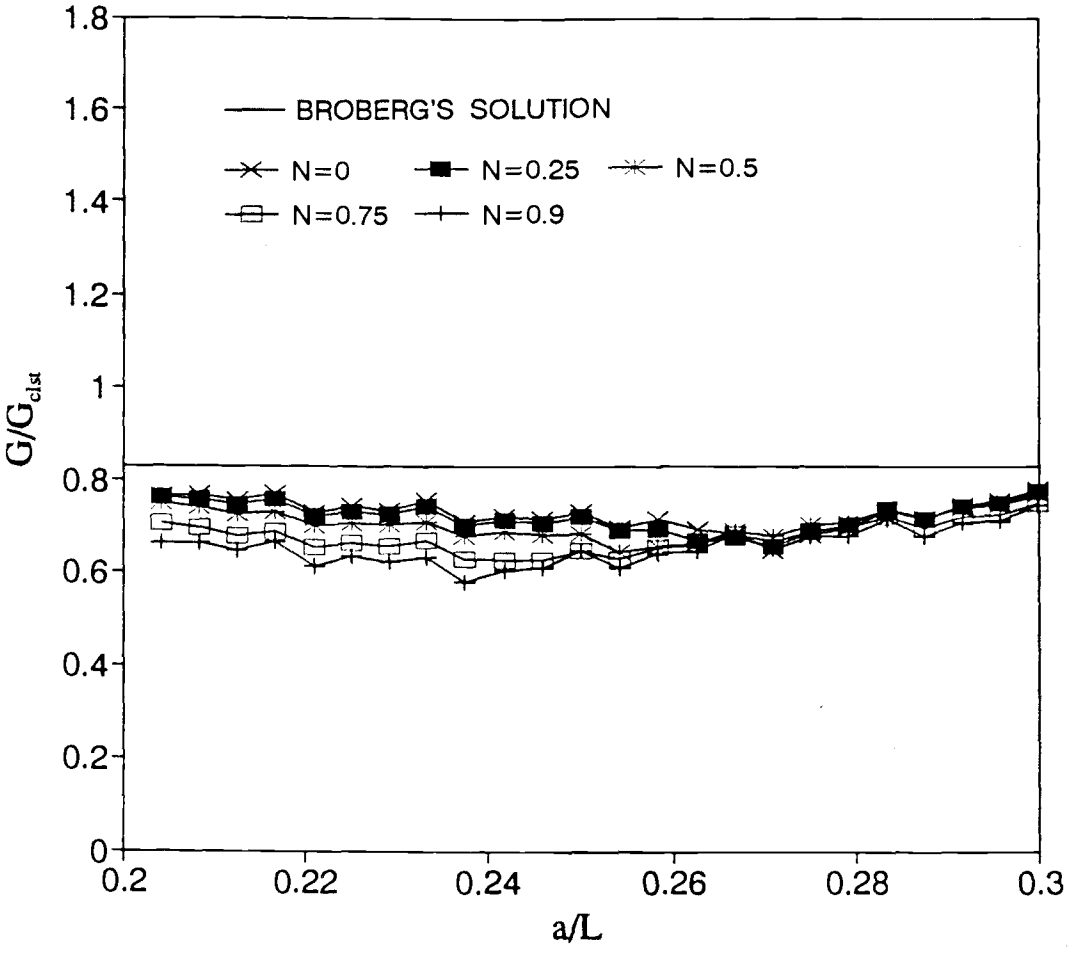

Figure 5.27 Energy release rate versus crack length for a crack propagating at the velocity 0.11 C_d, $a_0/c = 4$.

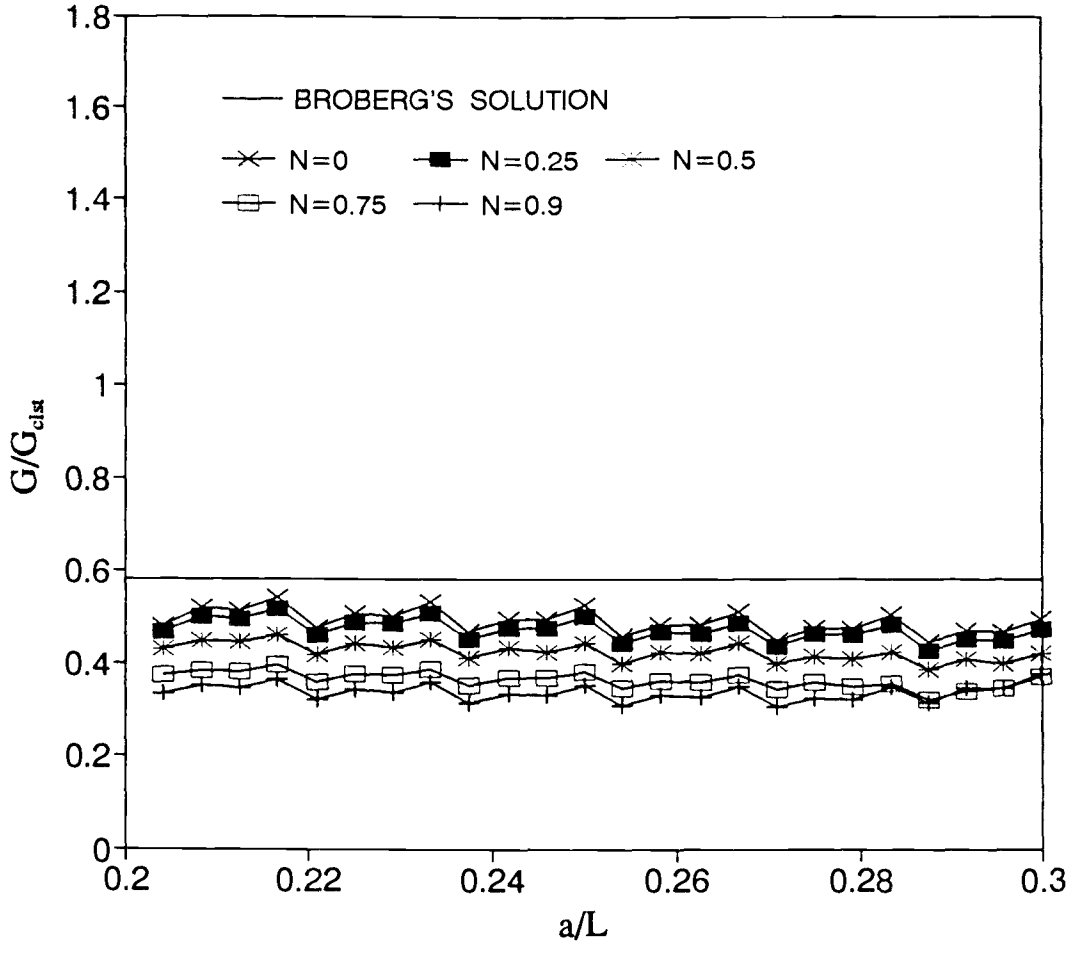

Figure 5.28 Energy release rate versus crack length for a crack propagating at the velocity 0.219 C_d, $a_0/c = 0.25$.

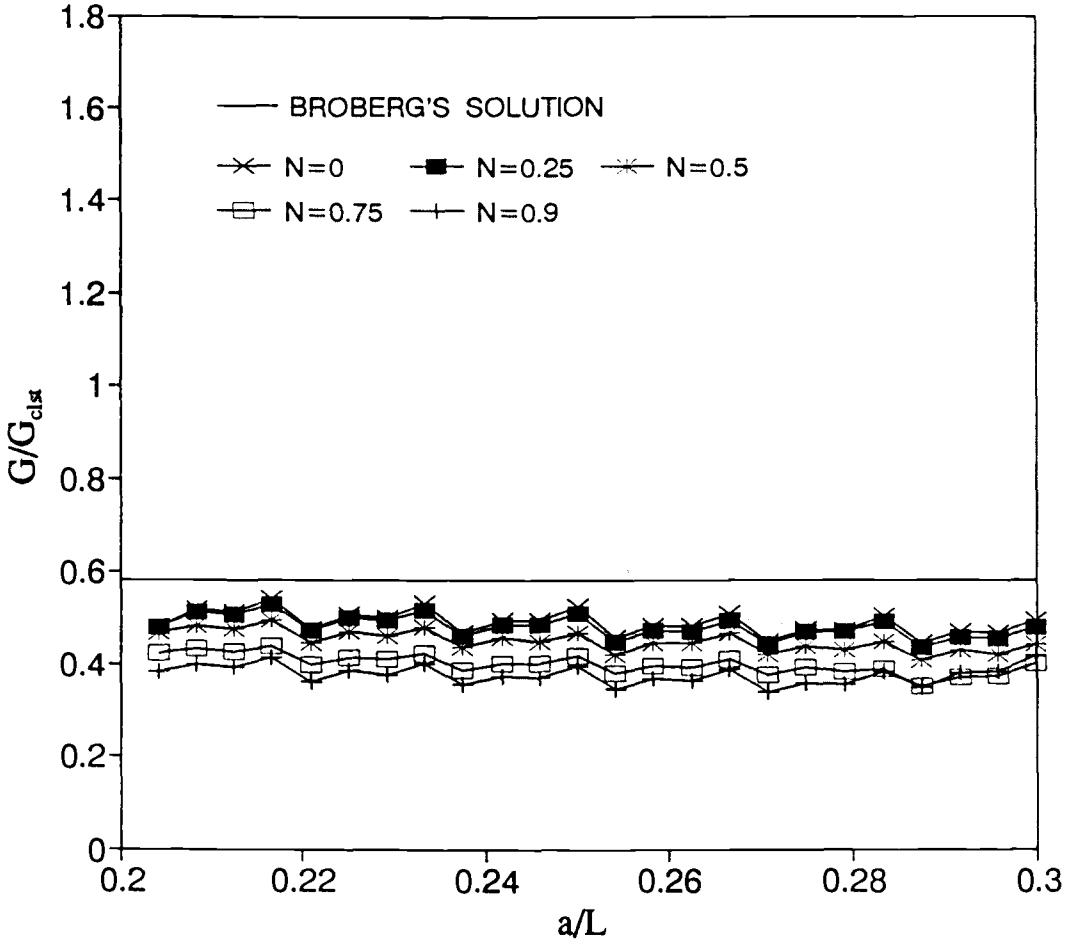

Figure 5.29 Energy release rate versus crack length for a crack propagating at the velocity 0.219 C_d, $a_0/c = 1$.

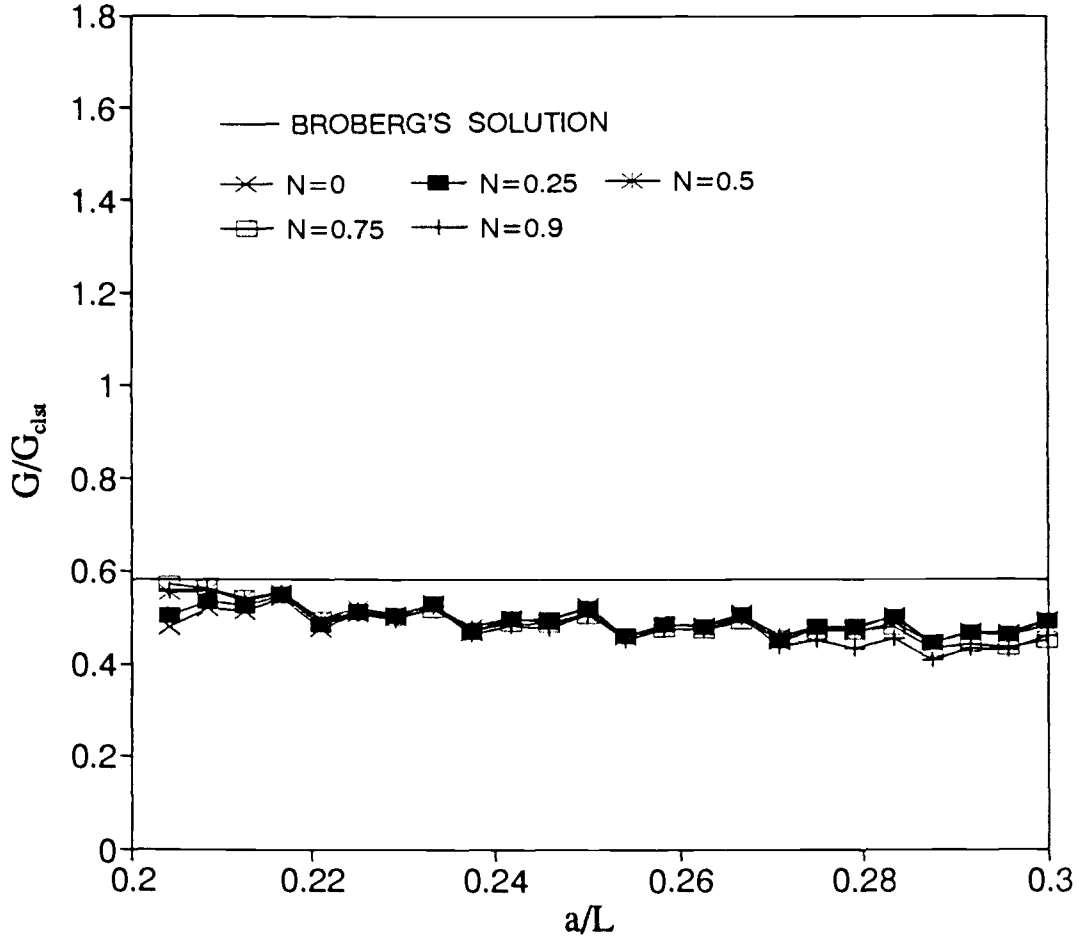

Figure 5.30 Energy release rate versus crack length for a crack propagating at the velocity 0.219 C_d, $a_0/c = 4$.

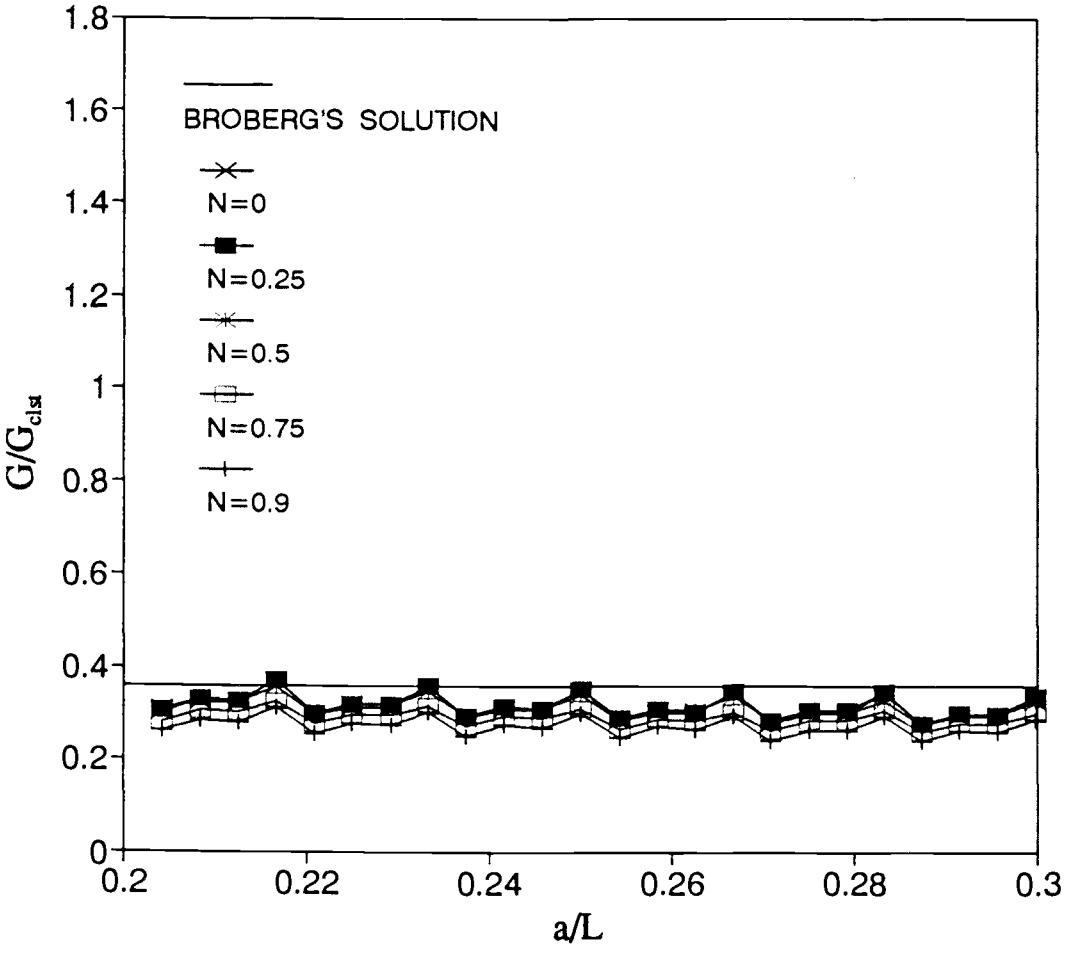

Figure 5.31 Energy release rate versus crack length for a crack propagating at the velocity 0.328 C_d, $a_0/c = 0.25$.

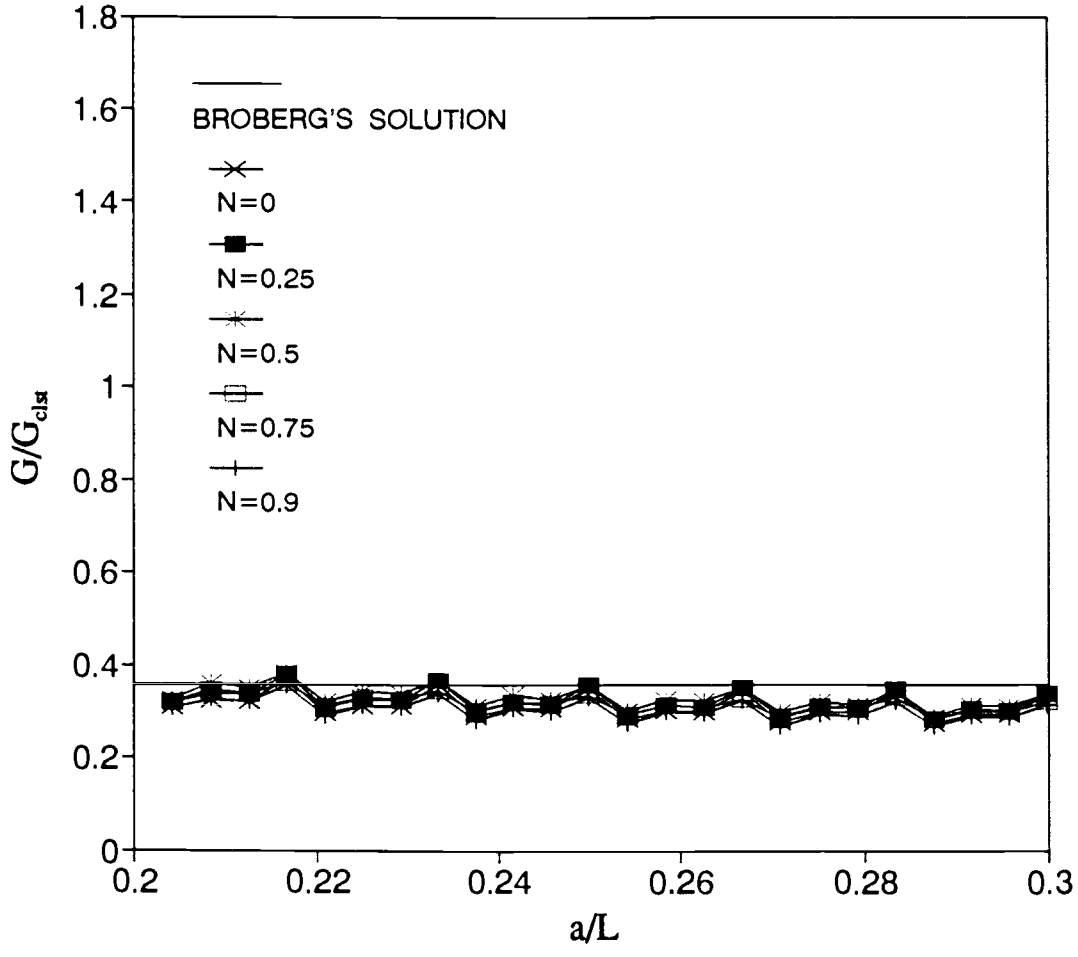

Figure 5.32 Energy release rate versus crack length for a crack propagating at the velocity 0.328 C_d, $a_0/c = 1$.

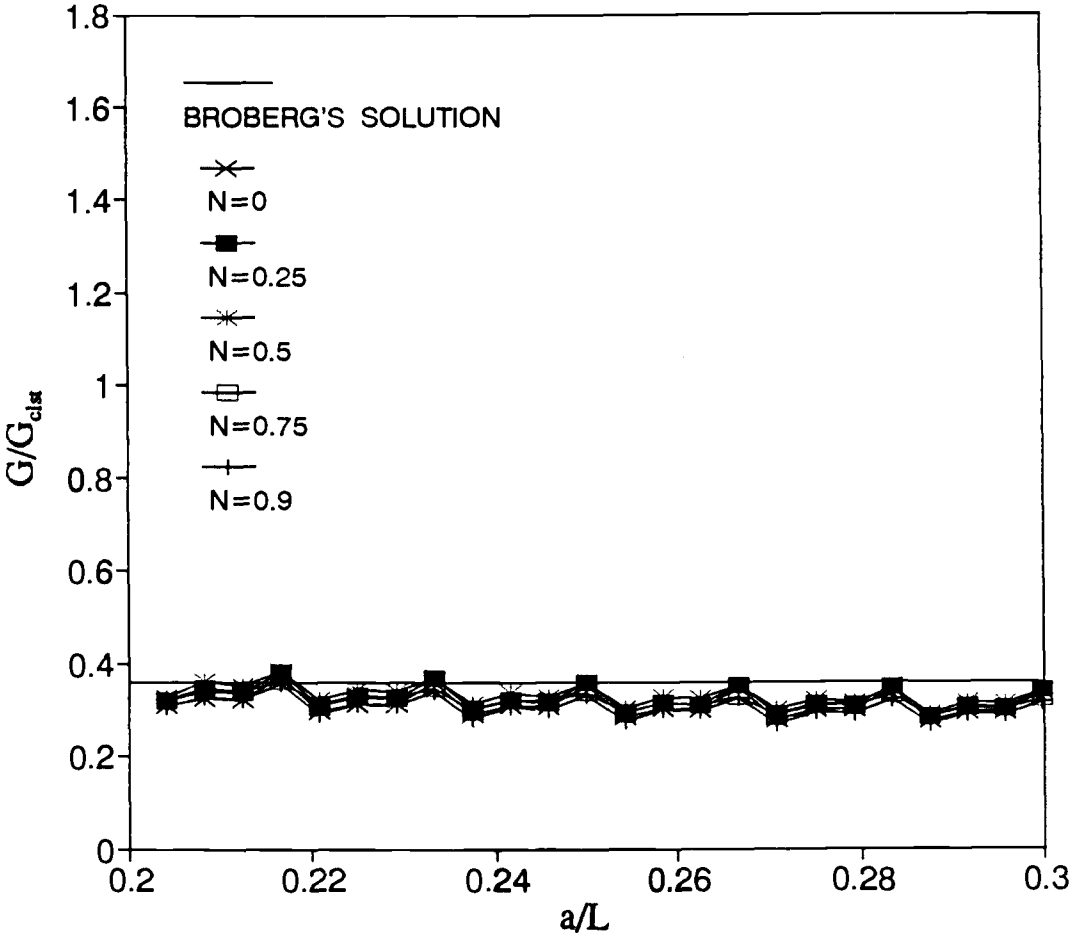

Figure 5.33 Energy release rate versus crack length for a crack propagating at the velocity 0.328 C_d, $a_0/c = 4$.

6. CONCLUSIONS AND DISCUSSION

For the current study, a dynamic finite element method for plane-strain micropolar elasticity theory was developed, based upon the use of a virtual work principle for a two-dimensional, eight-node, isoparametric quadrilateral element, with three degrees of freedom (i.e., two displacements and one microrotation independent of displacements) for each node. The Newmark time integration scheme and a consistent mass matrix were employed in the development of the finite element program. The effects of micropolar elasticity could be of considerable importance where large gradients in stress occur over distances that are of the same order of magnitude as the internal structure of the material. This is a likely occurrence in particulate composites, or in other fibrous materials containing small flaws or holes.

The feasiblity of this program was examined by comparing its predictive abilities to finite difference solutions for the problem of micropolar half-spaces, the surfaces of which were subject to shear stresses that were uniform and harmonic in time. Transient solutions obtained by the application of two different methods were observed to be in very close agreement.

The occurrence of a suddenly applied, normal stress on the surface of a plate containing circular or elliptical holes was considered. When the micropolar coupling factor N was zero, the solution was almost identical to the case of classical elasticity. The peak stress rate obtained from application of the dynamic finite element method was within one percent of the analytical solution obtained by Baron and Matthews [99]. It was observed that as the influence of the micropolar properties was streng-

thened (i.e., N became larger, while a/c and R/c, respectively, for the case of circular and elliptical holes, became smaller), dynamic stress concentration at the edges of the hole was reduced significantly. Furthermore, as expected in the case of an elliptical hole, larger stress concentrations were obtained in proportion to the narrowness of the elliptical opening.

The method for the calculation of dynamic energy release rates and the linear node-releasing technique were extended to the case of micropolar elasticity. In addition, a stationary crack in a body subject to dynamic, mode-I loading, as well as a body with a static load containing a crack suddenly propagating at constant velocities, were examined. The micropolar effects were found to be most pronounced in those cases where the crack length was not significantly larger than the characteristic dimensions of the material microstructure; that is, a/c was small. For the case of a dynamically loaded stationary crack, it was determined that the micropolar effects influenced the reduction of the dynamic energy release rate by as much as 55 percent $(a/c = 0.25,\ N = 0.9)$. The maximum energy release rate obtained by application of the dynamic finite element program for the case $N = 0$ (i.e., identical to the case of classical elasticity) was compared to a known analytical solution [103], resulting in agreement within a range of two percent. Moreover, increase in the coupling factor N resulted in the lowering of the maximum dynamic energy release rate. For the case of a crack propagating at a constant velocity, the micropolar effects exercise an equally dramatic influence in reducing the energy release rate for a low velocity crack. However, these effects became less pronounced in proportion to the increase in the velocity of crack propagation. The significance of these results can be assessed only by the development of a comprehensive method for the analysis of relationships between micropolar elastic constants and microstructural properties.

The following recommendations for areas of further study are included. The full understanding of relationships between micropolar elastic moduli and microstructural properties will be derived only from further experimentation. To date, the determination of the properties of micropolar materials has been the subject of several investigations [102,105-108]. However, additional experimental inquiry will be required for full evaluation of the usefulness of the theory of micropolar elasticity as a model for materials with relatively large internal structures. In the area of dynamic fracture mechanics in micropolar elasticity, methods for the evaluation of dynamic stress intensity factors, and the determination of the relationship between dynamic energy release rates and stress intensity factors, should be the subject of further study. Finally, it is recommended that improved and increasingly accurate methods for the simulation of propagating cracks be developed.

REFERENCES

[1] A.C. Eringen and E.S. Suhubi, Non-linear theory of microelastic solids--I, *Int. J. Eng. Sci. 2*, 189-203 (1964).

[2] A.C.Eringen and E.S. Suhubi, Non-linear theory of microelastic solids--II, *Int.J.Eng.Sci.2* , 389-404 (1964).

[3] A.C. Eringen, Linear theory of micropolar elasticity, *J. Math. Mech. 15*, 909-923 (1966).

[4] A.C. Eringen, Theory of micropolar elasticity, in *Fractures*, Vol.2 (Edited by H.Liebowitz), Academic Press, New York, 621-729 (1968).

[5] R.D. Mindlin, Influence of couple stress on stress concentrations, *Exp. Mech. 3*, 1-7 (1963).

[6] P.N. Kaloni and T. Ariman, Stress concentration effects in micropolar elasticity, *Z. Angew. Math. Phys. 18*, 136-141 (1967).

[7] B.S. Kim and A.C. Eringen, Stress distribution around an elliptic hole in an infinite micropolar elastic plate, *Lett. Appl. Engr. Sci. 1*, 381-390 (1973).

[8] E. Sternberg and R. Muki, The effect of couple stress on the stress concentration around a crack, *Int. J. Sol. Struct. 3*, 69-95 (1967).

[9] C. Atkinson and F.G. Leppington, The effect of couple stresses on the tip of cracks, *Int. J. Sol. Struct. 13*, 1103-1122 (1977).

[10] H.S. Paul and K. Sridharan, The penny-shaped crack problem in micropolar elasticity, *Int. J. Engr. Sci. 18*, 651-664 (1980).

[11] J. Sladec and V. Sladec, The effect of couple stresses on the stress field around a penny-shaped crack, *Int. J. Fract. 25*, 109-119 (1984).

[12] D.J. Malcolm, Orthotropic fiber composite as micromorphic materials, *Int. J. Engr. Sci. 20*, 1111-1124 (1982).

[13] L.R. Hermann, Mixed finite elements for couple stress theory, in *Hybrid and Mixed Finite Element Methods* (Edited by S.N. Atluri et al.), John Wiley & Sons, 1-17 (1983).

[14] S. Nakamura, R. Benedict, and R. Lakes, Finite element method for orthotropic micropolar elasticity, *Int. J. Engr. Sci. 22*, 319-330 (1984).

[15] T.C. Kennedy and J.B. Kim, Finite element analysis of a crack in a micropolar elastic material, in *Computers in Engineering 1987*, Vol.3 (Edited by R. Raghavan and T.J. CoKonis), ASME, New York, 439-444 (1987).

[16] S. Nakamura and R.S. Lakes, Finite element analysis of stress concentration around a blunt crack in a Cosserat elastic solid, *Comp. Meth. Appl. Mech. Engr. 66*, 257-266 (1988).

[17] R.S. Wood, Finite element analysis of plane couple stress problems using first order stress functions, *Int. J. Num. Meth. Engr. 26*, 489-509 (1988).

[18] G.C. Sih, *Elastodymic Crack Problems*, in *Mechanics of Fractures*, Vol.4, Noordhoff International Publishing (1977).

[19] M.L. Williams and W.G. Knauss, *Dynamic Fracture*, Martinus Nijhoff Publishers (1985).

[20] M.F. Kanninen and C.H. Popelar, *Advanced Fracture Mechanics*, Oxford University Press, New York (1985).

[21] V.Z. Parton and V.G. Boriskovsky, *Stationary Cracks*, Vol. 1 in *Dynamic Fracture Mechanics*, Hemisphere Publishing Co. (1989).

[22] V.Z. Parton and V.G. Boriskovsky, *Propagating Cracks*, Vol. 2 in *Dynamic Fracture Mechanics*, Hemisphere Publishing Co. (1989).

[23] W. Nowacki, *Theory of Asymmetric Elasticity*, Pergamon Press, New York (1986).

[24] D. Iesan, On the crack propagation in micropolar elastic solids, *Int. J. Engr. Sci. 22*, 547-555 (1984).

[25] K.M. Rao, Longitudinal wave propagation in a micropolar wave guide, *Int. J. Eng. Sci. 26*, 135-141 (1988).

[26] M.DJ. Vukobrat, Conservation laws in micropolar elastodynamics and path-independent integrals, *Int. J. Engr. Sci. 27*, 1093-1106 (1989).

[27] J.R. Rice, A path independent integral and approximate analysis of strain concentration by notches and cracks, *J. Appl. Mech. 35*, 379-386 (1968).

[28] S.Y. Han, M.N.L. Narasimhan, and T.C. Kennedy, Dynamic propagation of a finite crack in a micropolar elastic solid, *Act. Mech. 85*, 179-191 (1990).

[29] T. Belytschko, N. Holmes, and R. Mullen, Explicit integration-stability, solution properties, cost, *AMD, ASME 14*, 1-12 (1975).

[30] J.C. Houbolt, A recurrence matrix solution for the dynamic response of elastic aircraft, *J. Aeronautical Sciences 17*, 540-555 (1950).

[31] N.M. Newmark, A method of computation for structural dynamics, *J. Engr. Mech. 85*, 67-94 (1959).

[32] E.L. Wilson, I. Farhoomand, and K.J. Bathe, *Nonlinear Dynamic Analysis of Complex Structures, Earthquake Engineering and Structural Dynamics*, Vol. 1, 241-252 (1973).

[33] H.M. Hilber, T.J.R. Hughes, and R.L. Taylor, Improved numerical dissipation for time integration algorithms, in *Structural Dynamics,Earthquake Engineering and Structural Dynamics*, Vol. 5, 283-292 (1977).

[34] H.M. Hilber and T.J.R. Hughes, Collocation dissipation and overshoot for time integration scheme, in *Structural Dynamics, Earthquake Engineering and Structural Dynamics*, Vol. 6, 99-118 (1978).

[35] G. Bazzi, and E. Anderheggen, The ρ-family of algorithms for time step integration with improved numerical dissipation, in *Earthquake Engineering and Structural Dynamics 10*, 10, 537-550 (1982).

[36] K.C. Park, An improved stiffy-stable method for direct integration of nonlinear structural dynamics equations, *J. Appl. Mech. 42*, 464-470 (1975).

[37] C.W. Gear, *Numerical Initial Value Problems in Ordinary Differential Equations*, Prentice Hall, Englewood Cliffs, NJ (1971).

[38] O.C. Zienkiewicz, W.L. Wood, N.W. Hine, and R.L. Taylor, A unified set of single step algorithms, Part I: General formulation and applications, *Int. J. Num. Meth. Engr. 20*, 1529-1552 (1984).

[39] T. Belytschko, and R. Mullen, Mesh partitions of explicit-implicit time integration, formulation and computational algorithms, in *Finite Element Analysis*, M.I.T. Press, Cambridge, MA, 673-690 (1977).

[40] T.J.R. Hughes, and W.K. Liu, Implicit-explicit finite elements in transient analysis, *J. Appl. Mech. 45*, 371-378 (1978).

[41] W.K. Liu, and T. Belytschko, Mixed-time implicit-explicit finite elements, in *Transient Analysis, Computers and Structures*, Vol. 5, 445-450 (1982).

[42] T. Belytschko, B.E. Engelmann, and W.K. Liu, A review of recent developments in time integration, in *State of the Art Surveys on Computational Mechanics*, Ed. A.K. Noor, ASME, New York (1988).

[43] K.J. Bathe, *Finite Element Procedures in Engineering Analysis*, Prentice Hall, Englewood Cliffs, NJ (1982).

[44] R.D. Cook, D.S. Malkus, and M.E. Plesha, *Concepts and Applications of Finite Element Analysis* (3rd ed.), John Wiley & Sons, New York (1989).

[45] T.J.R. Hughes, *The Finite Element Method-Linear Static and Dynamic Finite Element Analysis*, Prentice Hall, Englewood Cliffs, NJ (1987).

[46] W.B. Bickford, *A First Course in the Finite Element Method*, IRWIN, Homewood, IL (1990).

[47] O.C. Zienkiewicz, and R.L. Taylor, *Solid and Fluid Mechanics Dynamics and Nonlinearity*, in Vol. 2, *The Finite Element Method*, 4th ed.: McGraw Hill, London (1991).

[48] J.S. Archer, Consistent mass matrix for distributed systems, *Proceedings of ASCE*, Vol. 89, 161-178 (1963).

[49] J.S. Archer, Consistent matrix formulation for structural analysis using finite element techniques, *AIAA J. 3*, 1910-1918 (1965).

[50] E. Hinton, T. Rock, and O.C. Zienkiewicz, A note on mass lumping and related processes in finite element method, in *Earthquake Engineering Structural Dynamics*, Vol. IV, 245-249 (1976).

[51] I. Fried, and D.S. Malkus, Finite element mass matrix lumping by numerical integration without convergence rate loss, *Int. J. Solids. Struct. 11*, 461-466 (1976).

[52] D.S. Malkus, and M.E. Plesha, Zero and negative masses in finite element vibration and transient analysis, *Comp. Meth. Appl. Mech. Engng. 59*, 281-306 (1986).

[53] D.S. Malkus, M.E. Plesha, and M.R. Liu, Reversed stability conditions in transient finite element analysis, *Comp. Meth. Appl. Mech. Engng. 68*, 97-114 (1988).

[54] M.F. Kanninen, A critical appraisal of solution techniques in dynamic fracture mechanics, in *Proceedings of the 1st International Conference on Numerical Methods in Fracture Mechanics* (Edited by A.R. Luxmoore and D.R.J. Owen), Swansea, 612-633 (1978).

[55] S.N. Atluri and T. Nishioka, Numerical studies in dynamic fracture mechanics, *Int. J. Fract. 27*, 245-261 (1985).

[56] H. Liebowitz and E.T. Moyer, Jr., Finite element methods in fracture mechanics, *Computers & Structures 31*, 1-9 (1989).

[57] R.D. Henshell and K.G. Shaw, Crack-tip elements are unnecessary, *Int. J. Num. Meth. Engng. 9*, 495-507 (1975).

[58] R.S. Barsoum, On the use of isoparametric finite elements in linear fracture mechanics, *Int. J. Num. Meth. Engng. 10*, 25-37 (1976).

[59] R.S. Barsoum, Triangular quarter-point elements as elastic and perfectly-plastic crack-tip element, *Int. J. Num. Meth. Engng. 11*, 85-98 (1977).

[60] S. Mall, Dynamic finite element analysis of cracked bodies with stationary cracks, *ASTM-STP 700*, 453-465 (1980).

[61] V. Murti and S. Valliappan, The use of quarter point element in dynamic crack analysis, *Engr. Fract. Mech. 23*, 585-614 (1986).

[62] J.D. Morgan, J.M. Anderson, and W.W. King, Elastodynamics of cracked structures using finite elements, *AIAA J. 12*, 1767-1769 (1974).

[63] S. Aoki, K. Kishimoto, H. Kondo, and M. Sakata, Elastodynamic analysis of crack by finite element method using singular element, *Int. J. Fract. 14*, 59-68 (1978).

[64] Z.P. Bazant, J.L. Glazik, and J.D. Achenbach, Elastodynamic fields near running cracks by finite elements, *Computers & Structures 8*, 193-198 (1978).

[65] W.W. King and J.E. Malluck, Toward a singular element for propagating cracks, *Int. J. Fract. 14*, R7-R11 (1978).

[66] S.N. Atluri and T. Nishioka, Dyanmic fracture analysis: A translating singularity finite element procedure, in *Proceedings of the 2nd International Conference on Numerical Methods in Fracture Mechanics* (Edited by D.R.J. Owen and A.R. Luxmoore), Swansea, 2163-2170 (1980).

[67] T. Nishioka and S.N. Atluri, Numerical modeling of dynamic crack propagation in finite bodies, by moving singular elements, Part 1: Formulation, *J. Appl. Mech. 47*, 570-576 (1980).

[68] T. Nishioka and S.N. Atluri, Numerical modeling of dynamic crack propagation in finite bodies, by moving singular elements, Part 2: Results, *J. Appl. Mech. 47*, 577-582 (1980).

[69] T. Nishioka, R.B. Stonesifer, and S.N. Atluri, An evaluation of several moving singularity finite element models for fast fracture analysis, *Engr. Frac. Mech. 15*, 205-218 (1981).

[70] T. Nishioka and S.N. Atluri, A numerical study of the use of path independent integrals in elastodynamic crack propagation, *Engr. Fract. Mech. 18*, 23-33 (1983).

[71] T. Nishioka and S.N. Atluri, Path-independent integrals, energy release rates, and general solutions of near-tip fields in mixed-mode dynamic fracture mechanics, *Engr. Fract. Mech. 18*, 1-22 (1983).

[72] T. Nishioka, Y. Takemoto, and R. Murakami, The dynamic J integral and its use in finite element simulation of dynamic crack propagation, *ASME-PVP 160*, 117-125 (1990).

[73] K. Kishimoto, S. Aoki, and M. Sakata, On the path independent integral $\hat{J}$, *Engr. Fract. Mech. 13*, 841-850 (1980).

[74] D.R.J. Owen and D. Shantaram, Numerical study of dynamic crack growth by the finite element method, *Int. J. Fract. 13*, 821-837 (1977).

[75] P.N.R. Keegstra, J.L. Head, and C.E. Turner, A two dimensional dynamic linear elastic finite element program for the analysis of unstable crack propagation and arrest, in *Proceedings of the 1st International Conference on Numerical Methods in Fracture Mechanics* (Edited by A.R. Luxmoore and D.R.J. Owen), Swansea, 634-647 (1978).

[76] J.F. Malluck and W.W. King, Fast fracture simulated by a finite element analysis which accounts for crack-tip energy dissipation, *Proceedings of the 1st International Conference on Numerical Methods in Fracture Mechanics* (Edited by A.R. Luxmoore and D.R.J. Owen), Swansea, 648-659 (1978).

[77] G. Rydholm, B. Fredriksson, and F. Nilsson, Numerical investigations of rapid crack propagation, *Proceedings of the 1st International Conference on Numerical Methods in Fracture Mechanics* (Edited by A.R. Luxmoore and D.R.J. Owen), Swansea, 660-672 (1978).

[78] A.S. Kobayashi, S. Mall, Y. Urabe, and A.F. Emery, a numerical dynamic fracture analysis of three wedge-loaded DCB specimens, *Proceedings of the 1st International Conference on Numerical Methods in Fracture Mechanics* (Edited by A.R. Luxmoore and D.R.J. Owen), Swansea, 673-684 (1978).

[79] J.F. Malluck and W.W. King, Fast fracture simulated by convential finite elements: A comparison of two energy release algorithms, *ASTM-STP 711*, 39-53 (1980).

[80] L. Hodulak, A.S. Kobayashi, and A.F. Emery, A critical examination of a numerical fracture dynamic code, *ASTM-STP 700*, 174-188 (1980).

[81] S. Mall and J. Luz, Use of an eight-node element for fast fracture problems, *Int. J. Fract. 16*, R33-R36 (1980).

[82] G.R. Irwin, Analysis of stresses and strains near the end of a crack traversing a plate, *J. Appl. Mech. 24*, 361-364 (1957).

[83] G.C. Sih and R.J. Hartranft, Variation of strain energy release rate with plate thickness, *Int. J. Fract. 9*, 75-82 (1973).

[84] E.F. Rybicki and M.F. Kanninen, A finite element calculation of stress intensity factors by a modified crack closure integral, *Engr. Fract. Mech. 9*, 931-938 (1977).

[85] C.J. Jih and C.T. Sun, Evaluation of a finite element based crack-closure method for calculating static and dynamic strain energy release rates, *Engr. Fract. Mech. 37*, 313-322 (1990).

[86] A.C. Eringen, Micropolar continua, in *Continuum Physics*, Vol. 4 (Ed. by A.C. Eringen), Academic Press, New York (1976).

[87] S.C. Cowin, An incorrect inequality in micropolar elasticity theory, *J. Appl. Math. Physics 21*, 494-497 (1970).

[88] E. Hinton and D.R.J. Owen, *Finite Element Programming*, Academic Press, New York (1977).

[89] R.L. Kuhlemeyer and J. Lysiner, Finite element method accuracy for wave propagation problems, *ASCE J. Soil Mech. Found. Div. 99*, 421-429 (1973).

[90] G. Segol, J.F. Abel, and P.C.Y. Lee, Finite element mesh gradation for surface waves, *ASCE J. Geo. Engr. Div. 101*, 1177-1181 (1975).

[91] Z.P. Bazant and J.L. Glazik, Finite element analysis of wave diffraction by a crack, *J. Eng. Mech. 102*, 479-496 (1976).

[92] Z.P. Bazant and Z. Celep, Spurious reflections of elastic waves in nonuniform meshes of constant and linear strain finite elements, *Comp. Struc. 15*, 451-459 (1982).

[93] R. Mullen and T. Belytschko, Dispersion analysis of finite element semidiscretizations of the two-dimensional wave equations, *Int. J. Num. Meth. Engr. 18*, 11-29 (1982).

[94] Z. Celep and Z.P. Bazant, Spurious reflection of elastic waves due to gradually changing finite element size, *Int. J. Num. Meth. Engr. 19*, 631-646 (1983)

[95] Z. Celep and D. Turhan, Finite element solution for reflection of plane harmonic waves from the free surface of a half-space, *Comp. Struc. 27*, 593-599 (1987).

[96] J.W. Tedesco, J.R. Hayes, and D.W. Landis, Dynamic response of layered structures subject to blast effects of non-nuclear weaponry, *Comp. Struc. 26*, 79-86 (1987).

[97] F.G. Laturelle, Finite element analysis of wave propagation in an elastic half-space under step loading, *Comp. Struc. 32*, 721-735 (1989).

[98] J.W. Tedesco and D.W. Landis, Wave propagation through layered systems, *Comp. Struc. 32*, 625-638 (1989).

[99] M.L. Baron and A.T. Matthews, Diffraction of a pressure wave by a cylindrical cavity in an elastic medium, *J. Appl. Mech. 28*, 347-354 (1961).

[100] R. Courant, K.O. Friedrichs, and H. Lewy, On the partial differential equations of mathematical physics, *Math. Ann. 100*, 32-74 (1928).

[101] E. Rank, C. Katz, and H. Werner, On the importance of the discrete maximum principle in transient analysis using finite element methods, *Int. J. Num. Meth. Engr. 19*, 1771-1782 (1983).

[102] R.D. Gauthier, Experimental investigations on micropolar media, in *Mechanics of Micropolar Media* (Edited by O. Brulin and R.K.T. Hsieh), World Scientific Publishing, 395-463 (1981).

[103] G.S. Sih, G.T. Embley, and R.S. Ravera, Impact response of a finite crack in plane extension, *Int. J. Sol. Struct. 8*, 977-993 (1972).

[104] K.B. Broberg, The propagation of a brittle crack, *Arkiv for Fysik 18*, 159-192 (1960).

[105] J.F.C. Yang and R.S. Lakes, Transient study of couple stress effects in compact bone: Torsion, *J. Biomech. Engr. 103*, 275-279 (1981).

[106] R.S. Lakes, Dynamical study of couple stress effects in human compact bone, *J. Biomech. Engr. 104*, 6-11 (1982).

[107] J.F.C. Yang and R.S. Lakes, Experimental study of micropolar and couple stress elasticity in compact bone in bending, *J. Biomech. 15*, 91-98 (1982).

[108] R.S. Lakes, Experimental microelasticity of two porous solids, *Int. J. Sol. Struct. 22*, 55-63 (1985).

APPENDICES

Appendix A

Two-Dimensional Gaussian Quadrature

In the finite element method, certain integrals must be evaluated, including equations (3.28)—(3.30), which are, respectively, the mass matrix, the stiffness matrix, and applied nodal force. For reason of their inherent advantages with respect to analytical integration procedures, Gauss quadrature routines were used with two- or three-point integration rules. It should be noted that an n-point rule integrates any polynomial of the degree x^{2n-1}, or less, exactly.

For two dimensions, the integration of a certain function $f(\xi,\eta)$, with respect to ξ and then with respect to η, using the n-point rule, may be expressed as

$$I = \int_{-1}^{1}\int_{-1}^{1} f(\xi,\eta)\,d\xi\,d\eta = \sum_{k=1}^{n}\sum_{l=1}^{n} W_k W_l f(\xi_k,\eta_l) \ , \qquad \text{(A.1)}$$

where ξ and η represent the natural coordinates, W_k and W_l are the weighting factors, ξ_k is the ξ coordinate of the kth Gauss point, and η_l is the η coordinate of the lth Gauss point. For the three-point rule, the weighting factors are 5/9, 8/9, and 5/9, respectively, for the three Gauss points $-\sqrt{0.6}$, 0, and $\sqrt{0.6}$. For the two-point rule, the weighting factor was 1 for both Gauss points (i.e., $\pm 1/\sqrt{3}$).

The finite element mesh shown in Figure 5.2 was used to compare the effects of the use of either the two- or three-point rule. The size of the mesh was 0.356 m in width and 0.178 m in height, with a hole radius of 0.025 m; the Young's modulus was 68.96 GPa, the Poisson's ratio was 0.25, and the mass density was 2768 Kg/m^3. The Newmark parameters β and γ were, respectively, 0.25 and 0.5, indicating that

algorithmic damping was not applied. A time-step size of 1 microsecond was used and the results are shown in Figure A.1. The use of four-point integration (i.e., the two-point rule in two-dimensional space) caused more high frequency oscillations than the use of nine-point integration (i.e., the three-point rule in two-dimensional space). Thus, the three-point rule was adopted for use in this study.

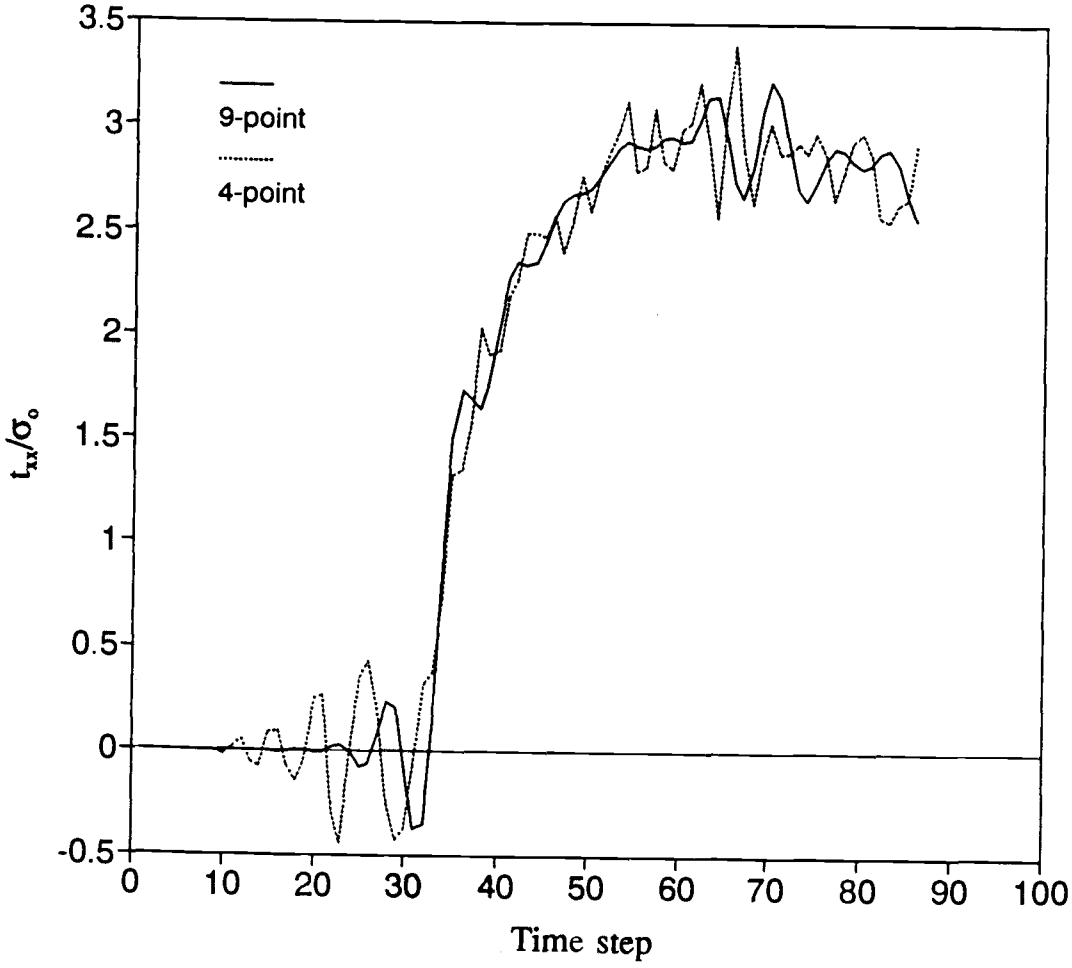

Figure A.1 Comparisons between 9-point and 4-point integration.

Appendix B

Examples of Explicit vs. Implicit Time Integration and Consistent Mass vs. Lumped Mass

Examples of comparisons between the use of explicit (i.e., the central difference method) and implicit time integration schemes (i.e., the Newmark method) with either lumped or consistent mass matrices are considered.

Figure B.1 shows the finite element mesh used for the first example, in which a plate, 0.254 m in width and 0.152 m in height, under suddenly applied normal harmonic loads (magnitude = 44.5 N, frequency = 1.0×10^5 sec^{-1}) was considered. The Young's modulus was 3.79 GPa, the Poisson's ratio was 0.4, and the dilatational wave speed was 1926 m/sec. A time-step of 3 microseconds was selected to satisfy the conditions described in Chapter 3.

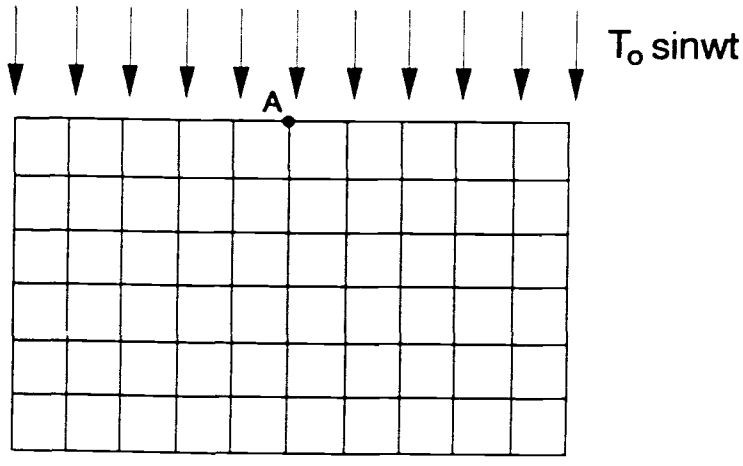

Figure B.1 Finite element mesh for a plate under normal harmonic loads.

The results of vertical displacements at point A are shown in Figure B.2 for three cases: 1) The Newmark method with consistent mass in the absence of algorthmic damping (i.e., $\beta = 0.25$ and $\gamma = 0.5$); 2) the explicit method with consistent mass matrix; and 3) the explicit method with lumped mass matrix.

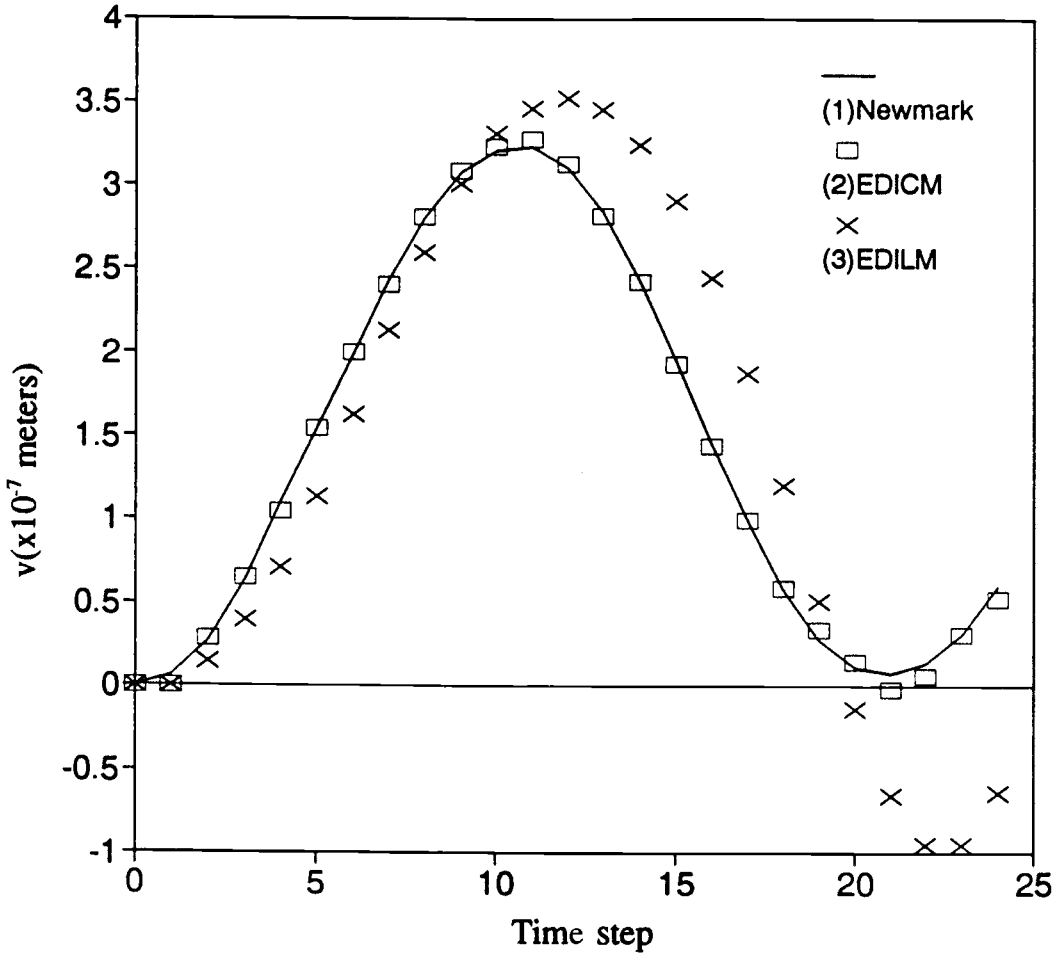

Figure B.2 Vertical displacements using: 1) Newmark time integration and consistent mass; 2) Explicit time integration and consistent mass; 3) Explicit time integration and lumped mass.

Among the three cases considered in Figure B.2, the combination of the Newmark integration scheme and a consistent mass matrix generated the results which were closest to those obtained for a known analytical solution (i.e., a maximum value of 3.05×10^{-7} m); the use of the explicit method with a lumped mass generated the least favorable results. Since, for reason of the stability problem, the explicit method requires smaller time steps than the implicit method, a smaller time step (i.e., 0.3 microseconds) was used for the second and third cases. The corresponding Courant number was 0.023 and approximately 200 point per cycle of applied load were used. Figure B.3 indicates that for these cases, compared to the values used for Figure B.1, there was no solution improvement.

To determine the effect of mass matrices (i.e., a consistent mass matrix and a special lumped mass matrix) when used with the Newmark time integration method, the problem outlined in Appendix A, for $\nu = 0.0$, was considered. As shown in Figure B.4, the results obtained with the lumped mass were close to those obtained with a consistent mass. When compared to the known analytical solution (i.e., maximum value = 3.28) of Baron and Matthews [99], the lumped mass matrix produced fewer spurious oscillations and yielded magnified maximum value. However, since the use of a lumped mass with the Newmark method requires a matrix solver, this approach resulted in no savings in computational time.

The procedures to generate a lumped mass matrix (i.e., using the HRZ special lumping technique [50]) are as follows: 1) Compute only the diagonal coefficients of the consistent mass matrix and calculate the total mass for the element, m; 2) compute a number s by adding the diagnonal coefficients m_{kk} associated with translational degrees of freedom that are mutually perpendicular in the same direction; and 3) scale all diagonal coefficients by multiplication by the ratio m/s. These procedures produce a reliable positive diagonal mass matrix.

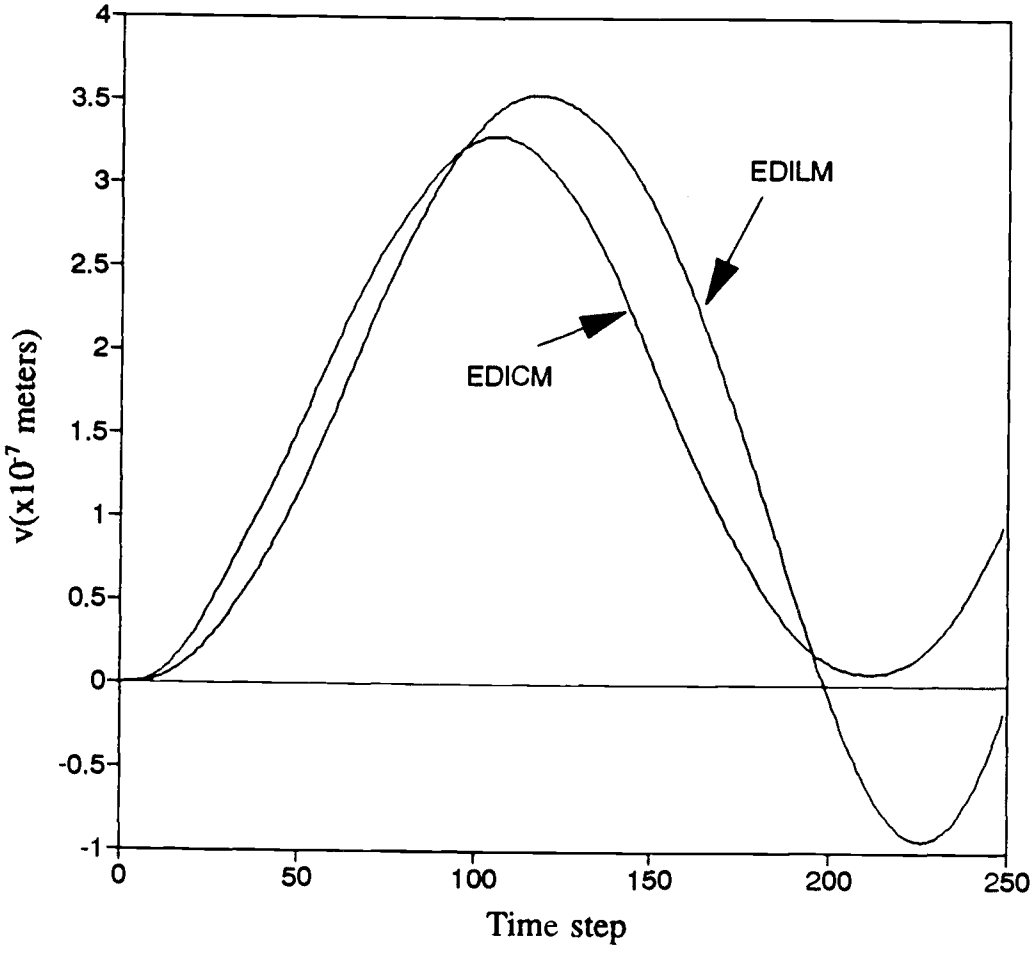

Figure B.3 Vertical displacements using smaller time step size.

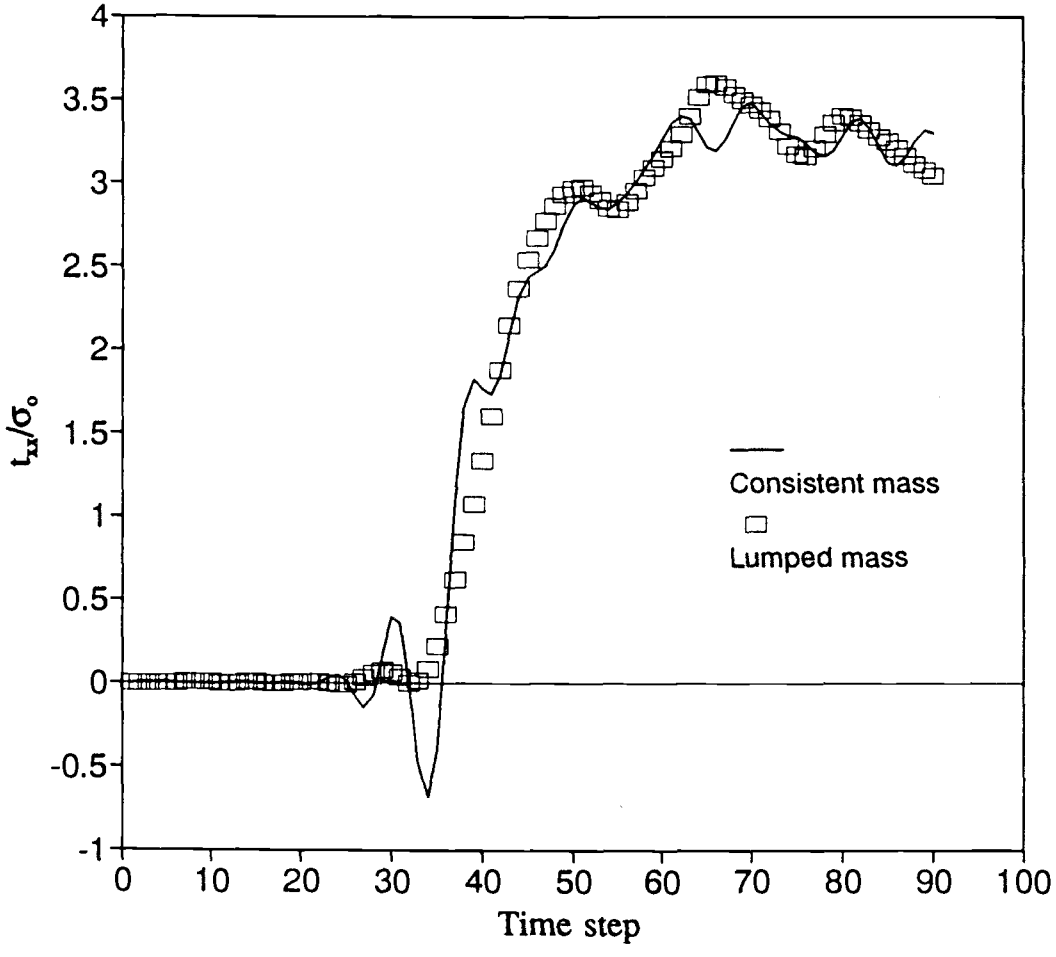

Figure B.4 Consistent vs. lumped mass (applied with the Newmark method).

Appendix C

Effect of Newmark Parameters for Stress Concentrations Around a Circular Hole

Three sets of Newmark parameters were tested for the solution of the problem proposed in Appendix A: 1) $\beta = 0.25$ and $\gamma = 0.5$ (i.e., in the absence of algorithmic damping); 2) $\beta = 0.3025$ and $\gamma = 0.6$; and 3) $\beta = 0.36$ and $\gamma = 0.7$. From Figure C.1, the use of option 3 produced the most apparently favorable results without degradation of accuracy. Thus, it was concluded that the use of a proper damping algorithm is necessary for the suppression of undesired spurious oscillations, an effect which was readily apparent in option 1.

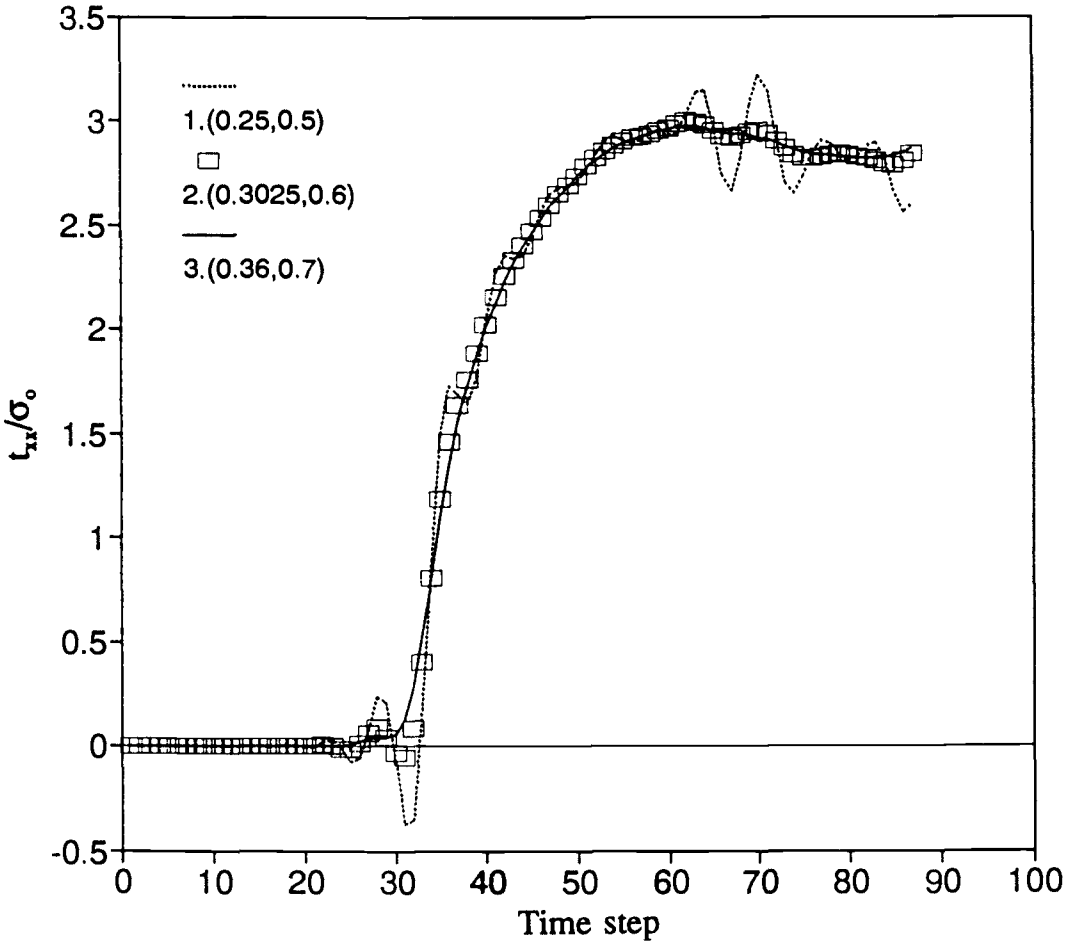

Figure C.1 Comparison of three damping ratios: 1) $\beta = 0.25$ and $\gamma = 0.5$; 2) $\beta = 0.3025$ and $\gamma = 0.6$; and 3) $\beta = 0.36$ and $\gamma = 0.7$.

Appendix D

Examples of Time Step Sizes for the Newmark Method

Since the Newmark method is unconditionally stable, only the Courant condition, equation (3.42), need be considered. As shown in Figure 5.2, the problem of stress concentration around a circular hole was analyzed. The size of the mesh was 35.56 mm width and 17.78 mm height, with a hole radius of 2.54 mm. The dilatational wave speed (C_d) was 126.37 m/sec and three different time step sizes were considered: Δt at 1, 2, and 3 microseconds. The smallest element (h) was 0.51 mm, thus the corresponding Courant numbers ($\rho_c = (C_d \cdot \Delta t)/h$) were, respectively, 0.25, 0.5, and 0.75.

The results, as shown in Figure D.1, indicated that there were no significant differences among the three outputs, although the case of $\Delta t = 3$ microseconds produced slightly fewer spurious oscillations at the early time steps. It should be noted that a second-order scheme of time integration accuracy was used since algorithmic damping was not employed for this experiment.

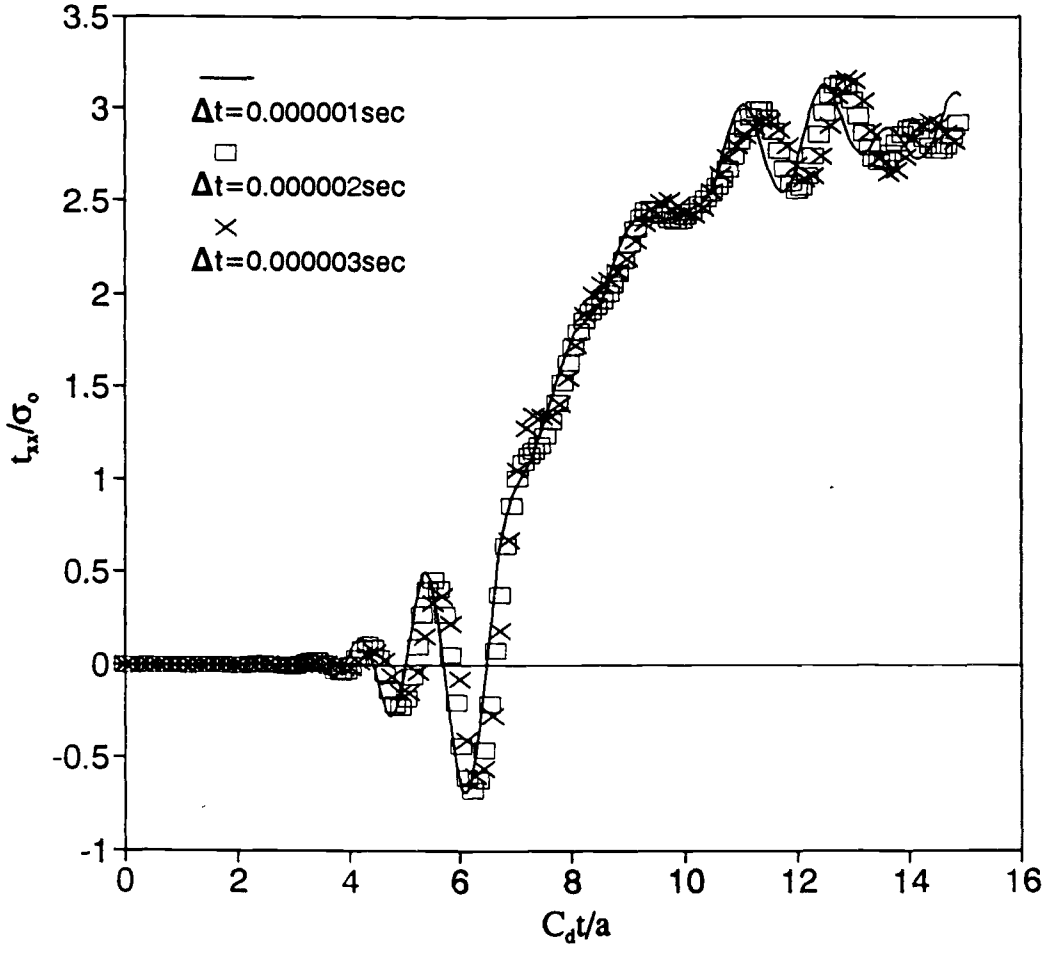

Figure D.1 Three time steps used for the problem of stress concentration around a circular hole in the absence of damping.

Appendix E

Nowacki's Steady-State Solution

Nowacki [23] investigated the problem of the coupled transverse shear wave in a micropolar elastic half-space (section 3.4, Figure 3.2), the field equations for which are:

$$(\mu + \kappa)\frac{\partial^2 v}{\partial x^2} - \kappa\frac{\partial \phi}{\partial x} = \rho\frac{\partial^2 v}{\partial t^2} \tag{E.1}$$

and

$$\gamma\frac{\partial^2 \phi}{\partial x^2} + \kappa\frac{\partial v}{\partial x} - 2\kappa\phi = \rho j\frac{\partial^2 \phi}{\partial t^2}\ , \tag{E.2}$$

where μ, κ, and γ are micropolar elastic constants, ρ and j, respectively, are density and microinertia, v is displacement in the y-direction, and ϕ is microrotation perpendicular to the xy-plane. The boundary conditions on the plane $x = 0$ are

$$t_{xy} = (\mu + \kappa)\frac{\partial v}{\partial x} - \kappa\phi = -T_0 e^{-i\omega t} \tag{E.3}$$

and

$$m_{xz} = \gamma\frac{\partial \phi}{\partial x} = 0\ , \tag{E.4}$$

where T_0 and ω are the magnitude and frequency of applied harmonic force.

Harmonic solutions for the wave equation,

$$v = V e^{-i(\omega t - kx)} \tag{E.5}$$

and

$$\phi = \Phi e^{-i(\omega t - kx)} , \tag{E.6}$$

are immediately considered. Substituting equations (E.5) and (E.6) into equations (E.1) and (E.2) and rearranging gives

$$\left(\sigma_2^2 - k^2\right) V - isk\,\Phi = 0 \tag{E.7}$$

and

$$ipk\,V + \left(\sigma_4^2 - k^2 - 2p\right)\Phi = 0 , \tag{E.8}$$

where $s = \kappa/(\mu+\kappa)$, $p = \kappa/\gamma$, $\sigma_2 = \omega/c_2$, $\sigma_4 = \omega/c_4$, $c_2 = \sqrt{(\mu+\kappa)/\rho}$, and $c_4 = \sqrt{\gamma/\rho j}$. Equations (E.7) and (E.8) are then written in matrix form as

$$\begin{bmatrix} (\sigma_2^2 - k^2) & -isk \\ ipk & (\sigma_4^2 - k^2 - 2p) \end{bmatrix} \begin{Bmatrix} V \\ \Phi \end{Bmatrix} = \begin{Bmatrix} 0 \\ 0 \end{Bmatrix} . \tag{E.9}$$

The determinant of equation (E.9) should be zero for a nontrivial solution of V and Φ:

$$k^4 - \left(\sigma_2^2 + \sigma_4^2 + p(s-2)\right)k^2 + \sigma_2^2\left(\sigma_4^2 - 2p\right) = 0 . \tag{E.10}$$

Solving the biquadratic equation (E.10) results in

$$k_{1,2}^2 = \frac{1}{2}\left[\sigma_2^2+\sigma_4^2+p(s-2) \pm \sqrt{(\sigma_2^2+\sigma_4^2+p(s-2))^2-4\sigma_2^2(\sigma_4^2-2p)}\right] . \tag{E.11}$$

The phase velocity v_β is defined by

$$v_\beta = \frac{\omega}{k_\beta} , \qquad \beta = 1, 2$$

and two positive values for k_1 and k_2 can be obtained from equation (E.11) if the following condition is satisfied:

$$\sigma_4^2 - 2p > 0 , \qquad (\text{i.e., } \omega^2 > \omega_0^2)$$

where the critical frequency ω_0 is $\sqrt{2\kappa/\rho j}$.

Solutions for equations (E.1) and (E.2) may be expressed by the linear superpositions:

$$v = V_1 e^{-i(\omega t - k_1 x)} + V_2 e^{-i(\omega t - k_2 x)} \tag{E.13}$$

and

$$\phi = \Phi_1 e^{-i(\omega t - k_1 x)} + \Phi_2 e^{-i(\omega t - k_2 x)} . \tag{E.14}$$

Substituting equations (E.13) and (E.14) into equations (E.1) and (E.2), and equating each part, respectively, results in

$$\left(k_1^2 - \sigma_2^2\right)V_1 + isk_1\Phi_1 = 0 , \tag{E.15}$$

$$\left(k_2^2 - \sigma_2^2\right)V_2 + isk_2\Phi_2 = 0 , \tag{E.16}$$

$$ipk_1 V_1 + \left(\sigma_4^2 - 2p - k_1^2\right)\Phi_1 = 0 , \tag{E.17}$$

and

$$ipk_2 V_2 + \left(\sigma_4^2 - 2p - k_2^2\right)\Phi_2 = 0 . \tag{E.18}$$

Substituting boundary conditions, equations (E.3) and (E.4), into equations (E.1) and (E.2), based upon equations (E.15)—(E.18), provides the solutions

$$v = V_1 e^{-i(\omega t - k_1 x)} + \frac{isk_2}{\sigma_2^2 - k_2^2}\Phi_2 e^{-i(\omega t - k_2 x)} \tag{E.19}$$

and

$$\phi = \frac{(\sigma_2^2 - k_1^2)}{isk_1} V_1 e^{-i(\omega t - k_1 x)} + \Phi_2 e^{-i(\omega t - k_2 x)} , \tag{E.20}$$

where

$$\Phi_2 = \frac{-T_0 k_1 p}{(k_2 - k_1)\left((\mu + \alpha)(\sigma_4^2 - 2p + k_1 k_2) + 2\alpha p\right)} \tag{E.21}$$

and

$$V_1 = -\Phi_2 \frac{isk_2}{(\sigma_2^2 - k_1^2)} . \tag{E.22}$$

Equations (E.19) and (E.20) are the harmonic displacement and microrotation solutions for the field equations (E.1) and (E.2), and the force and couple stresses, respectively, t_{xy}, t_{yx}, and m_{xz}, m_{zx} may be computed by equations (2.9) and (2.20).

Note that the transient solution for equations (E.1) and (E.2) may be obtained from the use of both the boundary conditions and the initial conditions, which are not considered in this harmonic solution procedure. A transient solution is not available from the literature, nor would such a solution appear to be easy to generate.

Appendix F

Dynamic Finite Element Program for Plane-Strain Micropolar Elasticity Theory

```
      PROGRAM DYCOUPLE
C-----------------------------------------------------------------------
C     PROGRAM DYCOUPLE.FOR
C     Dynamic finite element method for micropolar elasticity theory.
C     This program includes crack closure integral algorithm to
C     calculate dynamic energy release rate.
C     Note: 1) Each node has three-degrees of freedom in
C              two-dimensional space.
C           2) Plane-strain condition is applied.
C           3) Step pressure type load is used.
C-----------------------------------------------------------------------
C
      INCLUDE 'JEIBI.INC'
      DIMENSION TITLE(80)
      COMMON/ENERGY/NSEL(4),DLC
      OPEN(1,FILE='FILE1',STATUS='NEW',FORM='UNFORMATTED')
      OPEN(2,FILE='FILE2',STATUS='NEW',FORM='UNFORMATTED')
      OPEN(3,FILE='FILE3',STATUS='NEW',FORM='UNFORMATTED')
      OPEN(4,FILE='FILE4',STATUS='NEW',FORM='UNFORMATTED')
      OPEN(5,FILE='DYCOUP.DAT',STATUS='OLD')
      OPEN(6,FILE='DYCOUP1.OUT',STATUS='NEW')
      OPEN(7,FILE='FILE7',STATUS='NEW',FORM='UNFORMATTED')
      OPEN(9,FILE='DYCOUP2.OUT',STATUS='NEW')
      OPEN(10,FILE='DYCOUP3.OUT',STATUS='NEW')
      OPEN(11,FILE='DYCOUP4.OUT',STATUS='NEW')
      OPEN(12,FILE='DYCOUP5.OUT',STATUS='NEW')
      READ(5,900) NPROB
  900 FORMAT(I5)
      WRITE(6,905) NPROB
  905 FORMAT(1H0,5X,23HTOTAL NO. OF PROBLEMS =,I5)
      DO 20 IPROB=1,NPROB
      REWIND (1)
      REWIND (2)
      REWIND (3)
      REWIND (4)
      REWIND (7)
      READ(5,910) TITLE
  910 FORMAT(80A1)
      WRITE(6,915) IPROB,TITLE
```

```
  915 FORMAT(//////,6X,12HPROBLEM NO. ,I3,10X,80A1)
C
C     CALL THE SUBROUTINE WHICH READS MOST OF
C     THE PROBLEM DATA
C
      CALL INPUT
C
C     NEXT CREATE THE EFFECTIVE ELEMENT STIFFNESS FILE
C
      CALL STIEPS
      DO 10 ISTEP=1,NSTEP
C
C     COMPUTE LOADS, AFTER READING THE RELEVANT
C     EXTRA DATA
C
      IF(ISTEP.EQ.1) THEN
      DO 100 IELEM=1,NELEM
      DO 100 IEVAB=1,NEVAB
  100 ELOAD(IELEM,IEVAB)=0.0
      IGISH=0
      DO 110 IPOIN=1,NPOIN
      DO 110 IDOFN=1,NDOFN
      IGISH=IGISH+1
      ASDISH(IGISH)=0.0
      ASVELH(IGISH)=0.0
      ASACCELH(IGISH)=0.0
  110 CONTINUE
      ELSE
      CALL LOADPS
      ENDIF
C
C     MERGE AND SOLVE THE RESULTING EQUATIONS
C     BY THE FRONTAL SOLVER
C
      CALL FRONT
C
C     COMPUTE THE STRESSES IN ALL THE ELEMENTS
C
      CALL STREPS
   10 CONTINUE
   20 CONTINUE
      STOP
      END
C
      SUBROUTINE INPUT
C
C     TO READ ALL INPUT DATA EXCEPT LOADS
C
      INCLUDE 'JEIBI.INC'
      COMMON/ENERGY/NSEL(4),DLC
C
```

```
C     READ THE FIRST DATA CARD, AND ECHO IT
C     IMMEDIATELY
C
      READ(5,900) NPOIN,NELEM,NVFIX,NSTEP,NTYPE,
     , NNODE,NDOFN,NMATS,NPROP,NGAUS,NDIME,NSTRE
  900 FORMAT(12I5)
C
C     READ ELEMENT NUMBER OF WHICH STRESS OUTPUT IS NEEDED
C
      READ(5,777) NWANT,(IWANT(I),I=1,NWANT)
  777 FORMAT(11I5)
      NEVAB=NDOFN*NNODE
      WRITE(6,905) NPOIN,NELEM,NVFIX,NSTEP,NTYPE,
     , NNODE,NDOFN,NMATS,NPROP,NGAUS,NDIME,
     ,NSTRE,NEVAB
  905 FORMAT(//8H NPOIN =,I4,4X,8H NELEM =,I4,
     , 4X,8H NVFIX =,I4,4X,8H NSTEP =,I4,4X,
     , 8H NTYPE =,I4//8H NNODE =,I4,4X,
     , 8H NDOFN =,I4,4X,8H NMATS =,I4,4X,
     , 8H NPROP =,I4,4X,8H NGAUS =,I4//
     , 8H NDIME =,I4,4X,8H NSTRE =,I4,4X,
     , 8H NEVAB =,I4)
      READ(5,906) BETA,DELTA,DTIME
  906 FORMAT(4X,F6.4,4X,F6.4,6X,E14.6)
      WRITE(6,800) BETA,DELTA,DTIME
  800 FORMAT(/7H BETA =,F6.4,4X,8H DELTA =,F6.4,
     , 4X,8H DTIME =,E14.6)
C
C     CALCULATE THE COEFFICIENTS A0 THROUGH A7
C
      A0=1.0/(BETA*DTIME*DTIME)
      A1=DELTA/(BETA*DTIME)
      A2=1.0/(BETA*DTIME)
      A3=1.0/(2.0*BETA)-1.0
      A4=DELTA/BETA-1.0
      A5=DTIME*(DELTA/BETA-2.0)/2.0
      A6=DTIME*(1.0-DELTA)
      A7=DELTA*DTIME
C
C     NODES FOR THE CALCULATION OF ENERGY RELEASE RATES
C
      READ(5,902) (NSEL(I),I=1,4),DLC
  902 FORMAT(4I5,F10.5)
      CALL CHECK1
      CALL CHECK1
C
C     READ THE ELEMENT NODAL CONNECTIONS, AND
C     THE PROPERTY NUMBERS
```

```
C
      WRITE(6,910)
  910 FORMAT(//8H ELEMENT,3X,8HPROPERTY,6X,
     , 12HNODE NUMBERS)
      DO 10 IELEM=1,NELEM
      READ(5,900) NUMEL,MATNO(NUMEL),
     , (LNODS(NUMEL,INODE),INODE=1,NNODE)
   10 WRITE(6,915) NUMEL,MATNO(NUMEL),
     , (LNODS(NUMEL,INODE),INODE=1,NNODE)
  915 FORMAT(1X,I5,I9,6X,8I5)
C
C     ZERO ALL THE NODAL COORDINATES, PRIOR
C     TO READING SOME OF THEM
C
      DO 20 IPOIN=1,NPOIN
      DO 20 IDIME=1,NDIME
   20 COORD(IPOIN,IDIME)=0.0
C
C     READ SOME NODAL COORDINATES, FINISHING
C     WITH THE LAST NODE OF ALL
C
      WRITE(6,920)
  920 FORMAT(//25H  NODAL POINT COORDINATES)
      WRITE(6,925)
  925 FORMAT(6H  NODE,7X,1HX,9X,1HY)
   30 READ(5,930) IPOIN,(COORD(IPOIN,IDIME),
     , IDIME=1,NDIME)
  930 FORMAT(I5,5F15.9)
      IF(IPOIN.NE.NPOIN) GO TO 30
C
C     INTERPOLATE COORDINATES OF MID-SIDE NODES
C
      IF(NDIME.EQ.1) GO TO 40
      CALL NODEXY
   40 CONTINUE
      DO 50 IPOIN=1,NPOIN
   50 WRITE(6,935) IPOIN,(COORD(IPOIN,IDIME),
     , IDIME=1,NDIME)
  935 FORMAT(1X,I5,5F15.9)
C
C    READ THE FIXED VALUES,
C
      WRITE(6,940)
  940 FORMAT(//17H RESTRAINED NODES)
      WRITE(6,945)
  945 FORMAT(5H NODE,1X,4HCODE,6X,
     , 12HFIXED VALUES)
      IF(NDOFN.NE.3) GO TO 70
      DO 60 IVFIX=1,NVFIX
      READ(5,950) NOFIX(IVFIX),(IFPRE(IVFIX,
     , IDOFN),IDOFN=1,NDOFN),(PRESC(IVFIX,IDOFN),
```

```
     , IDOFN=1,NDOFN)
   60 WRITE(6,950) NOFIX(IVFIX),(IFPRE(IVFIX,
     , IDOFN),IDOFN=1,NDOFN),(PRESC(IVFIX,IDOFN),
     , IDOFN=1,NDOFN)
  950 FORMAT(1X,I4,2X,3I1,3F10.6)
      GO TO 90
   70 DO 80 IVFIX=1,NVFIX
      READ(5,955) NOFIX(IVFIX),(IFPRE(IVFIX,
     , IDOFN),IDOFN=1,NDOFN),(PRESC(IVFIX,
     , IDOFN),IDOFN=1,NDOFN)
   80 WRITE(6,955) NOFIX(IVFIX),(IFPRE(IVFIX,
     , IDOFN),IDOFN=1,NDOFN),(PRESC(IVFIX,
     , IDOFN),IDOFN=1,NDOFN)
  955 FORMAT(1X,I4,2X,3I1,3F10.6)
   90 CONTINUE
C
C     READ THE AVAILABLE SELECTION OF ELEMENT
C     PROPERTIES
C
      WRITE(6,960)
  960 FORMAT(//21H  MATERIAL PROPERTIES)
      WRITE(6,965)
  965 FORMAT(8H  NUMBER,7X,10HPROPERTIES)
      DO 100 IMATS=1,NMATS
      READ(5,*) NUMAT,(PROPS(NUMAT,IPROP),
     , IPROP=1,7)
      READ(5,*) (PROPS(NUMAT,IPROP),IPROP=8,9)
  975 FORMAT(5F14.6)
  100 WRITE(6,970) NUMAT,(PROPS(NUMAT,IPROP),
     , IPROP=1,5)
      WRITE(6,980) (PROPS(NUMAT,IPROP),IPROP=6,9)
  970 FORMAT(I4,4X,9E14.6)
  980 FORMAT(8X,5E14.6)
C
C     SET UP GAUSSIAN INTEGRATION CONSTANTS
C
      CALL GAUSSQ
      CALL CHECK2
      RETURN
      END
C
      SUBROUTINE NODEXY
C
C     LOOP OVER EACH ELEMENT
C
      INCLUDE 'JEIBI.INC'
      DO 30 IELEM=1,NELEM
C
C     LOOP OVER EACH ELEMENT EDGE
C
      DO 20 INODE=1,NNODE,2
```

```
C
C     COMPUTE THE NODE NUMBER OF THE FIRST NODE
C
       NODST=LNODS(IELEM,INODE)
       IGASH=INODE+2
       IF(IGASH.GT.NNODE) IGASH=1
C
C     COMPUTE THE NODE NUMBER OF THE LAST NODE
C
       NODFN=LNODS(IELEM,IGASH)
       MIDPT=INODE+1
C
C     COMPUTE THE NODE NUMBER OF THE
C     INTERMEDIATE NODE
C
       NODMD=LNODS(IELEM,MIDPT)
       TOTAL=ABS(COORD(NODMD,1))+
     , ABS(COORD(NODMD,2))
C
C     IF THE COORDINATES OF THE INTERMEDIATE
C     NODE ARE BOTH ZERO INTERPOLATE BY A
C     STRAIGHT LINE
C
       IF(TOTAL.GT.0.0) GO TO 20
       KOUNT=1
   10 COORD(NODMD,KOUNT)=(COORD(NODST,KOUNT)+
     , COORD(NODFN,KOUNT))/2.0
      KOUNT=KOUNT+1
      IF(KOUNT.EQ.2) GO TO 10
   20 CONTINUE
   30 CONTINUE
      RETURN
      END
C
      SUBROUTINE GAUSSQ
C
C     SET UP GAUSS POINTS FOR INTEGRATION IN SPACE
C
      INCLUDE 'JEIBI.INC'
      IF(NGAUS.GT.2) GO TO 10
      POSGP(1)=-0.577350269190
      WEIGP(1)=1.0
      GO TO 20
   10 POSGP(1)=-0.774596669241
      POSGP(2)=0.0
      WEIGP(1)=0.555555555556
      WEIGP(2)=0.888888888889
   20 KGAUS=NGAUS/2
      DO 30 IGASH=1,KGAUS
      JGASH=NGAUS+1-IGASH
      POSGP(JGASH)=-POSGP(IGASH)
```

```
      WEIGP(JGASH)=WEIGP(IGASH)
   30 CONTINUE
      RETURN
      END
C
      SUBROUTINE DBE
C
C     CALCULATES (D-MATRIX) x (B-MATRIX)
C
      INCLUDE 'JEIBI.INC'
      DO 10 ISTRE=1,NSTRE
      DO 10 IEVAB=1,NEVAB
      DBMAT(ISTRE,IEVAB)=0.0
      DO 10 JSTRE=1,NSTRE
      DBMAT(ISTRE,IEVAB)=DBMAT(ISTRE,IEVAB)+
     ,DMATX(ISTRE,JSTRE)*BMATX(JSTRE,IEVAB)
   10 CONTINUE
      RETURN
      END

      SUBROUTINE SFR2(S,T)
C
C     CALCULATES SHAPE FUNCTIONS AND THEIR
C     DERIVATIVES FOR 2D ELEMENTS
C
      INCLUDE 'JEIBI.INC'
      S2=S*2.0
      T2=T*2.0
      SS=S*S
      TT=T*T
      ST=S*T
      SST=S*S*T
      STT=S*T*T
      ST2=S*T*2.0
C
C     SHAPE FUNCTIONS
C
      SHAPE(1)=(-1.0+ST+SS+TT-SST-STT)/4.0
      SHAPE(2)=(1.0-T-SS+SST)/2.0
      SHAPE(3)=(-1.0-ST+SS+TT-SST+STT)/4.0
      SHAPE(4)=(1.0+S-TT-STT)/2.0
      SHAPE(5)=(-1.0+ST+SS+TT+SST+STT)/4.0
      SHAPE(6)=(1.0+T-SS-SST)/2.0
      SHAPE(7)=(-1.0-ST+SS+TT+SST-STT)/4.0
      SHAPE(8)=(1.0-S-TT+STT)/2.0
C
C     SHAPE FUNCTION DERIVATIVES
C
      DERIV(1,1)=(T+S2-ST2-TT)/4.0
      DERIV(1,2)=-S+ST
      DERIV(1,3)=(-T+S2-ST2+TT)/4.0
```

```
      DERIV(1,4)=(1.0-TT)/2.0
      DERIV(1,5)=(T+S2+ST2+TT)/4.0
      DERIV(1,6)=-S-ST
      DERIV(1,7)=(-T+S2+ST2-TT)/4.0
      DERIV(1,8)=(-1.0+TT)/2.0
      DERIV(2,1)=(S+T2-SS-ST2)/4.0
      DERIV(2,2)=(-1.0+SS)/2.0
      DERIV(2,3)=(-S+T2-SS+ST2)/4.0
      DERIV(2,4)=-T-ST
      DERIV(2,5)=(S+T2+SS+ST2)/4.0
      DERIV(2,6)=(1.0-SS)/2.0
      DERIV(2,7)=(-S+T2+SS-ST2)/4.0
      DERIV(2,8)=-T+ST
      RETURN
      END
C
      SUBROUTINE JACOB2(IELEM,DJACB,KGASP)
C
C     CALCULATES COORDINATES OF GAUSS POINTS
C     AND THE JACOBIAN MATRIX AND ITS DETERMINANT
C     AND THE INVERSE FOR 2D ELEMENTS
C
      INCLUDE 'JEIBI.INC'
      DIMENSION XJACM(2,2),XJACI(2,2)
C
C     CALCULATE COORDINATES OF SAMPLING POINT
C
      DO 10 IDIME=1,NDIME
      GPCOD(IDIME,KGASP)=0.0
      DO 10 INODE=1,NNODE
      GPCOD(IDIME,KGASP)=GPCOD(IDIME,KGASP)+
     , ELCOD(IDIME,INODE)*SHAPE(INODE)
   10 CONTINUE
C
C     CREATE JACOBIAN MATRIX XJACM
C
      DO 20 IDIME=1,NDIME
      DO 20 JDIME=1,NDIME
      XJACM(IDIME,JDIME)=0.0
      DO 20 INODE=1,NNODE
      XJACM(IDIME,JDIME)=XJACM(IDIME,JDIME)+
     , DERIV(IDIME,INODE)*ELCOD(JDIME,INODE)
   20 CONTINUE
C
C     CALCULATE DETERMINANT AND INVERSE OF
C     JACOBIAN MATRIX
C
      DJACB=XJACM(1,1)*XJACM(2,2)-XJACM(1,2)*
     , XJACM(2,1)
      IF(DJACB.GT.0.0) GO TO 30
      WRITE(6,900) IELEM
```

```
      STOP
   30 XJACI(1,1)=XJACM(2,2)/DJACB
      XJACI(2,2)=XJACM(1,1)/DJACB
      XJACI(1,2)=-XJACM(1,2)/DJACB
      XJACI(2,1)=-XJACM(2,1)/DJACB
C
C     CALCULATE CARTESIAN DERIVATIVES
C
      DO 40 IDIME=1,NDIME
      DO 40 INODE=1,NNODE
      CARTD(IDIME,INODE)=0.0
      DO 40 JDIME=1,NDIME
      CARTD(IDIME,INODE)=CARTD(IDIME,INODE)+
     , XJACI(IDIME,JDIME)*DERIV(JDIME,INODE)
   40 CONTINUE
  900 FORMAT(//,24HPROGRAM HALTED IN JACOB2,
     , /,11X,22H ZERO OR NEGATIVE AREA,/,
     , 10X,16H ELEMENT NUMBER ,I5)
      RETURN
      END
C
      SUBROUTINE BMATPS
C
C     THIS SUBROUTINE CALCULATE DERIVATIVES OF
C     B-MATRIX
C
      INCLUDE 'JEIBI.INC'
      KGASH=0
      DO 10 INODE=1,NNODE
      MGASH=KGASH+1
      NGASH=MGASH+1
      KGASH=NGASH+1
      BMATX(1,MGASH)=CARTD(1,INODE)
      BMATX(1,NGASH)=0.0
      BMATX(1,KGASH)=0.0
      BMATX(2,MGASH)=0.0
      BMATX(2,NGASH)=CARTD(2,INODE)
      BMATX(2,KGASH)=0.0
      BMATX(3,MGASH)=0.0
      BMATX(3,NGASH)=CARTD(1,INODE)
      BMATX(3,KGASH)=-SHAPE(INODE)
      BMATX(4,MGASH)=CARTD(2,INODE)
      BMATX(4,NGASH)=0.0
      BMATX(4,KGASH)=SHAPE(INODE)
      BMATX(5,MGASH)=0.0
      BMATX(5,NGASH)=0.0
      BMATX(5,KGASH)=CARTD(1,INODE)
      BMATX(6,MGASH)=0.0
      BMATX(6,NGASH)=0.0
      BMATX(6,KGASH)=CARTD(2,INODE)
   10 CONTINUE
```

```
      RETURN
      END
C
      SUBROUTINE MODPS(LPROP)
      INCLUDE 'JEIBI.INC'
      YOUNG=PROPS(LPROP,1)
      POISS=PROPS(LPROP,2)
      RAMDA=PROPS(LPROP,4)
      XXMUI=PROPS(LPROP,5)
      CAY=PROPS(LPROP,6)
      GAM=PROPS(LPROP,7)
      DO 10 ISTRE=1,NSTRE
      DO 10 JSTRE=1,NSTRE
      DMATX(ISTRE,JSTRE)=0.0
   10 CONTINUE
C
C     D MATRIX FOR PLANE STRAIN MICROPOLAR ELASTICITY CASE
C
      DMATX(1,1)=RAMDA+2.*XXMUI+CAY
      DMATX(2,2)=RAMDA+2.*XXMUI+CAY
      DMATX(1,2)=RAMDA
      DMATX(2,1)=RAMDA
      DMATX(3,3)=XXMUI+CAY
      DMATX(4,4)=XXMUI+CAY
      DMATX(3,4)=XXMUI
      DMATX(4,3)=XXMUI
      DMATX(5,5)=GAM
      DMATX(6,6)=GAM
   30 CONTINUE
      RETURN
      END
C
      SUBROUTINE STIEPS
C
C     TO GENERATE ELEMENT MASS MATRIX
C     AND ELEMENT STIFFNESS MATRIX,
C     ALSO ASSEMBLE EFFECTIVE STIFFNESS MATRIX
C     FOR NEWMARK METHOD
C
      INCLUDE 'JEIBI.INC'
      DIMENSION ESTIF(24,24),EMASS(24,24)
C
C     LOOP OVER EACH ELEMENT
C
       DO 70 IELEM=1,NELEM
       LPROP=MATNO(IELEM)
C
C     EVALUATE THE COORDINATES OF THE ELEMENT
C     NODAL POINTS
C
       DO 10 INODE=1,NNODE
```

```
      LNODE=LNODS(IELEM,INODE)
      DO 10 IDIME=1,NDIME
   10 ELCOD(IDIME,INODE)=COORD(LNODE,IDIME)
C
C     EVALUATE THE D-MATRIX
C
      CALL MODPS(LPROP)
      THICK=PROPS(LPROP,3)
      DENSE=PROPS(LPROP,8)
      DINERTIA=PROPS(LPROP,9)
C
C     INITIALIZE THE ELEMENT STIFFNESS MATRIX
C
      DO 20 IEVAB=1,NEVAB
      DO 20 JEVAB=1,NEVAB
      ESTIF(IEVAB,JEVAB)=0.0
   20 EMASS(IEVAB,JEVAB)=0.0
      KGASP=0
C
C     ENTER LOOPS FOR AREA NUMBERICAL INTEGRATION
C
      DO 50 IGAUS=1,NGAUS
      DO 50 JGAUS=1,NGAUS
      KGASP=KGASP+1
      EXISP=POSGP(IGAUS)
      ETASP=POSGP(JGAUS)
C
C     EVALUATE THE SHAPE FUNCTIONS,ELEMENTAL
C     VOLUME,ETC.
C
      CALL SFR2(EXISP,ETASP)
      CALL JACOB2(IELEM,DJACB,KGASP)
      DVOLU=DJACB*WEIGP(IGAUS)*WEIGP(JGAUS)
      IF(THICK.NE.0.0) DVOLU=DVOLU*THICK
      IF(DENSE.NE.0.0) DMASS=DVOLU*DENSE
      IF(DINERTIA.NE.0.0) DROT=DVOLU*DINERTIA
C
C     EVALUATE THE B AND DB MATRICES
C
      CALL BMATPS
      CALL DBE
C
C     CALCULATE THE ELEMENT STIFFNESSES
C
      DO 30 IEVAB=1,NEVAB
      DO 30 JEVAB=IEVAB,NEVAB
      DO 30 ISTRE=1,NSTRE
   30 ESTIF(IEVAB,JEVAB)=ESTIF(IEVAB,JEVAB)+
     , BMATX(ISTRE,IEVAB)*DBMAT(ISTRE,
     , JEVAB)*DVOLU
```

```
C
C     STORE THE COMPONENTS OF THE DB MATRIX FOR
C     THE ELEMENT
C
      DO 40 ISTRE=1,NSTRE
      DO 40 IEVAB=1,NEVAB
   40 SMATX(ISTRE,IEVAB,KGASP)=DBMAT(ISTRE,IEVAB)
C
C     CONSTRUCT THE CONSISTENT ELEMENT MASS MATRIX
C
      DO 65 INODE=1,NNODE
      DO 65 JNODE=1,NNODE
      DO 63 IDOFN=1,NDOFN
      DO 63 JDOFN=1,NDOFN
      IEVAB=3*(INODE-1)+IDOFN
      JEVAB=3*(JNODE-1)+JDOFN
      IF(IDOFN.EQ.3.AND.JDOFN.EQ.3) THEN
      EMASS(IEVAB,JEVAB)=EMASS(IEVAB,JEVAB)+
     ,SHAPE(INODE)*SHAPE(JNODE)*DROT
      ELSE
      EMASS(IEVAB,JEVAB)=EMASS(IEVAB,JEVAB)+
     ,SHAPE(INODE)*SHAPE(JNODE)*DMASS
      ENDIF
      IF(IDOFN.NE.JDOFN) EMASS(IEVAB,JEVAB)=0.0
   63 CONTINUE
   65 CONTINUE
   50 CONTINUE
C
C     CONSTRUCT THE LOWER TRIANGLE OF THE
C     STIFFNESS MATRIX
C
      DO 60 IEVAB=1,NEVAB
      DO 60 JEVAB=1,NEVAB
   60 ESTIF(JEVAB,IEVAB)=ESTIF(IEVAB,JEVAB)
C
C     CONSTRUCT THE EFFECTIVE ELEMENT STIFFNESS MATRIX
C
      DO 67 IEVAB=1,NEVAB
      DO 67 JEVAB=1,NEVAB
   67 ESTIF(IEVAB,JEVAB)=ESTIF(IEVAB,JEVAB)+A0*EMASS(IEVAB,JEVAB)
C
C     STORE THE EFFECTIVE STIFFNESS MATRIX,MASS MATRIX,
C     STRESS MATRIX AND SAMPLING POINT COORDINATES FOR EACH
C     ELEMENT ON DISC FILE
C
      WRITE(1) ESTIF
      WRITE(7) EMASS
      WRITE(3) SMATX,GPCOD
   70 CONTINUE
      RETURN
      END
```

```
C
      SUBROUTINE STREPS
C
C     TO CALCULATE ELEMENT STRESSES AT GAUSS POINTS
C     OR NODES
C
      INCLUDE 'JEIBI.INC'
      DIMENSION ELDIS(3,8),STRSG(6)
C
C     NOTE: IF HEADING FOR STRESS OUTPUT IS NECESSARY USE THIS.
C      WRITE(6,900) ISTEP
C      WRITE(6,905)
C  905 FORMAT(1H0,4HG,P.,2X,8HX-COORD.,2X,
C     , 8HY-COORD.,3X,8HX-STRESS,4X,8HY-STRESS,
C     , 3X,9HXY-STRESS,2X,9HYX-STRESS,3X,
C     , 9HXZ-COUPLE,3X,9HYZ-COUPLE)
      KGAST=0
      REWIND (3)
C
C     LOOP OVER EACH ELEMENT
C
      DO 60 IELEM=1,NELEM
      LPROP=MATNO(IELEM)
      POISS=PROPS(LPROP,2)
C
C     READ THE STRESS MATRIX, SAMPLING POINT
C     COORDINATES FOR THE ELEMENT
C
      READ(3) SMATX,GPCOD
C
C     PRINT ELEMENT NUMBER OF WHICH OUTPUT IS WANTED
C      DO 444 IWAN=1,NWANT
C      IF(IELEM.EQ.IWANT(IWAN)) WRITE(6,910) IELEM
C  444 CONTINUE
C
C     IDENTIFY THE DISPLACEMENTS OF THE
C     ELEMENT NODAL POINTS
C
      DO 10 INODE=1,NNODE
      LNODE=LNODS(IELEM,INODE)
      NPOSN=(LNODE-1)*NDOFN
      DO 10 IDOFN=1,NDOFN
      NPOSN=NPOSN+1
      ELDIS(IDOFN,INODE)=ASDIS(NPOSN)
   10 CONTINUE
      KGASP=0
C
C     ENTER LOOPS OVER EACH SAMPLING POINT
C
      DO 50 IGAUS=1,NGAUS
      DO 50 JGAUS=1,NGAUS
```

```
      KGAST=KGAST+1
      KGASP=KGASP+1
C
C     COMPUTE THE CARTESIAN STRESS COMPONENTS
C     AT THE SAMPLING POINTS
C
      DO 20 ISTRE=1,NSTRE
      STRSG(ISTRE)=0.0
      KGASH=0
      DO 20 INODE=1,NNODE
      DO 20 IDOFN=1,NDOFN
      KGASH=KGASH+1
      STRSG(ISTRE)=STRSG(ISTRE)+SMATX(ISTRE,
     , KGASH,KGASP)*ELDIS(IDOFN,INODE)
   20 CONTINUE
C
C     OUTPUT THE STRESSES FOR THE SELECTED GAUSS POINT
C     OF THE SELECTED ELEMENTS
C
C     DO 45 IWA=1,NWANT
      IF(IELEM.EQ.IWANT(1)) THEN
      IF(KGASP.EQ.1) THEN
      WRITE(9,915) KGASP,(GPCOD(IDIME,KGASP),
     ,IDIME=1,NDIME),(STRSG(ISTR1),ISTR1=1,NSTRE)
      ENDIF
      IF(KGASP.EQ.7) THEN
      WRITE(10,915) KGASP,(GPCOD(IDIME,KGASP),
     ,IDIME=1,NDIME),(STRSG(ISTR1),ISTR1=1,NSTRE)
      ENDIF
      ENDIF
      IF(IELEM.EQ.IWANT(2)) THEN
      IF(KGASP.EQ.1) THEN
      WRITE(11,915) KGASP,(GPCOD(IDIME,KGASP),
     ,IDIME=1,NDIME),(STRSG(ISTR1),ISTR1=1,NSTRE)
      ENDIF
      IF(KGASP.EQ.7) THEN
      WRITE(12,915) KGASP,(GPCOD(IDIME,KGASP),
     ,IDIME=1,NDIME),(STRSG(ISTR1),ISTR1=1,NSTRE)
      ENDIF
      ENDIF
C  45 CONTINUE
   50 CONTINUE
   60 CONTINUE
  900 FORMAT(/,10X,8H ISTEP =,I3,4X,8HSTRESSES,/)
  910 FORMAT(/,5X,12HELEMENT NO.=,I5)
  915 FORMAT(I1,2F15.9,6(1X,E12.5))
      RETURN
      END
C
      SUBROUTINE LOADPS
C
```

```
C     TO GENERATE INPUT LOADS
C
      INCLUDE 'JEIBI.INC'
      DIMENSION TITLE(80),POINT(3),PRESS(3,3),PGASH(2)
     ,,DGASH(2),TEMPE(300),STRAN(3),STRES(3),NOPRS(3),EMASS(24,24)
      IF(ISTEP.GT.2) GO TO 715
      DO 10 IELEM=1,NELEM
      DO 10 IEVAB=1,NEVAB
   10 ELOAD1(IELEM,IEVAB)=0.0
      READ(5,900) TITLE
  900 FORMAT(80A1)
C
C     READ DATA CONTROLLING LOADING TYPES
C     TO BE INPUT
C
      READ(5,910) IPLOD,IGRAV,IEDGE,ITEMP
      WRITE(6,910) IPLOD,IGRAV,IEDGE,ITEMP
  910 FORMAT(4I5)
C
C     READ NODAL POINT LOADS
C
      IF(IPLOD.EQ.0) GO TO 500
   20 READ(5,915) LODPT,(POINT(IDOFN),IDOFN=
     , 1,NDOFN)
      WRITE(6,915) LODPT,(POINT(IDOFN),IDOFN=
     , 1,NDOFN)
  915 FORMAT(I5,3F10.3)
C
C     ASSOCIATE THE NODAL POINT LOADS WITH
C     AN ELEMENT
C
      DO 30 IELEM=1,NELEM
      DO 30 INODE=1,NNODE
      NLOCA=LNODS(IELEM,INODE)
      IF(LODPT.EQ.NLOCA) GO TO 40
   30 CONTINUE
   40 DO 50 IDOFN=1,NDOFN
      NGASH=(INODE-1)*NDOFN+IDOFN
   50 ELOAD(IELEM,NGASH)=POINT(IDOFN)
      IF(LODPT.LT.NPOIN) GO TO 20
  500 CONTINUE
      IF(IGRAV.EQ.0) GO TO 600
  600 CONTINUE
      IF(IEDGE.EQ.0) GO TO 700
C
C     DISTRIBUTED EDGE LOADS SECTION
C
      READ(5,930) NEDGE
  930 FORMAT(I5)
C     WRITE(6,935) NEDGE
C 935 FORMAT(1H0,5X,21HNO. OF LOADED EDGES =,I5)
```

```
C     WRITE(6,940)
C 940 FORMAT(1H0,5X,
C    , 38HLIST OF LOADED EDGES AND APPLIED LOADS)
      NODEG=3
C
C     LOOP OVER EACH LOADED EDGE
C
      DO 160 IEDGE=1,NEDGE
C
C     READ DATA LOCATING THE LOADED EDGE AND
C     APPLIED LOAD
C
      READ(5,945) NEASS,(NOPRS(IODEG),IODEG=
     , 1,NODEG)
  945 FORMAT(4I5)
C     WRITE(6,950) NEASS,(NOPRS(IODEG),IODEG=
C    , 1,NODEG)
C 950 FORMAT(I10,5X,3I5)
      READ(5,955) ((PRESS(IODEG,IDOFN),IODEG=
     , 1,NODEG),IDOFN=1,NDOFN)
C     WRITE(6,955) ((PRESS(IODEG,IDOFN),IODEG=
C    , 1,NODEG),IDOFN=1,NDOFN)
  955 FORMAT(6F10.3,3F6.3)
      ETASP=-1.0
C
C     CALCULATE THE COORDINATES OF THE NODES
C     OF THE ELEMENT EDGE
C
      DO 100 IODEG=1,NODEG
      LNODE=NOPRS(IODEG)
      DO 100 IDIME=1,NDIME
  100 ELCOD(IDIME,IODEG)=COORD(LNODE,IDIME)
C
C     ENTER LOOP FOR LINEAR NUMERICAL INTEGRATION
C
      DO 150 IGAUS=1,NGAUS
      EXISP=POSGP(IGAUS)
C
C     EVALUATE THE SHAPE FUNCTIONS AT THE
C     SAMPLING POINTS
C
      CALL SFR2(EXISP,ETASP)
C
C     CALCULATE THE COMPONENTS OF THE EQUIVALENT
C     NODAL LOADS
C
      DO 110 IDOFN=1,2
      PGASH(IDOFN)=0.0
      DGASH(IDOFN)=0.0
      DO 110 IODEG=1,NODEG
      PGASH(IDOFN)=PGASH(IDOFN)+PRESS(IODEG,
```

```
     , IDOFN)*SHAPE(IODEG)
  110 DGASH(IDOFN)=DGASH(IDOFN)+ELCOD(IDOFN,
     , IODEG)*DERIV(1,IODEG)
      DVOLU=WEIGP(IGAUS)
      PXCOM=DGASH(1)*PGASH(2)-DGASH(2)*PGASH(1)
      PYCOM=DGASH(1)*PGASH(1)+DGASH(2)*PGASH(2)
      POCOM=0.0
C
C     ASSOCIATE THE EQUIVALENT NODAL EDGE
C     LOADS WITH AN ELEMENT
C
      DO 120 INODE=1,NNODE
      NLOCA=LNODS(NEASS,INODE)
      IF(NLOCA.EQ.NOPRS(1)) GO TO 130
  120 CONTINUE
  130 JNODE=INODE+NODEG-1
      KOUNT=0
      DO 140 KNODE=INODE,JNODE
      KOUNT=KOUNT+1
      NGASH=(KNODE-1)*NDOFN+1
      MGASH=(KNODE-1)*NDOFN+2
      KGASH=(KNODE-1)*NDOFN+3
      IF(KNODE.GT.NNODE) NGASH=1
      IF(KNODE.GT.NNODE) MGASH=2
      IF(KNODE.GT.NNODE) KGASH=3
      ELOAD1(NEASS,NGASH)=ELOAD1(NEASS,NGASH)+
     , SHAPE(KOUNT)*PXCOM*DVOLU
      ELOAD1(NEASS,MGASH)=ELOAD1(NEASS,MGASH)+
     , SHAPE(KOUNT)*PYCOM*DVOLU
  140 ELOAD1(NEASS,KGASH)=ELOAD1(NEASS,KGASH)+
     , SHAPE(KOUNT)*POCOM*DVOLU
  150 CONTINUE
  160 CONTINUE
  700 CONTINUE
      IF(ITEMP.EQ.0) GO TO 800
  800 CONTINUE
C     WRITE(6,970)
C 970 FORMAT(1H0,5X,
C    , 36H TOTAL NODAL FORCES FOR EACH ELEMENT)
C     DO 290 IELEM=1,NELEM
C 290 WRITE(6,975) IELEM,(ELOAD1(IELEM,IEVAB),
C    , IEVAB=1,NEVAB)
C 975 FORMAT(1X,I4,5X,8E12.4/(10X,8E12.4)/(10X,8E12.4))
  715 CONTINUE
C
C     CONSTRUCT THE EFFECTIVE DYNAMIC LOADS
C
      DO 725 IELEM=1,NELEM
      DO 725 IEVAB=1,NEVAB
      ELOAD(IELEM,IEVAB)=0.0
```

```
  725 ELOAD2(IELEM,IEVAB)=0.0
      NGISH=0
      DO 730 IPOIN=1,NPOIN
      DO 730 IDOFN=1,NDOFN
      NGISH=NGISH+1
      ASDISH(NGISH)=ASDIS(NGISH)
      ASVELH(NGISH)=ASVEL(NGISH)
      ASACCELH(NGISH)=ASACCEL(NGISH)
      ASDIST(NGISH)=A0*ASDISH(NGISH)+A2*ASVELH(NGISH)+
     ,A3*ASACCELH(NGISH)
  730 CONTINUE
      REWIND (7)
      DO 745 IELEM=1,NELEM
      READ(7) EMASS
      DO 745 IEVAB=1,NEVAB
      DO 750 INODE=1,NNODE
      DO 750 IDOFN=1,NDOFN
      NPOSI=(INODE-1)*NDOFN+IDOFN
      LOCNO=LNODS(IELEM,INODE)
      ICOLUMN=(LOCNO-1)*NDOFN+IDOFN
      ELOAD2(IELEM,IEVAB)=ELOAD2(IELEM,IEVAB)+
     ,EMASS(IEVAB,NPOSI)*ASDIST(ICOLUMN)
  750 CONTINUE
      ELOAD(IELEM,IEVAB)=ELOAD1(IELEM,IEVAB)+ELOAD2(IELEM,IEVAB)
  745 CONTINUE
      RETURN
      END
C
      SUBROUTINE FRONT
C
C     MATRIX SOLVER
C
      INCLUDE 'JEIBI.INC'
      DIMENSION FIXED(3000),EQUAT(200),VECRV(3000),
     , GLOAD(200),GSTIF(20100),ESTIF(24,24),
     , IFFIX(3000),NACVA(200),LOCEL(24),NDEST(24)
      COMMON/ENERGY/NSEL(4),DLC
      NFUNC(I,J)=(J*J-J)/2+I
      MFRON=200
      MSTIF=20100
C
C     INTERPRET FIXITY DATA IN VECTOR FORM
C
      NTOTV=NPOIN*NDOFN
      DO 100 ITOTV=1,NTOTV
      IFFIX(ITOTV)=0
  100 FIXED(ITOTV)=0.0
      DO 110 IVFIX=1,NVFIX
      NLOCA=(NOFIX(IVFIX)-1)*NDOFN
      DO 110 IDOFN=1,NDOFN
      NGASH=NLOCA+IDOFN
```

```
      IFFIX(NGASH)=IFPRE(IVFIX,IDOFN)
  110 FIXED(NGASH)=PRESC(IVFIX,IDOFN)
C
C     CHANGE THE SIGN OF THE LAST APPEARANCE
C     OF EACH NODE
C
      DO 140 IPOIN=1,NPOIN
      KLAST=0
      DO 130 IELEM=1,NELEM
      DO 120 INODE=1,NNODE
      IF(LNODS(IELEM,INODE).NE.IPOIN) GO TO 120
      KLAST=IELEM
      NLAST=INODE
  120 CONTINUE
  130 CONTINUE
      IF(KLAST.NE.0) LNODS(KLAST,NLAST)=-IPOIN
  140 CONTINUE
C
C     START BY INITIALIZING EVERYTHING THAT
C     MATTERS TO ZERO
C
      DO 150 ISTIF=1,MSTIF
  150 GSTIF(ISTIF)=0.0
      DO 160 IFRON=1,MFRON
      GLOAD(IFRON)=0.0
      EQUAT(IFRON)=0.0
      VECRV(IFRON)=0.0
  160 NACVA(IFRON)=0
C
C     AND PREPARE FOR DISC READING AND WRITING
C     OPERATIONS
C
      REWIND (1)
      REWIND (2)
      REWIND (3)
      REWIND (4)
C
C     ENTER MAIN ELEMENT ASSEMBLY-REDUCTION LOOP
C
      NFRON=0
      KELVA=0
      DO 380 IELEM=1,NELEM
      KEVAB=0
      READ(1) ESTIF
      DO 170 INODE=1,NNODE
      DO 170 IDOFN=1,NDOFN
      NPOSI=(INODE-1)*NDOFN+IDOFN
      LOCNO=LNODS(IELEM,INODE)
      IF(LOCNO.GT.0) LOCEL(NPOSI)=(LOCNO-1)*
     , NDOFN+IDOFN
      IF(LOCNO.LT.0) LOCEL(NPOSI)=(LOCNO+1)*
```

```
     , NDOFN-IDOFN
  170 CONTINUE
C
C     START BY LOOKING FOR EXISTING DESTINATIONS
C
      DO 210 IEVAB=1,NEVAB
      NIKNO=IABS(LOCEL(IEVAB))
      KEXIS=0
      DO 180 IFRON=1,NFRON
      IF(NIKNO.NE.NACVA(IFRON)) GO TO 180
      KEVAB=KEVAB+1
      KEXIS=1
      NDEST(KEVAB)=IFRON
  180 CONTINUE
      IF(KEXIS.NE.0) GO TO 210
C
C     WE NOW SEEK NEW EMPTY PLACES FOR
C     DESTINATION VECTOR
C
      DO 190 IFRON=1,MFRON
      IF(NACVA(IFRON).NE.0) GO TO 190
      NACVA(IFRON)=NIKNO
      KEVAB=KEVAB+1
      NDEST(KEVAB)=IFRON
      GO TO 200
  190 CONTINUE
C
C     THE NEW PLACES MAY DEMAND AN INCREASE
C     IN CURRENT FRONTWIDTH
C
  200 IF(NDEST(KEVAB).GT.NFRON) NFRON=NDEST(KEVAB)
  210 CONTINUE
C
C     ASSEMBLE ELEMENT LOADS
C
      DO 240 IEVAB=1,NEVAB
      IDEST=NDEST(IEVAB)
      GLOAD(IDEST)=GLOAD(IDEST)+ELOAD(IELEM,IEVAB)
C
C     ASSEMBLE THE ELEMENT STIFFNESSES
C     - BUT NOT IN RESOLUTION
C
      IF(ISTEP.GT.1) GO TO 230
      DO 220 JEVAB=1,IEVAB
      JDEST=NDEST(JEVAB)
      NGASH=NFUNC(IDEST,JDEST)
      NGISH=NFUNC(JDEST,IDEST)
      IF(JDEST.GE.IDEST) GSTIF(NGASH)=
     , GSTIF(NGASH)+ESTIF(IEVAB,JEVAB)
      IF(JDEST.LT.IDEST) GSTIF(NGISH)=
     ,GSTIF(NGISH)+ESTIF(IEVAB,JEVAB)
```

```
  220 CONTINUE
  230 CONTINUE
  240 CONTINUE
C
C     RE-EXAMINE EACH ELEMENT NODE, TO
C     ENQUIRE WHICH CAN BE ELIMINATED
C
      DO 370 IEVAB=1,NEVAB
      NIKNO=-LOCEL(IEVAB)
      IF(NIKNO.LE.0) GO TO 370
C
C     FIND POSITIONS OF VARIABLES READY
C     FOR ELIMINATION
C
      DO 350 IFRON=1,NFRON
      IF(NACVA(IFRON).NE.NIKNO) GO TO 350
C
C     EXTRACT THE COEFFICIENTS OF THE
C     NEW EQUATION FOR ELIMINATION
C
      IF(ISTEP.GT.1) GO TO 260
      DO 250 JFRON=1,MFRON
      IF(IFRON.LT.JFRON) NLOCA=NFUNC(IFRON,JFRON)
      IF(IFRON.GE.JFRON) NLOCA=NFUNC(JFRON,IFRON)
      EQUAT(JFRON)=GSTIF(NLOCA)
  250 GSTIF(NLOCA)=0.0
  260 CONTINUE
C
C     AND EXTRACT THE CORRESPONDING RIGHT
C     HAND SIDES
C
      EQRHS=GLOAD(IFRON)
      GLOAD(IFRON)=0.0
      KELVA=KELVA+1
C
C     WRITE EQUATIONS TO DISC OR TO TAPE
C
      IF(ISTEP.GT.1) GO TO 270
      WRITE(2) EQUAT,EQRHS,IFRON,NIKNO
      GO TO 280
  270 WRITE(4) EQRHS
      READ(2) EQUAT,DUMMY,IDUMM,NIKNO
  280 CONTINUE
C
C     DEAL WITH PIVOT
C
      PIVOT=EQUAT(IFRON)
      EQUAT(IFRON)=0.0
C
C     ENQUIRE WHETHER PRESENT VARIABLE IS
C     FREE OR PRESCRIBED
```

```
C
      IF(IFFIX(NIKNO).EQ.0) GO TO 300
C
C     DEAL WITH A PRESCRIBED DEFLECTION
C
      DO 290 JFRON=1,NFRON
  290 GLOAD(JFRON)=GLOAD(JFRON)-FIXED(NIKNO)*
     , EQUAT(JFRON)
      GO TO 340
C
CZ    ELIMINATE A FREE VARIABLE - DEAL WITH
C     THE RIGHT HAND SIDE FIRST
C
  300 DO 330 JFRON=1,NFRON
      GLOAD(JFRON)=GLOAD(JFRON)-EQUAT(JFRON)*
     , EQRHS/PIVOT
C
C     NOW DEAL WITH THE COEFFICIENTS IN CORE
C
      IF(ISTEP.GT.1) GO TO 320
      IF(EQUAT(JFRON).EQ.0.0) GO TO 330
      NLOCA=NFUNC(0,JFRON)
      DO 310 LFRON=1,JFRON
      NGASH=LFRON+NLOCA
  310 GSTIF(NGASH)=GSTIF(NGASH)-EQUAT(JFRON)*
     , EQUAT(LFRON)/PIVOT
  320 CONTINUE
  330 CONTINUE
  340 EQUAT(IFRON)=PIVOT
C
C     RECORD THE NEW VACANT SPACE, AND REDUCE
C     FRONTWIDTH IF POSSIBLE
C
      NACVA(IFRON)=0
      GO TO 360
C
C     COMPLETE THE ELEMENT LOOP IN THE FORWARD
C     ELIMINATION
C
  350 CONTINUE
  360 IF(NACVA(NFRON).NE.0) GO TO 370
      NFRON=NFRON-1
      IF(NFRON.GT.0) GO TO 360
  370 CONTINUE
  380 CONTINUE
C
C     ENTER BACK-SUBSTITUTION PHASE, LOOP
C     BACKWARDS THROUGH VARIABLES
C
      DO 410 IELVA=1,KELVA
C
```

```
C     READ A NEW EQUATION
C
      BACKSPACE (2)
      READ(2) EQUAT,EQRHS,IFRON,NIKNO
      BACKSPACE (2)
      IF(ISTEP.EQ.1) GO TO 390
      BACKSPACE (4)
      READ(4) EQRHS
      BACKSPACE (4)
  390 CONTINUE
C
C     PREPARE TO BACK-SUBSTITUTE FROM THE
C     CURRENT EQUATION
C
      PIVOT=EQUAT(IFRON)
      IF(IFFIX(NIKNO).EQ.1) VECRV(IFRON)=
     , FIXED(NIKNO)
      IF(IFFIX(NIKNO).EQ.0) EQUAT(IFRON)=0.0
C
C     BACK-SUBSTITUTE IN THE CURRENT EQUATION
C
      DO 400 JFRON=1,MFRON
  400 EQRHS=EQRHS-VECRV(JFRON)*EQUAT(JFRON)
C
C     PUT THE FINAL VALUES WHERE THEY BELONG
C
      IF(IFFIX(NIKNO).EQ.0) VECRV(IFRON)=
     , EQRHS/PIVOT
      IF(IFFIX(NIKNO).EQ.1) FIXED(NIKNO)=-EQRHS
      ASDIS(NIKNO)=VECRV(IFRON)
  410 CONTINUE
C
C     CALCULATE ACCELERATION AND VELOCITY
C
      NGISH=0
      DO 700 IPOIN=1,NPOIN
      DO 700 IDOFN=1,NDOFN
      NGISH=NGISH+1
      ASACCEL(NGISH)=A0*(ASDIS(NGISH)-ASDISH(NGISH))-
     ,A2*ASVELH(NGISH)-A3*ASACCELH(NGISH)
      ASVEL(NGISH)=ASVELH(NGISH)+A6*ASACCELH(NGISH)+
     ,A7*ASACCEL(NGISH)
  700 CONTINUE
C
C     NOTE: IF DISPLACEMENT OUTPUT IS NEEDED USE THIS SECTION.
C     DISPLACEMENTS & REACTIONS AT EACH TIME STEP
C     WRITE(6,900)
C 900 FORMAT(1HO,5X,13HDISPLACEMENTS)
C     WRITE(6,910)
C 910 FORMAT(1HO,5X,4HNODE,5X,7HX-DISP.,
C    , 7X,7HY-DISP.,7X,8HROTATION)
```

```
C
C     PRINT DISPLACEMENT OUTPUT AT SELECTED NODES
C
C      DO 450 IPOIN=1,NPOIN
C      NGASH=IPOIN*NDOFN
C      NGISH=NGASH-NDOFN+1
C      IF(IPOIN.EQ.115) THEN
C      WRITE(10,920) IPOIN,(ASDIS(IGASH),IGASH=
C     , NGISH,NGASH)
C      ENDIF
C      IF(IPOIN.EQ.117) THEN
C      WRITE(11,920) IPOIN,(ASDIS(IGASH),IGASH=
C     , NGISH,NGASH)
C      ENDIF
C  920 FORMAT(I10,3E14.6)
C  450 CONTINUE
c
C     CALCULATE ENERGY RELEASE RATE USING
C     CRACK CLOSURE METHOD (i.e.,SINGLE ANALYSIS)
C     note: only for a horizontal crack
C
      NGISH1=NSEL(1)*NDOFN
      NGISH2=NSEL(2)*NDOFN
      NGISH3=NSEL(3)*NDOFN
      NGISH4=NSEL(4)*NDOFN
      NGISH5=NGISH1-1
      NGISH6=NGISH2-1
      NGISH7=NGISH3-1
      NGISH8=NGISH4-1
      DOA=ASDIS(NGISH1)
      DOB=ASDIS(NGISH2)
      DMC=FIXED(NGISH3)
      DMD=FIXED(NGISH4)
      DDA=ASDIS(NGISH5)
      DDB=ASDIS(NGISH6)
      DFC=FIXED(NGISH7)
      DFD=FIXED(NGISH8)
      ENER=-(DDA*DFC+DDB*DFD+DOA*DMC+DOB*DMD)/DLC
      WRITE(6,926) ENER
  926 FORMAT(1H0,5X,6H  Gcc=,E14.7)
C
C     IF REACTION OUTPUT IS NEEDED USE BELOW
C     WRITE(6,925)
C 925 FORMAT(1H0,5X,9HREACTIONS)
C     WRITE(6,925)
C 925 FORMAT(1H0,5X,9HREACTIONS)
C     WRITE(6,935)
C 935 FORMAT(1H0,5X,4HNODE,5X,7HX-FORCE,7X,
C    , 7HY-FORCE,7X,6HCOUPLE)
C     DO 510 IPOIN=1,NPOIN
C     NLOCA=(IPOIN-1)*NDOFN
```

```
C     DO 490 IDOFN=1,NDOFN
C     NGUSH=NLOCA+IDOFN
C     IF(IFFIX(NGUSH).GT.0) GO TO 500
C 490 CONTINUE
C     GO TO 510
C 500 NGASH=NLOCA+NDOFN
C     NGISH=NLOCA+1
C     WRITE(6,945) IPOIN,(FIXED(IGASH),IGASH=
C    , NGISH,NGASH)
C 510 CONTINUE
C 945 FORMAT(I10,3E14.6)
C
C     POST FRONT = RESET ALL ELEMENT CONNECTION
C     NUMBERS TO POSITIVE VALUES FOR SUBSEQUENT
C     USE IN STRESS CALCULATION
C
      DO 520 IELEM=1,NELEM
      DO 520 INODE=1,NNODE
  520 LNODS(IELEM,INODE)=IABS(LNODS(IELEM,INODE))
      RETURN
      END
C
      SUBROUTINE CHECK1
C
C     TO CRITICIZE THE DATA CONTROL CARD AND
C     PRINT ANY DIAGNOSTICS
C
      INCLUDE 'JEIBI.INC'
      DO 10 IEROR=1,24
   10 NEROR(IEROR)=0
C
C     CREATE THE DIAGNOSTIC MESSAGES
C
      IF(NPOIN.LE.0) NEROR(1)=1
      IF(NELEM*NNODE.LT.NPOIN) NEROR(2)=1
      IF(NVFIX.LT.1.OR.NVFIX.GT.NPOIN) NEROR(3)=1
      IF(NSTEP.LE.0) NEROR(4)=1
      IF(NTYPE.LT.0.OR.NTYPE.GT.2) NEROR(5)=1
      IF(NNODE.LT.3.OR.NNODE.GT.8) NEROR(6)=1
      IF(NDOFN.LT.2.OR.NDOFN.GT.3) NEROR(7)=1
      IF(NMATS.LE.0.OR.NMATS.GT.NELEM) NEROR(8)=1
      IF(NPROP.LT.3.OR.NPROP.GT.9) NEROR(9)=1
      IF(NGAUS.LT.2.OR.NGAUS.GT.3) NEROR(10)=1
      IF(NDIME.LT.1.OR.NDIME.GT.2) NEROR(11)=1
      IF(NSTRE.LT.2.OR.NSTRE.GT.6) NEROR(12)=1
C
C     EITHER RETURN,OR ELSE PRINT THE ERRORS
C     DIAGNOSED
C
      KEROR=0
      DO 20 IEROR=1,12
```

```
      IF(NEROR(IEROR).EQ.0) GO TO 20
      KEROR=1
      WRITE(6,900) IEROR
  900 FORMAT(//24H *** DIAGNOSIS BY CHECK1,
     , 6H ERROR,I3)
   20 CONTINUE
      IF(KEROR.EQ.0) RETURN
C
C     OTHERWISE ECHO ALL THE REMAINING DATA
C     WITHOUT FURTHER COMMENT
C
      CALL ECHO
      END
C
      SUBROUTINE ECHO
      INCLUDE 'JEIBI.INC'
      DIMENSION NTITL(80)
      WRITE(6,900)
  900 FORMAT(//25H NOW FOLLOWS A LISTING OF,
     , 25H POST-DISASTER DATA CARDS/)
   10 READ(5,905) NTITL
  905 FORMAT(80A1)
      WRITE(6,910) NTITL
  910 FORMAT(20X,80A1)
      GO TO 10
      END
C
      SUBROUTINE CHECK2
C
C     TO CRITICIZE THE DATA FROM SUBROUTINE INPUT
C
      INCLUDE 'JEIBI.INC'
      DIMENSION NDFRO(300)
      MFRON=200
C
C     CHECK AGAINST TWO IDENTICAL NONZERO
C     NODAL COORDINATES
C
      DO 10 IELEM=1,NELEM
   10 NDFRO(IELEM)=0
      DO 40 IPOIN=2,NPOIN
      KPQIN=IPOIN-1
      DO 30 JPOIN=1,KPOIN
      DO 20 IDIME=1,NDIME
      IF(COORD(IPOIN,IDIME).NE.COORD(JPOIN,
     , IDIME)) GO TO 30
   20 CONTINUE
      NEROR(13)=NEROR(13)+1
   30 CONTINUE
   40 CONTINUE
C
```

```
C     CHECK THE LIST OF ELEMENT PROPERTY NUMBERS
C
      DO 50 IELEM=1,NELEM
   50 IF(MATNO(IELEM).LE.0.OR.MATNO(IELEM).GT.
     , NMATS) NEROR(14)=NEROR(14)+1
C
C     CHECK FOR IMPOSSIBLE NODE NUMBERS
C
      DO 70 IELEM=1,NELEM
      DO 60 INODE=1,NNODE
      IF(LNODS(IELEM,INODE).EQ.0) NEROR(15)=
     , NEROR(15)+1
   60 IF(LNODS(IELEM,INODE).LT.0.OR.LNODS(IELEM,
     , INODE).GT.NPOIN) NEROR(16)=NEROR(16)+1
   70 CONTINUE
C
C     CHECK FOR ANY REPETITION OF A NODE
C     NUMBER WITHIN AN ELEMENT
C
      DO 140 IPOIN=1,NPOIN
      KSTAR=0
      DO 100 IELEM=1,NELEM
      KZERO=0
      DO 90 INODE=1,NNODE
      IF(LNODS(IELEM,INODE).NE.IPOIN) GO TO 90
      KZERO=KZERO+1
C     IF(KZERO.GT.1) NEROR(17)=NEROR(17)+1
C
C     SEEK FIRST,LAST AND INTERMEDIATE
C     APPEARANCES OF NODE IPOIN
      IF(KSTAR.NE.0) GO TO 80
C
      KSTAR=IELEM
C
C     CALCULATE INCREASE OR DECREASE IN
C     FRONTWIDTH AT EACH ELEMENT STAGE
C
      NDFRO(IELEM)=NDFRO(IELEM)+NDOFN
   80 CONTINUE
C
C     AND CHANGE THE SIGN OF THE LAST
C     APPEARANCE OF EACH NODE
C
      KLAST=IELEM
      NLAST=INODE
   90 CONTINUE
  100 CONTINUE
      IF(KSTAR.EQ.0) GO TO 110
      IF(KLAST.LT.NELEM) NDFRO(KLAST+1)=
     , NDFRO(KLAST+1)-NDOFN
      LNODS(KLAST,NLAST)=-IPOIN
```

```
      GO TO 140
C
C     CHECK THAT COORDINATES FOR AN UNUSED
C     NODE HAVE NOT BEEN SPECIFIED
C
  110 WRITE(6,900) IPOIN
  900 FORMAT(/15H CHECK WHY NODE,I4,
     , 14H NEVER APPEARS)
      NEROR(18)=NEROR(18)+1
      SIGMA=0.0
      DO 120 IDIME=1,NDIME
  120 SIGMA=SIGMA+ABS(COORD(IPOIN,IDIME))
      IF(SIGMA.NE.0.0) NEROR(19)=NEROR(19)+1
C
C     CHECK THAT AN UNUSED NODE NUMBER IS NOT
C     A RESTRAINED NODE
C
      DO 130 IVFIX=1,NVFIX
  130 IF(NOFIX(IVFIX).EQ.IPOIN) NEROR(20)=
     , NEROR(20)+1
  140 CONTINUE
C
C     CALCULATE THE LARGEST FRONTWIDTH
C
      NFRON=0
      KFRON=0
      DO 150 IELEM=1,NELEM
      NFRON=NFRON+NDFRO(IELEM)
  150 IF(NFRON.GT.KFRON) KFRON=NFRON
      WRITE(6,905) KFRON
  905 FORMAT(//28HMAX FRONTWIDTH ENCOUNTERED =,I5)
      IF(KFRON.GT.MFRON) NEROR(21)=1
C
C     CONTINUE CHECKING THE DATA FOR THE
C     FIXED VALUES
C
      DO 170 IVFIX=1,NVFIX
      IF(NOFIX(IVFIX).LE.0.OR.NOFIX(IVFIX)
     ,.GT.NPOIN) NEROR(22)=NEROR(22)+1
      KOUNT=0
      DO 160 IDOFN=1,NDOFN
  160 IF(IFPRE(IVFIX,IDOFN).GT.0) KOUNT=1
      IF(KOUNT.EQ.0) NEROR(23)=NEROR(23)+1
      KVFIX=IVFIX-1
      DO 170 JVFIX=1,KVFIX
  170 IF(IVFIX.NE.1.AND.NOFIX(IVFIX).EQ.
     , NOFIX(JVFIX)) NEROR(24)=NEROR(24)+1
      KEROR=0
      DO 180 IEROR=13,24
      IF(NEROR(IEROR).EQ.0) GO TO 180
      KEROR=1
```

```
      WRITE(6,910) IEROR,NEROR(IEROR)
  910 FORMAT(//30H*** DIAGNOSIS BY CHECK2, ERROR,
     , I3,6X,18H ASSOCIATED NUMBER,I5)
  180 CONTINUE
      IF(KEROR.NE.0) GO TO 200
C
C     RETURN ALL NODAL CONNECTION NUMBERS TO
C     POSITIVE VALUES
C
      DO 190 IELEM=1,NELEM
      DO 190 INODE=1,NNODE
  190 LNODS(IELEM,INODE)=IABS(LNODS(IELEM,INODE))
      RETURN
  200 CALL ECHO
      END
C     END OF PROGRAM DYCOUPLE.FOR
C
C     Next is the INCLUDE file which contains common-blocks
C     for the whole program. (File name = JEIBI.INC)
C
      COMMON/CONTRO/NPOIN,NELEM,NNODE,NDOFN,NDIME,NSTRE,NTYPE,NGAUS,
     , NPROP,NMATS,NVFIX,NEVAB,ISTEP,NSTEP,ITEMP,IPROB,NPROB,
     , DTIME,NWANT
      COMMON/LGDATA/COORD(1000,2),PROPS(10,9),PRESC(111,3),ASDIS(3000),
     , ELOAD(300,24),STRIN(6,2700),NOFIX(111),IFPRE(111,3),
     , LNODS(300,8),MATNO(300),ASVEL(3000),ASACCEL(3000),ASDISH(3000),
     , ASDIST(3000),ASVELH(3000),ASACCELH(3000),IWANT(10),
     , ELOAD1(300,24),ELOAD2(300,24)
      COMMON/WORK/ELCOD(2,8),SHAPE(8),DERIV(2,8),DMATX(6,6),
     , CARTD(2,8),DBMAT(6,24),BMATX(6,24),SMATX(6,24,9),POSGP(3),
     , WEIGP(3),GPCOD(2,9),NEROR(24)
      COMMON/CONSTA/BETA,DELTA,A0,A1,A2,A3,A4,A5,A6,A7
C     END OF THE INCLUDE-FILE.
```

Appendix G

Finite Difference Program for a Micropolar Body Subject to Harmonic Surface Shear Loads

```
      PROGRAM FDMICRO
C-----------------------------------------------------------------------
C     Finite difference methods for to solve coupled transverse
C     wave problem which was introduced in Chapter 3.4.
C     (Case of one-dimensional micropolar elasticity)
C-----------------------------------------------------------------------
C
      INTEGER*4 ITIME,NTIME,M,I
      REAL*8 L,A,B,C,D,E,T,W,T0,DT,DX,AMU,AKA,RHO,AJ,GAM,
     ,       VN(1602),VC(1602),VH(1602),PN(1602),PC(1602),PH(1602),
     ,       SIG(1602),COU(1602)
      OPEN(5,FILE='FDM.DAT',STATUS='OLD')
      OPEN(6,FILE='FDM.OUT')
C
C     Setup program parameters:
C     L=length of dimension; M=number of space discretization;
C     DT=time step size; NTIME=total number of time step used;
C     T0=the magnitude of tangential surface loads;
C     W=the frequency of loads; AMU,AKA, and GAM are micropolar
C     material moduli; RHO=material mass density;
C     AJ=microinertia density
C
      READ(5,*)L,M,DT,NTIME,T0,W
      READ(5,*)AMU,AKA,RHO,AJ,GAM
      DX=L/M
      A=DT*DT*(AMU+AKA)/(RHO*DX*DX)
      B=DT*DT*AKA/(2.*RHO*DX)
      C=DT*DT*GAM/(AJ*DX*DX)
      D=DT*DT*AKA/(2.*AJ*DX)
      E=DT*DT*2.*AKA/AJ
C
C     Initial conditions VC(*) & PC(*) are specified .
C     Right end boundary conditions (i.e,fixed at M+2) are included.
C
      ITIME=1
      DO 10 I=1,M+2
      VN(I)=0.0
      VC(I)=0.0
      VH(I)=0.0
```

```
      PN(I)=0.0
      PC(I)=0.0
   10 PH(I)=0.0
      I=2
      T=0.0
      VN(2)=0.5*(2*A*VC(3)+2*(1.-A)*VC(2)-(A*2*DX/(AMU+AKA))*
     , (AKA*PC(2)-T0*SIN(W*T)))
      PN(2)=0.5*(C*PC(3)+(2.-2*C-E)*PC(2)+C*PC(3)+
     , (D*2*DX/(AMU+AKA))*(AKA*PC(2)-T0*SIN(W*T)))
      DO 20 I=3,M+1
      VN(I)=0.5*(A*VC(I+1)+2*(1.-A)*VC(I)+A*VC(I-1)-
     , B*PC(I+1)+B*PC(I-1))
      PN(I)=0.5*(C*PC(I+1)+(2.-2*C-E)*PC(I)+C*PC(I-1)+
     , D*VC(I+1)-D*VC(I-1))
   20 CONTINUE
      DO 25 I=3,M+1
      SIG(I)=(AMU+AKA)*(VN(I+1)-VN(I-1))/(2*DX)-AKA*PN(I)
   25 COU(I)=GAM*(PN(I+1)-PN(I-1))/(2*DX)
      WRITE(6,100)ITIME,VN(2),PN(2)
C
C     Now find next time step solutions.
C     Index I=2 represents the surface of body.
C
      DO 30 ITIME=2,NTIME
      DO 40 I=2,M+1
      VH(I)=VC(I)
      VC(I)=VN(I)
      PH(I)=PC(I)
   40 PC(I)=PN(I)
      I=2
      T=(ITIME-1)*DT
      VN(2)=2*A*VC(3)+2*(1.-A)*VC(2)-VH(2)-
     , (A*2*DX/(AMU+AKA))*(AKA*PC(2)-T0*SIN(W*T))
      PN(2)=C*PC(3)+(2.-2*C-E+D*AKA*2*DX/(AMU+AKA))*PC(2)+
     , C*PC(3)-PH(2)-(D*2*DX/(AMU+AKA))*T0*SIN(W*T)
      DO 50 I=3,M+1
      VN(I)=A*VC(I+1)+2*(1.-A)*VC(I)+A*VC(I-1)-B*PC(I+1)-
     , VH(I)+B*PC(I-1)
      PN(I)=C*PC(I+1)+(2.-2*C-E)*PC(I)+C*PC(I-1)+
     , D*VC(I+1)-PH(I)-D*VC(I-1)
   50 CONTINUE
      DO 55 I=3,M+1
      SIG(I)=(AMU+AKA)*(VN(I+1)-VN(I-1))/(2*DX)-AKA*PN(I)
   55 COU(I)=GAM*(PN(I+1)-PN(I-1))/(2*DX)
      WRITE(6,100)ITIME,VN(2),PN(2)
   30 CONTINUE
  100 FORMAT(I5,6(1X,E13.7))
      STOP
      END
```